UNIVERSITY OF SOUTHERN CALIFORNIA

DEPARTMENT OF CIVIL ENGINEERING

PRELIMINARY EMPIRICAL MODELS FOR SCALING ABSOLUTE ACCELERATION SPECTRA

by

Mihailo D. Trifunac and John G. Anderson

Report No. 77-03

A Report on the Research Conducted Under a Contract from

the U.S. Nuclear Regulatory Commission

Los Angeles, California

August, 1977

ABSTRACT

We present two preliminary models for the frequency dependent scaling of absolute acceleration spectra (SA) of strong earthquake ground motion. One of these models describes SA in terms of magnitude, epicentral distance, and site conditions; the other characterizes the dependence of SA on Modified Mercalli Intensity and site conditions.

The regression analyses have been carried out independently at 91 periods between 0.04 sec and 15 sec to permit the frequency dependent description of spectral amplitudes; the results are consistent with previous studies on the scaling of peak accelerations (Trifunac, 1976a) and of Fourier amplitude spectra (Trifunac, 1976b). One feature of these regressions is a description of the way amplitudes of SA scatter about the mean trend of the regression; this scatter is not inconsistent with a distribution curve derived from a Rayleigh distribution of response amplitudes.

INTRODUCTION

The purpose of this report is to explore the possibilities for improved characterization of absolute acceleration spectra of strong earthquake ground motion. It is motivated by the availability of uniformly processed strong-motion data which was obtained during the past several years and by the related work (Trifunac, 1976b) which demonstrated that empirical models for scaling the Fourier amplitudes of strong ground shaking in terms of earthquake magnitude, source to station distance, recording site conditions, component direction and the distribution of the observed amplitudes are now feasible.

The concept of the response spectrum was introduced into earthquake engineering by Biot (1941) and Benioff (1934). With the gradual accumulation of strong motion recordings since 1934, the response spectrum method for design of earthquake resistant structures (e.g., Hudson, et al., 1972) is now a part of or is being introduced into many modern design codes (Newmark et al., 1977). This popularity of the response spectrum method results partly from its property that it does not depend on the detailed characteristics of different structures, but only on the frequencies and the corresponding fractions of critical damping -- the two parameters which describe a single-degree-of-freedom, viscously damped, system. Hence, when available, a response spectrum can be utilized for the design of many different structural systems. Another important advantage of the response spectrum approach for the design of earthquake resistant structures

is that detailed real time response analysis, which often may represent an expensive undertaking, is not required. Even though the methodology for combining the contribution to the total response from several selected modes of vibration is only an approximate one, so far, it appears to be adequate for many design applications.

There are several difficulties which may result from the oversimplified methodology associated with the response spectrum approach. Some are caused by the lack of information contained in the response spectrum curve; these come from the definition of the spectrum, which is the maximum response to the entire time history of ground motion. Thus, many details on the duration of strong shaking and on the number and the distribution of peak amplitudes in the response are essentially eliminated. Other problems occur because the response analysis is linear; this makes any estimates of more realistic nonlinear response, at best, very difficult. It is clear, for example, that in a non-linear progressively deteriorating structural system, strong shaking with constant peak amplitudes may result in no damage, partial damage or total damage, depending on whether a structure was strained through one, several or through many cycles of nonlinear response. In spite of these and other well-known difficulties, the response spectrum approach in earthquake resistant design has gained considerable popularity among the engineering profession. If used judiciously and with the awareness of its limitations, it may offer convenient and simple means for the design of earthquake resistant structures in the absence of better and more reliable methodology.

It is likely that some form of the response spectrum approach will remain popular in engineering applications for some time in the future. It seems worthwhile, then, to explore the optimum methods for characterization of response spectra in terms of those parameters of strong ground motion which are most readily available to the engineering community. The physical phenomena which cause strong shaking are described by the parameters related to the earthquake source mechanism (e.g., moment, fault geometry, dislocation amplitudes, stress drop, radiation pattern, etc.) and the transmission path. For engineering analyses, however, at this point in time, one still has to utilize much less sophisticated parameters to describe strong shaking; e.g., earthquake magnitude, epicentral distance, site conditions, Modified Mercalli Intensity, etc. This is because those simple parameters are readily available and can be processed to yield desired statistical or deterministic estimates of future earthquake shaking (e.g., Anderson and Trifunac, 1977). The more detailed and informative parameters such as stress drop and seismic moment are not yet available for many past earthquakes and over sufficiently long intervals of time to warrant routine application of these parameters in a statistical or deterministic fashion.

Different types of response spectra are calculated from strong-motion accelerograms (Hudson et al., 1972). In this report our attention will be focused only on the absolute acceleration spectra, SA, which represent the maximum absolute acceleration of a single-degree-of-freedom system, with prescribed fraction of critical damping, during the excitation represented by a strong-motion accelerogram.

We shall address the scaling of the absolute acceleration spectra, SA, in terms of two groups of parameters. The first group will consist of earthquake magnitude, M, epicentral distance, R, recording site conditions, s (s = 0 will be assigned to alluvium sites, s = 2 to hard basement rock sites and s = 1 to intermediate sites; see Trifunac and Brady, 1975), component direction (v = 0 for horizontal and v = 1 for vertical) and a parameter, p, which will describe approximately the distribution of the spectral amplitudes. The second group will have the Modified Mercalli Intensity (M.M.I.) in place of M, and the epicentral distance, R, will be purposely omitted to avoid explicit emphasis on the rate of attenuation of M.M.I. in California. While this omission may increase the scatter of the observed spectral amplitudes with respect to the assumed empirical model, it permits the use of the derived correlations outside California, at least formally (e.g., see Trifunac and Westermo, 1976a, b for further discussion).

We are not suggesting that the above scaling parameters represent the best physical characterization of strong shaking; rather, they are based on the instrumental and qualitative information which is available to the engineering community in different parts of the United States and the world. While we are working towards better and more accurate characterization of strong earthquake ground motion, the present work accounts for the current limitations imposed by the data which is available now, and by the present status and completeness of the instrumental observations of earthquakes world-wide.

Following the first important recordings in 1934 and 1940 and in the early 1950's and the early systematic calculations of response

spectrum amplitudes (Alford et al., 1951) it became possible to study the shape of response spectra. This led to the development of "standard" spectral shapes for use in design. The development of a "standard" shape of the response spectrum was initiated in the mid and late 1950's (Housner, 1970) and extends through the early and mid 1970's (Trifunac, 1977). This work is usually characterized by the fixed shape of response spectrum whose amplitude depends on a single scaling parameter. Though spectra were also developed (Veletsos et al., 1965) which depended on peak acceleration, peak velocity and peak displacement, the direct availability of peak acceleration amplitudes from recorded accelerograms and the lack of accurate and uniformly processed peak velocities and peak displacements meant that most of these spectra were essentially scaled by the peak acceleration alone. Figure 1 shows the first "standard" shape of the absolute acceleration spectrum. It was intended that the spectrum intensity would be used as the amplitude scaling factor (Housner, 1970). However, because the spectral amplitudes tend toward the peak ground acceleration for $T \to 0$ for all fractions of critical damping, in applications, these and later fixed shape spectrum curves are often scaled in terms of peak acceleration. It was recognized that the shape of response spectra should depend on such parameters as earthquake magnitude, and source to station distance, but the data available in the mid and late 1950's did not allow more refined analysis; the curves in Figure 1 were developed by averaging over the spectra of strong-motion recordings of four representative earthquakes.

With the additional strong motion recordings obtained in the mid 1960's and early 1970's it has become possible to improve upon these

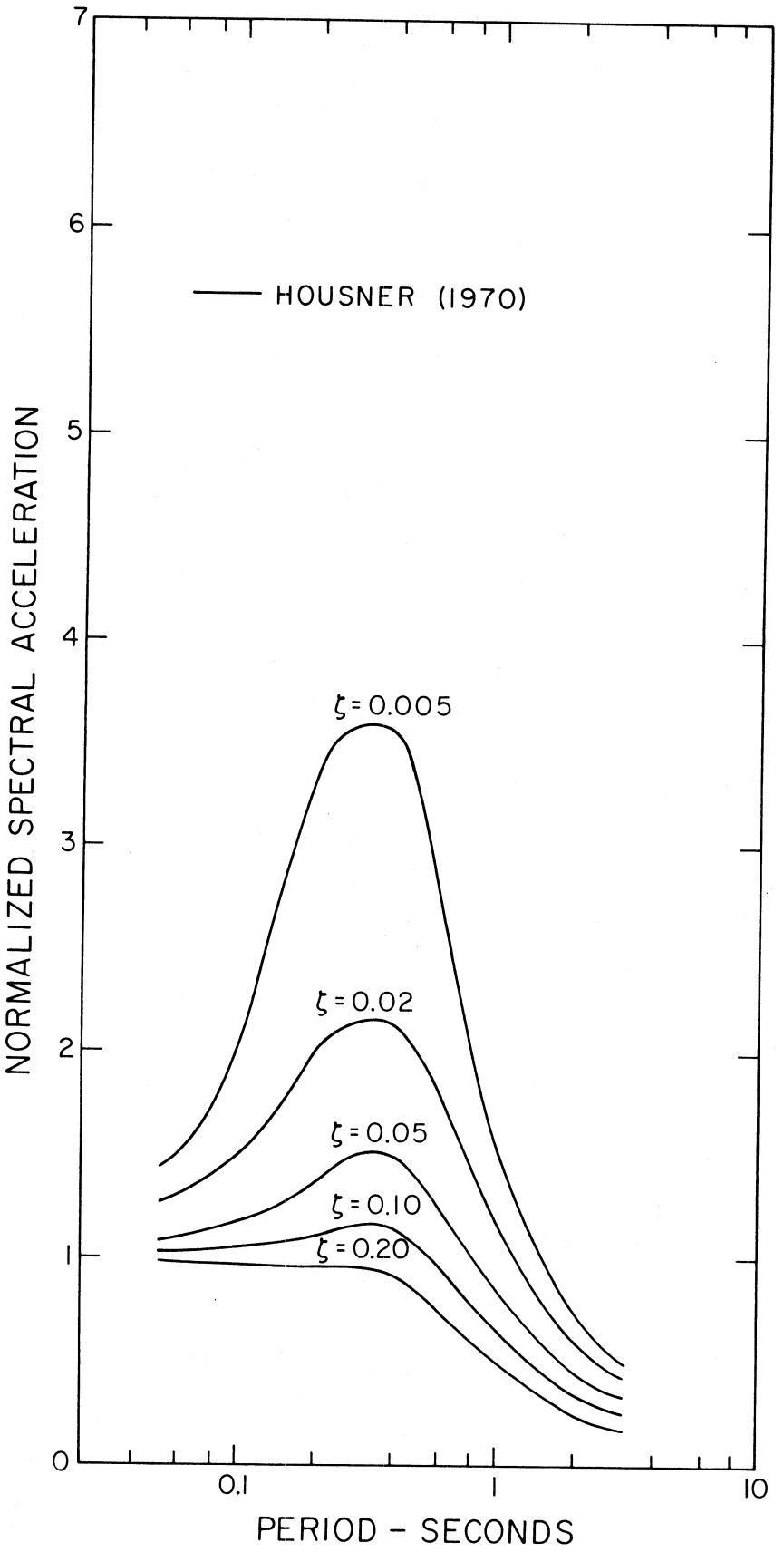
HOUSNER (1970)
ζ = 0.005
ζ = 0.02
ζ = 0.05
ζ = 0.10
ζ = 0.20
NORMALIZED SPECTRAL ACCELERATION
PERIOD - SECONDS
0
1
2
3
4
5
6
7
0.1
1
10

FIGURE 1

early studies. One recent example of a fixed shape absolute acceleration spectrum is shown in Figures 2 and 3 for horizontal and vertical strong shaking. These spectra are still scaled by peak acceleration amplitudes, and the effects of magnitude, source to station distance, attenuation with distance and site conditions are introduced only through the selected peak acceleration.

It has been recognized for some time that the level of the observed damage depends on the geologic and local soil conditions, and numerous attempts have been made to relate this observation to the recorded strong-motion accelerations (e.g., Duke, 1958) and to the recordings on more sensitive seismological instruments (e.g., Gutenberg, 1957; Borcherdt and Gibbs, 1976). With the exception of the work by Gutenberg (1957) most studies dealing with these effects attempted to relate the variations in damage to peak accelerations or peak velocity only and thus explicitly or implicitly eliminated the frequency dependent nature of this problem.

The spectra in Figure 4 (from Seed et al., 1974) represent one of the first attempts to study the frequency dependent variations of spectrum shape on the recording site conditions. In that analysis, the dependence of the shape of spectral amplitudes on site conditions was made possible by carrying out four independent statistical analyses on the normalized absolute acceleration spactra at many selected frequencies. The explicit dependence of spectrum shapes on magnitude and source to station distance were eliminated, however, by normalization of all spectral amplitudes to peak acceleration.

Since the completion of an important phase of the uniform data

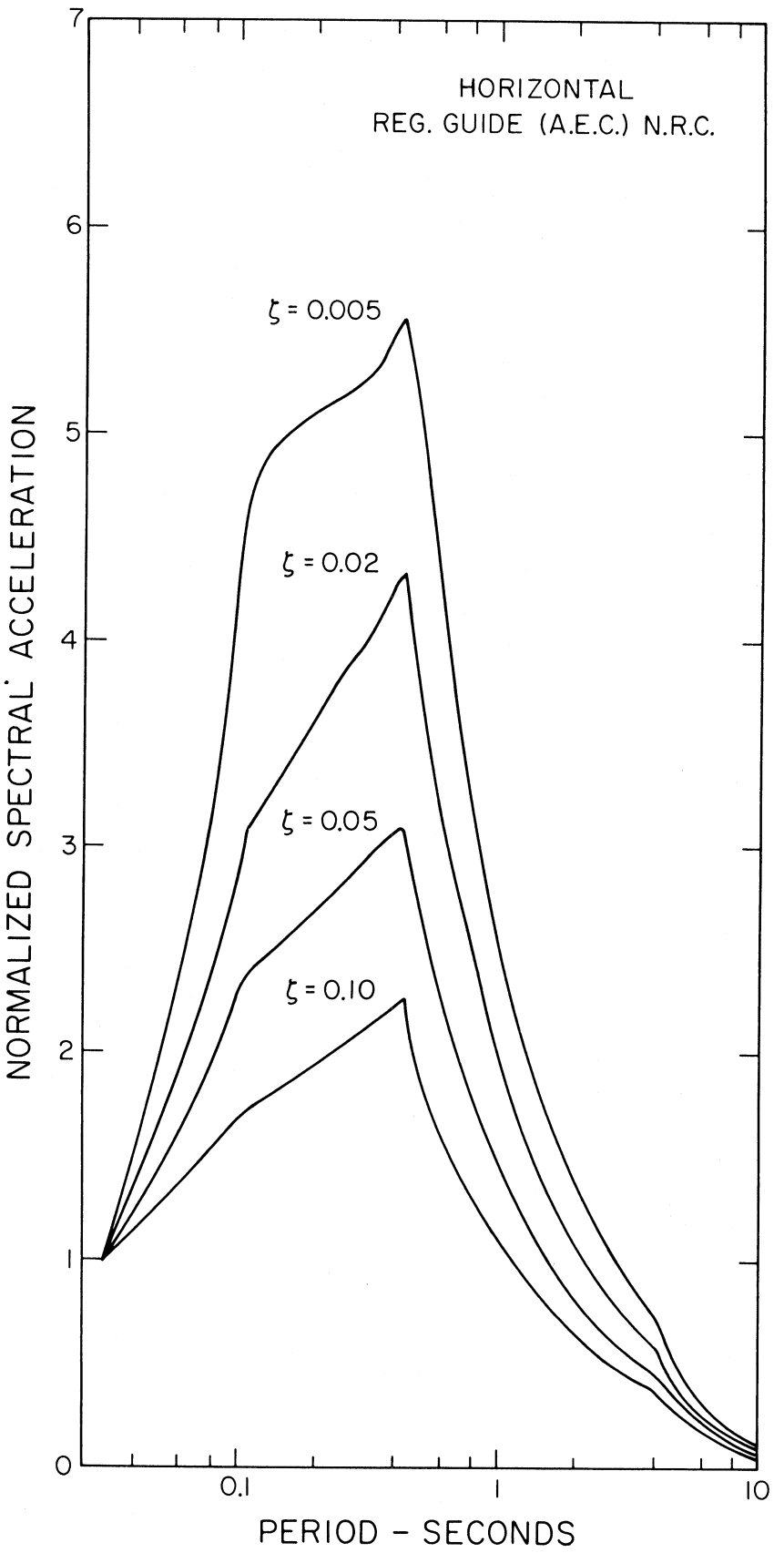
HORIZONTAL
REG. GUIDE (A.E.C.) N.R.C.
ζ = 0.005
ζ = 0.02
ζ = 0.05
ζ = 0.10
NORMALIZED SPECTRAL ACCELERATION
PERIOD - SECONDS
0
1
2
3
4
5
6
7
0.1
1
10

FIGURE 2

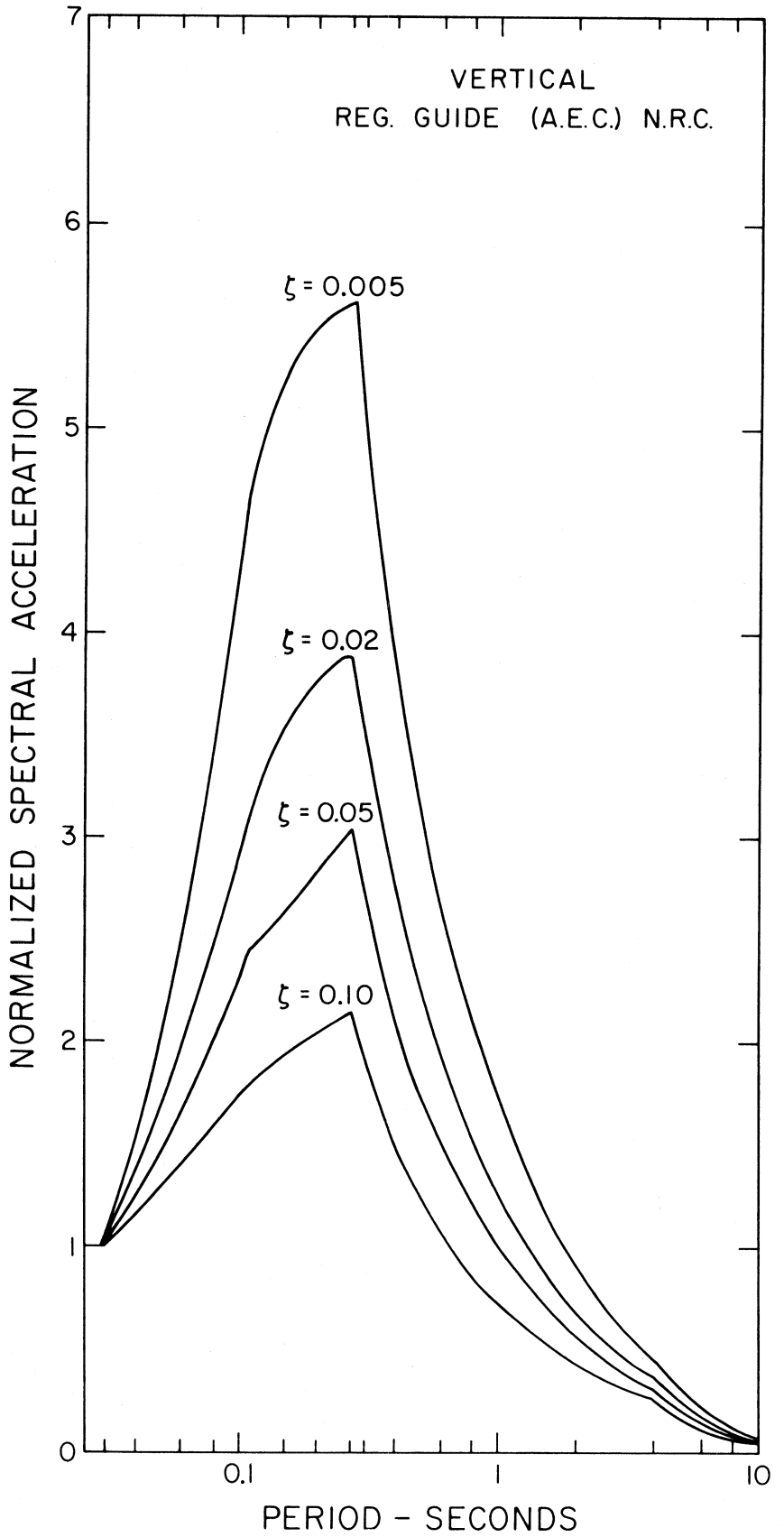
VERTICAL
REG. GUIDE (A.E.C.) N.R.C.
ζ = 0.005
ζ = 0.02
ζ = 0.05
ζ = 0.10
NORMALIZED SPECTRAL ACCELERATION
PERIOD - SECONDS
0
1
2
3
4
5
6
7
0.1
1
10

FIGURE 3

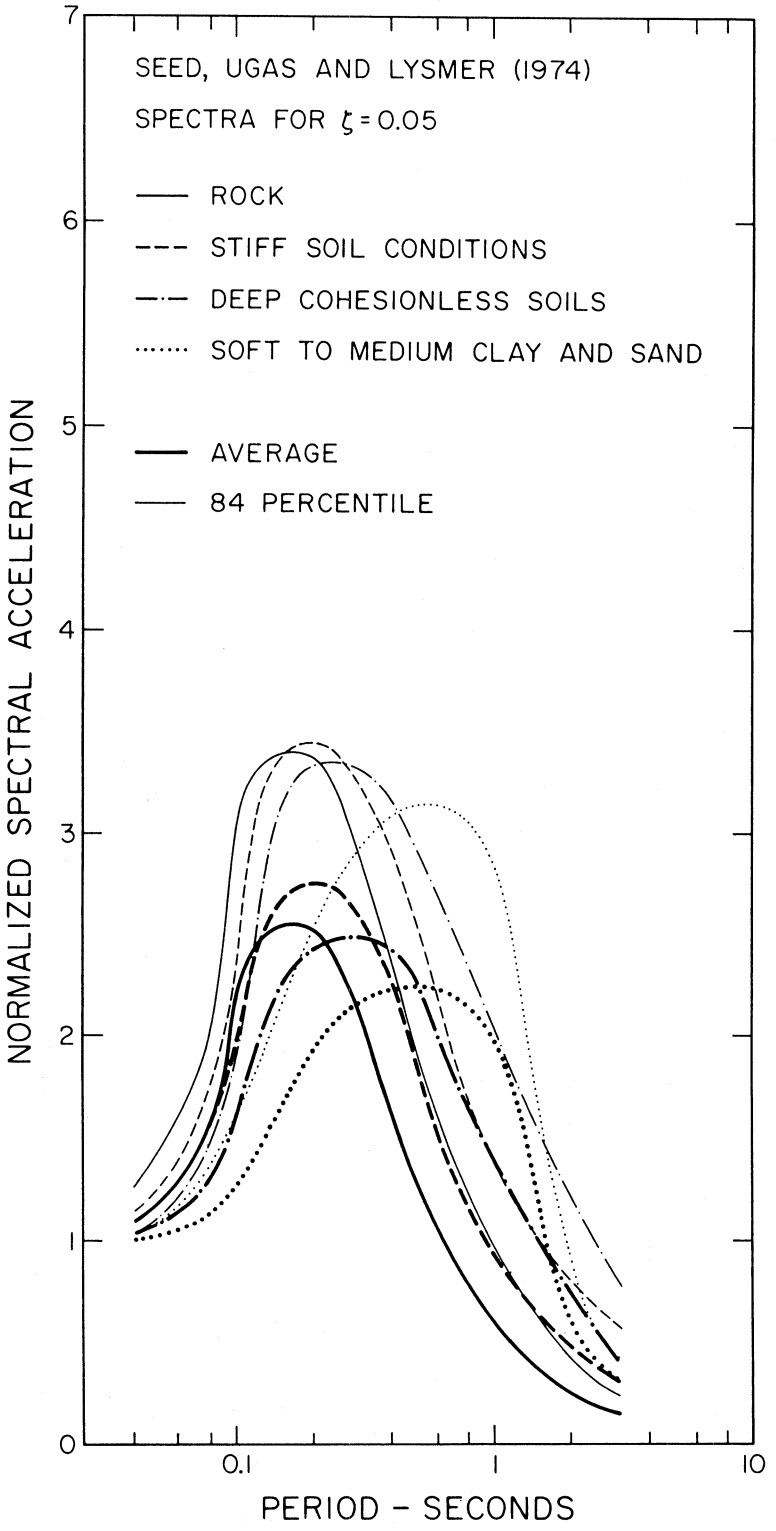
SEED, UGAS AND LYSMER (1974)
SPECTRA FOR ζ = 0.05
ROCK
STIFF SOIL CONDITIONS
DEEP COHESIONLESS SOILS
SOFT TO MEDIUM CLAY AND SAND
AVERAGE
84 PERCENTILE
NORMALIZED SPECTRAL ACCELERATION
PERIOD - SECONDS
0
1
2
3
4
5
6
7
0.1
1
10

FIGURE 4

processing effort (Hudson, 1976), it has become possible to develop multi-dimensional regression analyses of the shape and amplitudes of response spectra as those might depend not only on the recording site conditions but also on the other important parameters describing the strong ground motion. Preliminary studies of how the Fourier amplitude spectra depend on such scaling parameters (Trifunac, 1976b), have indicated that similar correlations for absolute acceleration and other response spectra may produce valuable results.

AVAILABLE DATA

The absolute acceleration spectra (SA) which are used in this study have been extracted from the Volume III tape (Trifunac and Lee, 1973) which contains absolute acceleration spectra (SA), relative displacement spectra (SD), relative velocity spectra (SV), pseudo relative velocity spectra (PSV) and Fourier amplitude spectra (FS) for 381 strong-motion accelerograms (Hudson et al., 1972). Of these 381 records, with two horizontal and one vertical component each, 186 accelerograms have been recorded at "free field" stations or in the basements of tall buildings. For the purpose of this analysis, it has been assumed that these recordings represent strong ground motion which is not seriously affected by the surroundings of the recording station. Detailed investigations will, no doubt, show that the records obtained in the basements of tall buildings or adjacent to some other large man-made or natural structure may be modified by the wave scattering and diffraction caused by these structures. However, for this analysis, these effects will not be considered.

These 381 accelerograph records resulted from 57 earthquakes in the Western United States and were recorded during the period from 1933 to 1971. From the 186 records that could be used as free-field data, only 182 were actually employed for the correlations with magnitude because no reliable magnitude estimates were available for four records (Table Ia). These 182 records were obtained during 46 earthquakes whose published magnitudes (Volume II reports, Parts A through Y, see Hudson et al., 1971) range from 3.8 to 7.7. The distribution of this data among five magnitude intervals is as follows: magnitude 3.0 to

3.9, 1 record; 4.0 to 4.9, 5 records; 5.0 to 5.9, 40 records; 6.0 to 6.9, 129 records; and 7.0 to 7.9, 7 records. As may be seen from this distribution, there is a concentration of data between magnitudes 5 and 7 with only 13 records available for magnitudes less than 5.0 and greater than 7.0. A majority (117) of the 182 records were registered at stations which were located on alluvium (classified under s = 0; see Trifunac and Brady, 1975 for more detailed description of this classification), 52 records were obtained on intermediate type rocks (s = 1) or close to boundaries between alluvium and basement rocks, and only 13 records came from stations on basement rocks (s = 2). Of these 182 records, slightly more than one half were recorded during the San Fernando, California, earthquake of 1971.

Clearly, the data used in this study are far from adequate to describe the magnitude range from M = 3 to M = 8 and all recording site conditions. The most serious shortage of recorded accelerograms is on basement rock sites (s = 2) and for magnitudes greater than M = 7. The following analysis is no doubt seriously affected by the non-uniformity of data and will have to be repeated and improved when more records become available. Nevertheless, these data do represent the largest collection of uniformly processed accelerograms so far, and can be used as an interim basis for the preliminary development of empirical models for the study of SA spectra.

The distribution of all 186 free-field accelerograms that could be used for the correlations with Modified Mercalli Intensities is given in Table Ib. It is clear from this distribution that most recordings

TABLE Ia

Summary of 186 Accelerograms Recorded at "Free Field" Stations or in Building Basements

Earthquake* No.	No. of Accelerograms Used in This Study	Magnitude	Caltech Report No.
1	3	6.3	B021, V314, V315
2	1	5.4	B023
3	-	-	U294
4	1	6.5	B024
5	1	6.0	B025
6	-	-	U295
8	-	-	U297
9	-	-	U298
13	1	5.5	B026
14	1	6.7	A001
15	1	6.4	B027
16	1	5.9	U299
17	1	6.4	U300
18	2	5.4	V316, V317
19	1	6.5	T286
20	1	5.3	U301
21	2	7.1	B028, B029
22	1	5.6	T287
23	1	5.8	A002
24	5	7.7	A003, A004, A005, A006, A007
26	1	5.5	B030
27	1	6.0	V319
28	1	5.5	T288
29	1	5.9	B031
30	1	5.3	U305
31	1	6.3	T289
32	2	6.5	A008, A009
33	1	5.8	A010
36	1	5.4	T292
37	1	6.8	A011
39	1	4.7	V329
40	1	3.8	V320
41	5	5.3	A013, A014, A015, A016, A017
42	2	4.4	V322, V323
43	1	4.0	V328
44	1	5.0	U307
45	1	5.7	U308
46	2	5.7	A018, U309

TABLE Ia (Continued)

Earthquake* No.	No. of Accelerogram Used in This Study	Magnitude	Caltech Report No.
47	1	5.0	V330
48	2	6.5	B032, U310
49	1	4.0	V331
50	6	5.6	B034, B035, B036, B037, B038, U311
51	1	6.3	T293
52	1	6.3	V332
53	2	5.8	B039, U312
54	1	5.2	U313
55	13	6.4	A019, A020, B040, Y370, Y371, Y372, Y373, Y375, Y376, Y377, Y378, Y379, Y380
56	7	5.4	W334, W335, W336, W338, W339, W342, W344
57	98	6.4	C041, C048, C051, C054, D056, D057, D058, D059, D062, D065, D068, E071, E072, E075, E078, E081, E083, F086, F087, F088, F089, F092, F095, F098, F101, F102, F103, F104, F105, G106, G107, G108, G110, G112, G114, H115, H118, H121, H124, I128, I131, I134, I137, J141, J142, J143, J144, J145, J148, K157, L166, L171, M176, M179, M180, M183, M184, N185, N186, N187, N188, N191, N192, N195, N196, N197,

TABLE Ia (Continued)

Earthquake* No.	No. of Accelerograms Used in This Study	Magnitude	Caltech Report No.
57 (Cont'd)			0198, 0199, 0204, 0205, 0206, 0207, 0208, 0210, P214, P217, P220, P221, P222, P223, P231, Q233, Q236, Q239, Q241, R244, R246, R246, R248, R249, R251, R253, S255, S258, S261, S262, S265, S266, S267

* For further details on these earthquakes, see Trifunac and Brady (1975). Records U296, T274, T275, T276, U302, U303, U204, T290, T291 and A012 which were recorded during the earthquakes numbered 7, 10, 11, 12, 25, 34, 35 and 38 were not included in this analysis. Six of these records represent incomplete time histories. For earthquakes 7 and 25 no reliable magnitude estimates were available.

TABLE Ib

Distribution of 186 Accelerograms Recorded at "Free Field" Stations or in Building Basements with Respect to M.M.I. and s=0, 1 and 2

M.M.I.	s = 0	s = 1	s = 2	N
III	1			1
IV	1	2		3
V	17	15	2	34
VI	43	16	7	66
VII	49	21	5	75
VIII	6			6
IX				
X			1	1

$n_{s=0} = 117$ $n_{s=1} = 54$ $n_{s=2} = 15$ $n_{total} = 186$

correspond to the M.M.I. levels V, VI, and VII with less than 3% of all data falling outside this range. It is also clear that recordings on hard rock (s = 2) are, again, not adequately represented.

ABSOLUTE ACCELERATION SPECTRA OF DIGITIZATION NOISE

Before proceeding with the regression analysis of absolute acceleration spectra, SA, it is necessary to examine the extent to which the computed SA spectra are affected by digitization and processing noise. Routine data processing techniques (Trifunac and Lee, 1973) which have been designed for typical accelerograms simply band-pass filter raw digitized data between 0.07 cps and 25 cps or between 0.125 cps and 25 cps depending on whether the raw data have been digitized from paper or 70-mm and 35-mm film records. However, since the digitization noise does not have constant spectral amplitudes in the respective frequency bands and since these amplitudes depend on the total length of record which has been digitized, for the analysis in this paper, it is necessary to extend the results presented by Trifunac et al., (1973) and compute the average SA spectra of digitization noise for different record durations.

Six operators digitized a straight line twice and one operator digitized it once, producing a total of thirteen digitizations. The straight line which they digitized extended diagonally from the lower left corner of a rectangular Mylar transparancy, 10 in. high and about 23 in. long. The total average number of digitized points has been selected to be about 700, which corresponds to about 30 pts/inch. This digitization rate was chosen to correspond to the average digitization rate for 4X enlargements of 10 to 15 cm long segments of 70-mm film records from which an average operator would digitize about 40 to 50 points per 4 cm, which corresponds to a time interval of one second. The reasons for selecting a sloping straight line to analyze digiti-

zation noise and other pertinent details of this and related procedures have been discussed by Trifunac et al., (1973) and will not be repeated here.

To simulate the effect of the fixed baseline on accelerograms, we decimated all raw digitizations of the straight line and kept only 16 points from the total sequence of about 700 points. For the 4X enlargements of 70-mm film records, this corresponds to digitization of the fixed baseline at equal intervals of about 1 sec long. By smoothing these decimated data with a $\frac{1}{4},\frac{1}{2},\frac{1}{4}$ filter and by subtracting the result from the raw digitization, the long-period drifts were eliminated from the raw data by following the same procedures used in routine processing of recorded accelerograms which contain fixed mirror traces. An example of a typical acceleration noise for a 15 sec long record is shown in Figure 5 after it has been processed through the routine Volume II (Trifunac and Lee, 1973) band-pass filtering. Once and twice integrated acceleration noise data are also shown in this figure to illustrate what may be the typical appearance of velocity and displacement curves which results from the digitization noise. Table II presents the average and standard deviations for the peaks of acceleration, velocity and displacement computed from 13 records for the duration of noise records equal to 15, 30, 60 and 100 seconds. The peak displacement amplitudes in this table are smaller by a factor of 2 or 3 than the estimates of the overall accuracy of computed ground displacements by Trifunac and Lee, 1974. This could be explained as follows: First the typical 70-mm record, which is longer than about 15 seconds, is digitized in segments which are about 10 to 15 sec long.

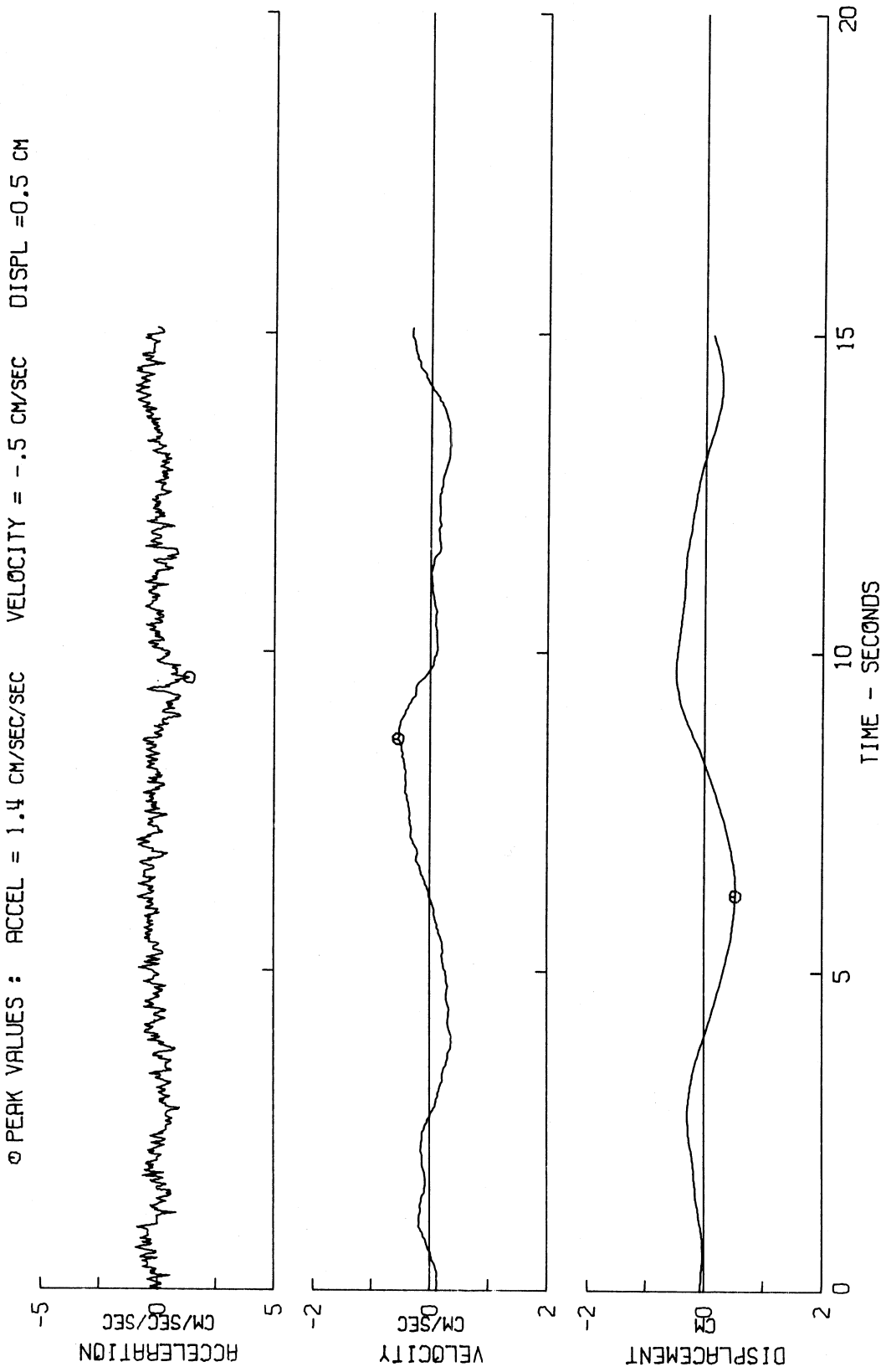
Ø PEAK VALUES : ACCEL = 1.4 CM/SEC/SEC VELØCITY = -.5 CM/SEC DISPL =0.5 CM
ACCELERATIØN
CM/SEC/SEC
VELØCITY
CM/SEC
DISPLACEMENT
CM
TIME - SECØNDS
-5
0
5
-2
0
2
-2
0
2
0
5
10
15
20

FIGURE 5

TABLE II

Averages and Standard Deviations of Peak Acceleration, Peak Velocity, and Peak Displacement That Resulted from Standard Processing of Digitization of Records containing Noise Alone

		Duration of Noise Record			
		15 sec	30 sec	60 sec	100 sec
acceleration (cm/sec^2)	ave. (13 records)	1.66	1.72	1.75	1.74
	st. dev.	0.48	0.48	0.46	0.46
velocity (cm/sec)	ave. (13 records)	0.46	0.55	0.59	0.58
	st. dev.	0.13	0.15	0.14	0.13
displacement (cm)	ave. (13 records)	0.49	0.61	0.68	0.73
	st. dev.	0.19	0.18	0.19	0.19

Moving the records to digitize successive segments adds a "saw-tooth" like sequence of straight lines to the digitized amplitudes and, thus, additional long period errors which are not present in the thirteen noise digitizations studied in this paper. The long-period noise contributions resulting from this "saw-tooth" like error are eliminated from the digitized data off 70-mm film records which have all been high-pass filtered from 0.125 cps rather than from 0.07 cps (see Trifunac et al., 1973), but some intermediate frequency errors are still present in the data. Second, and probably a more important reason for peak displacements in Table II being two to three times smaller than our previous estimates of the overall displacement errors (Trifunac and Lee, 1974), is that this noise study was carried out under more uniform and controlled conditions than the actual digitizations of the 381 accelerograph records, which took several years to complete and involved many more operators and different digitizing equipment as well.

For the purpose of this and other related investigations we will assume that the characteristics of the above described "noise" accelerograms are satisfactory to describe approximately the overall noise amplitudes in 182 records for short and intermediate periods, T, and we will use the average SA spectra of these thirteen digitizations to carry out an approximate scheme of noise subtraction from the computed SA spectra of 546 accelerograms. The amplitudes of the average and of the average plus one standard deviation of spectral amplitudes of noise are shown in many subsequent figures of this report where the amplitudes of SA spectra have been presented.

EMPIRICAL MODELS FOR SCALING ABSOLUTE ACCELERATION SPECTRA

In two recent studies, Trifunac (1976b, 1977) presented two approximate models for estimating the range of possible spectral amplitudes of strong ground motion for (a) known earthquake magnitude, source-to-station distance and recording site conditions, and (b) known Modified Mercalli Intensity at the site, and recording site conditions. The same empirical models will be applied in this report to scaling of absolute acceleration amplitudes at a selected set of discrete periods, T. For this purpose, the equations from the previous work can be modified to become

$$\log_{10}[SA(T)_{,p}] = M + \log_{10}A_o(R) - a(T)p - b(T)M - c(T) - d(T)s - e(T)v - f(T)M^2 - g(T)R \qquad (1)$$

and

$$\log_{10}[SA(T)_{,p}] = a(T)p + b(T)I_{MM} + c(T) + d(T)s + e(T)v \qquad (2)$$

where M is earthquake magnitude, usually M_L (Richter, 1958), s represents the type of site conditions (s = 0 for alluvium, s = 1 for intermediate rocks, and s = 2 for basement rocks), v designates the horizontal or vertical components (v = 0 for horizontal, v = 1 for vertical). The term $\log_{10}A_o(R)$ represents an empirical function (Richter, 1958) which describes the amplitude attenuation with distance R from the epicenter (in km); numerical values are listed in Table III. I_{MM} stands for a given M.M.I. level. The confidence level p, as used here, is not a probability. However, for values of p between 0.1 and 0.9, it approximates the probability that $SA(T)_{,p}$ will not be exceeded, given the other parameters of the regression. The units of SA are the fraction of the accelerations of gravity. Functions a(T), b(T),...,

TABLE III

$\log_{10}A_o(R)$ Versus Epicentral Distance R*

R (km)	$-\log_{10}A_o(R)$	R (km)	$-\log_{10}A_o(R)$	R (km)	$-\log_{10}A_o(R)$
0	1.400	140	3.230	370	4.336
5	1.500	150	3.279	380	4.376
10	1.605	160	3.328	390	4.414
15	1.716	170	3.378	400	4.451
20	1.833	180	3.429	410	4.485
25	1.955	190	3.480	420	4.518
30	2.078	200	3.530	430	4.549
35	2.199	210	3.581	440	4.579
40	2.314	220	3.631	450	4.607
45	2.421	230	3.680	460	4.634
50	2.517	240	3.729	470	4.660
55	2.603	250	3.779	480	4.685
60	2.679	260	3.828	490	4.709
65	2.746	270	3.877	500	4.732
70	2.805	280	3.926	510	4.755
80	2.920	290	3.975	520	4.776
85	2.958	300	4.024	530	4.797
90	2.989	310	4.072	540	4.817
95	3.020	320	4.119	550	4.835
100	3.044	330	4.164	560	4.853
110	3.089	340	4.209	570	4.869
120	3.135	350	4.253	580	4.885
130	3.182	360	4.295	590	4.900

* Only the first two digits may be assumed to be significant.

f(T) and g(T) in (1) and (2) are as yet unknown functions of T which will be determined in the following regression analyses. In this paper, as in the analysis of peak amplitudes and Fourier spectra (Trifunac, 1976a, b), the higher order terms in p, s and M and the terms which include different products of p, s and M will be neglected. The functions a(T), b(T), ..., in (1) and (2) are different functions which will be derived in two separate analyses, but their symbols have been selected to represent the corresponding types of data dependence in both (1) and (2). Their signs differ in (1) and (2) only for consistency with previous studies.

Equation (1) introduces a new term g(T)R, the analogue of which was not present in one of our previous studies (Trifunac, 1976a). This term now models the period dependent attenuation correction factor for distance R and its form corresponds to the usual amplitude attenuation $e^{-\frac{\pi R}{Q\beta T}}$, on a linear scale, which is often employed to model approximately the effect of anelastic attenuation. Here β stands for the shear wave velocity and Q is the attenuation constant. In (1) g(T) then might be thought of as corresponding to $\frac{\pi}{Q\beta T}\log_{10}e$.

If the $\log_{10}A_o(R)$ terms were to represent the geometric spreading only, then g(T)R would model the equivalent anelastic attenuation. However, $\log_{10}A_o(R)$, which has been derived empirically from the data on actual peak amplitudes of small earthquakes in Southern California, represents an average combination of geometric spreading and anelastic attenuation for a frequency band centered around 1 cps. Therefore, the term g(T)R cannot be thought of as modeling $\frac{\pi}{Q\beta T}\log_{10}e$ but rather

represents a correction to the average attenuation which is represented by $\log_{10}A_o(R)$. In the study of peak accelerations, peak velocities, and peak displacements (Trifunac, 1976a), a term like g(T)R was omitted on purpose to avoid undue emphasis and dependence in the model on the digitization noise which is reflected in larger peak amplitudes especially for peak displacement, at distances which are typically greater than 100 km. In this paper, because absolute acceleration spectral amplitudes are being studied, it is possible to subtract approximately the expected contributions to spectral amplitudes that results from noise; the g(T)R then reflects corrections to the $\log_{10}A_o(R)$ term.

REGRESSION ANALYSES

The computation of the coefficient functions a(T), b(T), ..., f(T) and g(T) in the equations (1) and (2) was carried out at 91 discrete periods T ranging from 0.04 sec to 15.0 sec. From each of the 546 SA spectra, for correlations with M, and 558 for correlations with M.M.I., an average noise spectrum was first subtracted.* This noise spectrum was obtained by linearly interpolating from the spectra which were computed for 15, 30, 60 and 100 seconds to obtain a noise spectrum which would apply for a record with the actual duration (Table IV) of each accelerogram. The data for fitting a(T), b(T),... in equation (1) were then computed by subtracting from $\log_{10}[SA(T)]$ the respective magnitude and $\log_{10}A_o(R)$ for the epicentral distance R corresponding to each of 182 records. Regression analysis was then carried out for each of 91 periods by fitting the remaining right hand side of equation (1) and the original data for equation (2).

To carry out these regression analyses with a(T), b(T), ..., f(T) and g(T) as coefficients at a fixed value of T, we began by (a) partitioning all data into five groups corresponding to magnitude groups 3.0-3.9, 4.0-4.9, 5.0-5.9, 6.0-6.9, and 7.0-7.9, and (b) partitioning into seven groups corresponding to M.M.I. levels III, IV, V, VI, VII, VIII and X. The data in each of these groups were next grouped according to the site classifications s=0, s=1 and s=2. The data within

---

* It is noted that $SA(\ddot{y}_1 + \ddot{y}_2) \neq SA(\ddot{y}_1) + SA(\ddot{y}_2)$, where $\ddot{y}_1$ and $\ddot{y}_2$ are two sources of ground shaking. Furthermore, if $\ddot{y}_1$ is the signal and $\ddot{y}_2$ is the noise, then the stochastic nature of $\ddot{y}_2$ prevents any exact noise elimination scheme from being carried out. Thus, this procedure is an approximation which, empirically, decreases the distortion by noise of the SA spectra when the signal to noise ratio is small.

TABLE IV

Total Duration and Low Cut-Off Frequency
for Acceleration Records Used in This Study

Record No.	Caltech Report No.	Total Duration*	Low Frequency Cut-Off (cps)
1	A001	54	0.07
2	A002	56	0.07
3	A003	77	0.07
4	A004	54	0.07
5	A005	75	0.07
6	A006	83	0.07
7	A007	79	0.07
8	A008	78	0.07
9	A009	42	0.07
10	A010	51	0.07
11	A011	90	0.07
12	A013	25	0.07
13	A014	26	0.07
14	A015	27	0.07
15	A016	25	0.07
16	A017	40	0.07
17	A018	40	0.07
18	A019	87	0.07
19	A020	79	0.07
20	B021	99	0.07
21	B023	75	0.07
22	B024	90	0.07
23	B025	51	0.07
24	B026	71	0.07
25	B027	67	0.07
26	B028	67	0.07
27	B029	89	0.07
28	B030	58	0.07
29	B031	65	0.07
30	B032	82	0.07
31	B034	44	0.07
32	B035	26	0.07
33	B036	44	0.07
34	B037	30	0.07
35	B038	30	0.07
36	B039	30	0.07
37	B040	45	0.07
38	C041	31	0.07
39	C048	59	0.07
40	C051	52	0.07
41	C054	57	0.07
42	D056	62	0.07

TABLE IV (Continued)

Record No.	Caltech Report No.	Total Duration*	Low Frequency Cut-Off (cps)
43	D057	82	0.07
44	D058	79	0.07
45	D059	57	0.07
46	D062	54	0.07
47	D065	41	0.07
48	D068	37	0.07
49	E071	30	0.07
50	E072	54	0.07
51	E075	44	0.07
52	E078	57	0.07
53	E081	50	0.07
54	E083	63	0.07
55	F086	78	0.07
56	F087	81	0.07
57	F088	30	0.07
58	F089	59	0.07
59	F092	34	0.07
60	F095	67	0.07
61	F098	56	0.07
62	F101	11	0.07
63	F102	10	0.07
64	F103	27	0.07
65	F104	11	0.07
66	F105	64	0.07
67	G106	31	0.125
68	G107	29	0.125
69	G108	99	0.125
70	G110	98	0.125
71	G112	52	0.125
72	G114	58	0.125
73	H115	40	0.125
74	H118	86	0.125
75	H121	46	0.125
76	H124	33	0.125
77	I128	27	0.125
78	I131	48	0.125
79	I134	49	0.125
80	I137	57	0.125
81	J141	60	0.07
82	J142	37	0.125
83	J143	35	0.07
84	J144	37	0.07
85	J145	99	0.125
86	J148	19	0.125
87	K157	32	0.125

TABLE IV (Continued)

Record No.	Caltech Report No.	Total Duration*	Low Frequency Cut-Off (cps)
88	L166	65	0.125
89	L171	53	0.07
90	M176	88	0.125
91	M179	13	0.07
92	M180	99	0.125
93	M183	20	0.125
94	M184	30	0.125
95	N185	44	0.125
96	N186	59	0.125
97	N187	30	0.125
98	N188	45	0.125
99	N191	70	0.125
100	N192	25	0.125
101	N195	99	0.125
102	N196	53	0.125
103	N197	43	0.125
104	O198	31	0.125
105	O199	35	0.125
106	O204	69	0.07
107	O205	99	0.07
108	O206	53	0.125
109	O207	62	0.07
110	O208	62	0.125
111	O210	54	0.125
112	P214	30	0.07
113	P217	30	0.07
114	P220	61	0.07
115	P221	30	0.07
116	P222	58	0.07
117	P223	33	0.07
118	P231	48	0.125
119	Q233	37	0.125
120	Q236	42	0.125
121	Q239	45	0.125
122	Q241	49	0.125
123	R244	42	0.125
124	R246	44	0.125
125	R248	45	0.125
126	R249	41	0.125
127	R251	31	0.125
128	R253	36	0.125
129	S255	30	0.125
130	S258	48	0.125
131	S261	39	0.125
132	S262	36	0.125

TABLE IV (Continued)

Record No.	Caltech Report No.	Total Duration*	Low Frequency Cut-Off (cps)
133	S265	21	0.125
134	S266	35	0.125
135	S267	49	0.125
136	T286	71	0.07
137	T287	60	0.07
138	T288	86	0.07
319	T289	78	0.07
140	T292	43	0.07
141	T293	75	0.07
142	U294**	59	0.07
143	U295**	21	0.07
144	U297**	9	0.07
145	U298**	76	0.07
146	U299	62	0.07
147	U300	68	0.07
148	U301	56	0.07
149	U305	57	0.07
150	U307	77	0.07
151	U308	82	0.07
152	U309	88	0.07
153	U310	74	0.07
154	U311	72	0.07
155	U312	93	0.07
156	U313	61	0.07
157	V314	99	0.07
158	V315	99	0.07
159	V316	67	0.07
160	V317	62	0.07
161	V319	49	0.07
162	V320	36	0.07
163	V322	49	0.07
164	V323	23	0.07
165	V328	26	0.07
166	V329	69	0.07
167	V330	75	0.07
168	V331	7	0.07
169	V332	43	0.07
170	W334	17	0.07
171	W335	38	0.07
172	W336	10	0.07
173	W338	30	0.07
174	W339	42	0.07
175	W342	23	0.07
176	W344	23	0.07

TABLE IV (Continued)

Record No.	Caltech Report No.	Total Duration*	Low Frequency Cut-Off (cps)
177	Y370	85	0.07
178	Y371	82	0.07
179	Y372	52	0.07
180	Y373	42	0.07
181	Y375	54	0.07
182	Y376	60	0.07
183	Y377	44	0.07
184	Y378	21	0.07
185	Y379	62	0.07
186	Y380	51	0.07

*Rounded to nearest second.

**Not included in the analysis because of incomplete information on earthquake magnitude.

each of these subgroups were then divided into two parts corresponding to v=0 and v=1. The n data remaining in each of these final parts were next rearranged so that the numerical values decrease monotonically. Then, if p=m/n, the m^{th} data point from a group of n points represents an estimate of (a) $\log_{10}[SA(T),_p] - M - \log_{10}A_o(R)$ or (b) $\log_{10}[SA(T),_p]$ which is to be associated with the approximate p-percent confidence level. If the number of data points, n, in each group was greater than 19, we used 19 levels for subsequent least squares fitting with the p levels equal to 0.5, 0.10, 0.15, ..., 0.9 and 0.95. If the number of data points in each group was less than 19, we used all data points and computed the estimates of the corresponding confidence levels p from the fraction of points that were smaller than a given level to the total number of points in that group of n. This approximate scheme has the effect of decreasing the "weight" of data groups for which many points are available in the subsequent least squares fitting.

For those accelerograms which were high-pass filtered from 0.125 cps rather than from 0.07 cps (Table IV) the data have not been included in the regression analysis for periods, T, longer than 8 seconds. This and the fact that for many intermediate and small earthquakes spectral amplitudes for the long period waves have a small signal-to-noise ratio led to the decision to terminate the final computation and presentation of a(T), b(T), ..., f(T) and g(T) for both correlations with M and M.M.I. at the long period end equal to 12 seconds rather than at 15 seconds.

a. Correlations in Terms of M, R, p, s and v

Figure 6 and Table V present the results of least squares fitting of equation (1) to the SA data. The 91 discrete estimates of a(T),

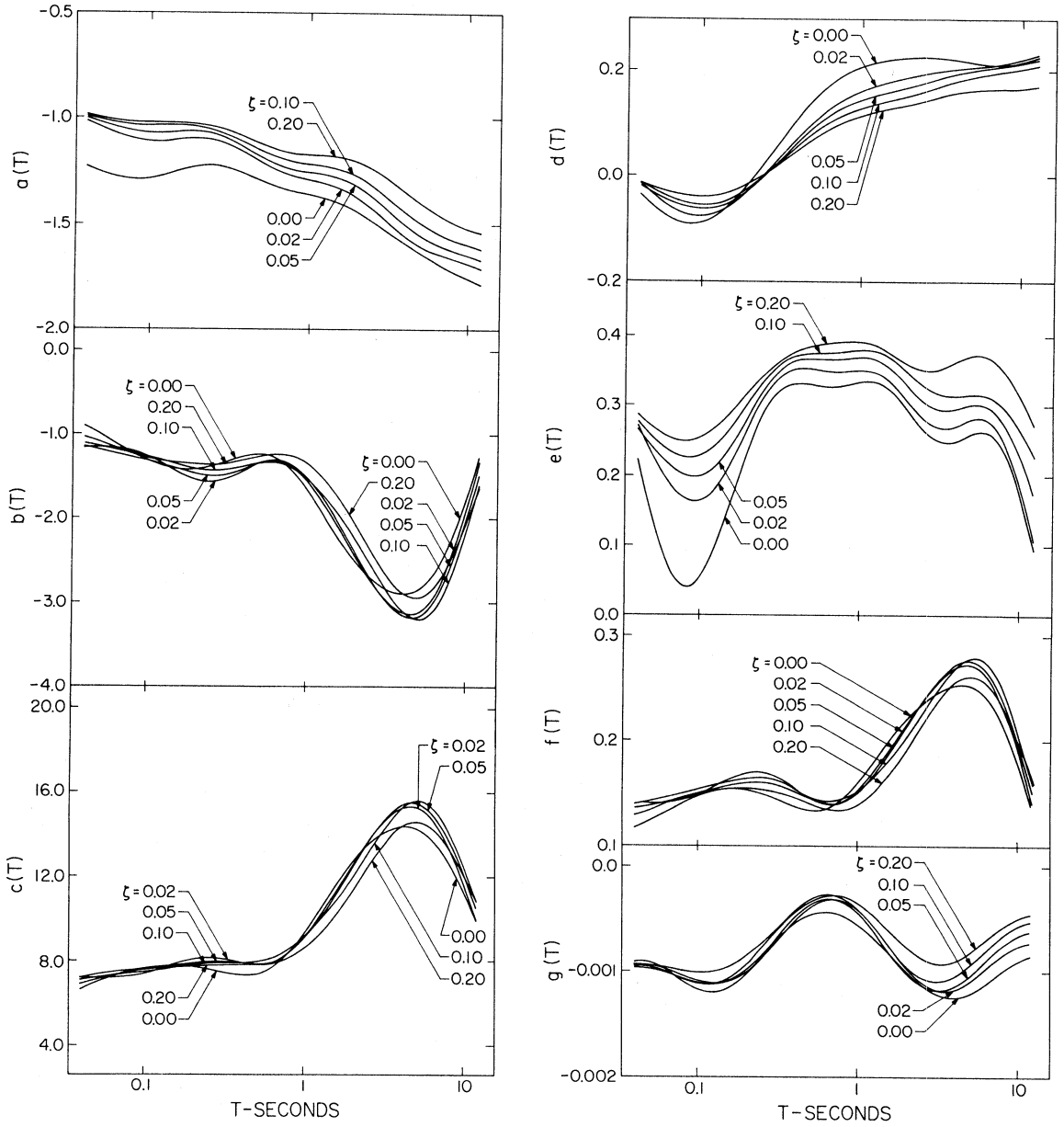
a (T)
-0.5
-1.0
-1.5
-2.0
ζ = 0.10
0.20
0.00
0.02
0.05
b (T)
0.0
-1.0
-2.0
-3.0
-4.0
ζ = 0.00
0.20
0.10
0.05
0.02
ζ = 0.00
0.20
0.02
0.05
0.10
c (T)
20.0
16.0
12.0
8.0
4.0
ζ = 0.02
0.05
ζ = 0.02
0.05
0.10
0.20
0.00
0.00
0.10
0.20
0.1
1
10
T-SECONDS
d (T)
0.2
0.0
-0.2
ζ = 0.00
0.02
0.05
0.10
0.20
e (T)
0.4
0.3
0.2
0.1
0.0
ζ = 0.20
0.10
0.05
0.02
0.00
f (T)
0.3
0.2
0.1
ζ = 0.00
0.02
0.05
0.10
0.20
g (T)
0.0
-0.001
-0.002
ζ = 0.20
0.10
0.05
0.02
0.00
0.1
1
10
T-SECONDS

FIGURE 6

TABLE V

Regression Parameters for Equation (1) and $\alpha(T)$, $\beta(T)$ and N(T)* at Eleven Selected Periods

$\log_{10}$T(sec)	-1.398	-1.171	-0.943	-0.716	-0.489	-0.261	-0.034	0.193	0.420	0.648	0.875
ζ = 0.0											
a(T)	-1.230	-1.284	-1.276	-1.229	-1.243	-1.312	-1.358	-1.405	-1.501	-1.617	-1.714
b(T)	-0.904	-1.146	-1.354	-1.418	-1.316	-1.244	-1.571	-2.219	-2.732	-2.884	-2.411
c(T)	6.601	7.317	7.701	7.695	7.413	7.446	8.875	11.436	13.576	14.366	13.105
d(T)	-0.036	-0.086	-0.078	-0.010	0.084	0.165	0.209	0.226	0.229	0.220	0.217
e(T)	0.223	0.057	0.081	0.231	0.325	0.329	0.334	0.321	0.260	0.257	0.243
10f(T)	1.163	1.342	1.500	1.535	1.427	1.336	1.553	2.019	2.398	2.548	2.232
1000g(T)	-0.915	-1.018	-1.198	-1.058	-0.679	-0.442	-0.523	-0.823	-1.144	-1.233	-1.025
α(T)	0.767	0.819	0.900	1.058	1.258	1.500	1.704	2.031	2.663	3.897	4.007
β(T)	1.339	1.201	1.047	0.846	0.620	0.314	0.042	-0.405	-1.216	-2.548	-2.586
N(T)	162	96	57	33	20	11	7	4	2	1	1
ζ = 0.02											
a(T)	-1.017	-1.084	-1.110	-1.097	-1.135	-1.228	-1.288	-1.334	-1.444	-1.580	-1.661
b(T)	-1.161	-1.172	-1.317	-1.532	-1.515	-1.327	-1.486	-2.089	-2.768	-3.138	-2.651
c(T)	7.203	7.226	7.506	8.019	8.038	7.794	8.749	11.126	13.766	15.289	13.942
d(T)	-0.015	-0.066	-0.071	-0.024	0.051	0.120	0.162	0.184	0.200	0.210	0.220
e(T)	0.272	0.181	0.174	0.264	0.345	0.352	0.351	0.333	0.277	0.278	0.257
10f(T)	1.401	1.411	1.527	1.685	1.637	1.428	1.494	1.930	2.439	2.740	2.407
1000g(T)	-0.972	-1.033	-1.122	-1.031	-0.693	-0.360	-0.377	-0.756	-1.123	-1.138	-0.868
α(T)	0.781	0.836	0.913	1.065	1.268	1.538	1.754	2.067	2.682	3.885	3.938
β(T)	1.336	1.200	1.049	0.851	0.620	0.291	0.004	-0.438	-1.236	-2.543	-2.547
N(T)	162	96	57	33	20	11	7	4	2	1	1
ζ = 0.05											
a(T)	-1.001	-1.054	-1.071	-1.064	-1.110	-1.204	-1.255	-1.287	-1.387	-1.528	-1.619
b(T)	-1.152	-1.248	-1.347	-1.463	-1.469	-1.322	-1.455	-2.031	-2.753	-3.178	-2.730
c(T)	7.189	7.480	7.635	7.866	7.960	7.849	8.716	10.983	13.734	15.444	14.249
d(T)	-0.019	-0.053	-0.060	-0.024	0.043	0.109	0.146	0.165	0.186	0.203	0.214
e(T)	0.266	0.210	0.207	0.281	0.355	0.368	0.370	0.352	0.302	0.301	0.281
10f(T)	1.387	1.470	1.557	1.640	1.609	1.433	1.478	1.898	2.440	2.775	2.462
1000g(T)	-0.941	-1.001	-1.108	-1.014	-0.655	-0.332	-0.401	-0.812	-1.145	-1.093	-0.787
α(T)	0.786	0.853	0.937	1.084	1.283	1.552	1.769	2.089	2.695	3.896	3.955
β(T)	1.332	1.195	1.041	0.842	0.613	0.287	-0.002	-0.451	-1.248	-2.553	-2.556
N(T)	162	96	57	33	20	11	7	4	2	1	1

TABLE V

(Continued)

ζ = 0.10

a(T)	-0.991	-1.028	-1.035	-1.040	-1.089	-1.170	-1.216	-1.244	-1.334	-1.470	-1.566
b(T)	-1.112	-1.197	-1.297	-1.408	-1.414	-1.335	-1.481	-1.937	-2.597	-3.161	-2.859
c(T)	7.084	7.340	7.518	7.768	7.886	7.980	8.873	10.721	13.226	15.365	14.646
d(T)	-0.013	-0.045	-0.052	-0.020	0.039	0.096	0.131	0.148	0.169	0.190	0.204
e(T)	0.278	0.232	0.238	0.301	0.363	0.376	0.380	0.367	0.325	0.317	0.302
10f(T)	1.348	1.424	1.516	1.596	1.567	1.445	1.504	1.833	2.332	2.773	2.565
1000g(T)	-0.956	-1.026	-1.128	-0.964	-0.579	-0.287	-0.362	-0.754	-1.070	-0.999	-0.691
α(T)	0.782	0.858	0.952	1.104	1.289	1.537	1.755	2.085	2.704	3.941	4.055
β(T)	1.339	1.194	1.034	0.832	0.608	0.292	0.003	-0.453	-1.252	-2.566	-2.581
N(T)	162	96	57	33	20	11	7	4	2	1	1

ζ = 0.20

a(T)	-0.987	-1.016	-1.022	-1.027	-1.068	-1.136	-1.174	-1.188	-1.252	-1.373	-1.482
b(T)	-1.039	-1.189	-1.307	-1.356	-1.341	-1.253	-1.308	-1.732	-2.431	-2.924	-2.612
c(T)	6.887	7.336	7.594	7.699	7.775	7.811	8.370	10.046	12.586	14.477	13.747
d(T)	-0.014	-0.034	-0.037	-0.012	0.035	0.084	0.116	0.132	0.150	0.166	0.170
e(T)	0.288	0.252	0.264	0.317	0.368	0.388	0.393	0.374	0.352	0.370	0.356
10f(T)	1.280	1.413	1.519	1.547	1.504	1.382	1.375	1.689	2.231	2.617	2.390
1000g(T)	-0.941	-0.974	-1.014	-0.879	-0.575	-0.310	-0.321	-0.609	-0.889	-0.866	-0.601
α(T)	0.787	0.867	0.968	1.114	1.292	1.539	1.759	2.096	2.772	4.079	4.200
β(T)	1.334	1.191	1.030	0.828	0.604	0.289	-0.004	-0.458	-1.268	-2.613	-2.673
N(T)	162	96	57	33	20	11	7	4	2	1	1

---

* See section entitled "Distribution of Spectral Amplitudes for Definition of α(T), β(T) and N(T).

b(T), ..., f(T) and g(T) for ζ = 0.0, 0.02, 0.05, 0.10 and 0.20 have been smoothed by low-pass filtering the data with an Ormsby filter along the $\log_{10}$T axis.

For fixed T, p, s, v and R, $\log_{10}\left[SA(T),_p\right] - M - \log_{10}A_o(R)$ represents a parabola when plotted versus M. The particular choice of a parabola in equation (1) has no physical significance since the functional growth of spectral amplitudes with M is not known at this time. Our choice is based on our previous work which dealt with peaks of strong ground motion (Trifunac, 1976a), with the Fourier amplitude spectra (Trifunac, 1976b), by the simplicity of its functional form and by the observation that the local amplitudes of near-field strong ground motion, for the limited range of periods considered in this analysis (T < 15 sec), seem to cease to grow appreciably with an increase in M for large earthquakes (Trifunac, 1973). Thus, by employing the approximate model which is defined by equation (1), and after the coefficients a(T), b(T), ..., f(T) and g(T) have been determined by regression, we assume that $\log_{10}\left[SA(T),_p\right]$ grows linearly with M up to some magnitude $M_{min} = -b(T)/2f(T)$. Above M_{min}, $\log_{10}\left[SA(T),_p\right]$ still grows with M but with a slope which is less than 1 unit until the maximum is reached at $M_{max} = [1 - b(T)]/2f(T)$. For magnitudes greater than M_{max} we assume that the amplitude of $\log_{10}\left[SA(T),_p\right]$ remains constant and equal to its value for $M = M_{max}$. With these arbitrary restrictions, equation (1) becomes

$$\log_{10}A_o(R) - \log_{10}\left[SA(T),_p\right] =$$

$$\begin{cases} -M_{max} + a(T)p + b(T)M_{max} + c(T) + d(T)s + e(T)v + f(T)M_{max}^2 + g(T)R & \text{for } M \geq M_{max} \\ -M + a(T)p + b(T)M + c(T) + d(T)s + e(T)v + f(T)M^2 + f(T)R & \text{for } M_{min} \leq M \leq M_{max} \\ -M + a(T)p + b(T)M_{min} + c(T) + d(T)s + e(T)v + f(T)M_{min}^2 + g(T)R & \text{for } M \leq M_{min} \end{cases} \quad (3)$$

Table VI presents the values and definitions of M_{min} and M_{max} for eleven selected periods which range from 0.04 to 7.5 seconds. As may be seen from this table and from Figure 7, this analysis suggests that $\log_{10}\left[SA(T),_p\right]$ may cease to grow linearly with M for earthquakes between M = 4 and M = 5.5 and that it perhaps reaches its maxima for magnitudes ranging from about M = 7.5 to about M = 8.5. These estimates of M_{min} and M_{max} are more reliable for periods, T, which are not close to the left and right limits of the T-interval considered in this study, because M_{min} and M_{max} depend on smoothed amplitudes of b(T) and f(T) which tend to be distorted in the vicinity of the left and right ends by the process of digital filtering. The range of estimates for M_{min} and M_{max} can, of course, only be taken as tentative, since there is not an adequate number of recordings for M greater than 7 and less than 5. Furthermore, our fitting procedure treats all events as if they have magnitudes between M_{min} and M_{max}; thus, if the assumed shape is reasonable, events outside that region which is quadratic in M will lead to distorted estimates of the parameters.

The range of values for M_{min} and M_{max} in Table VI is in fair agreement with similar estimates of M_{min} and M_{max} in the related analysis of the dependence of peak acceleration, peak velocity and peak displacement on magnitude (Trifunac, 1976a), and with the analysis of Fourier amplitude spectra (Trifunac, 1976b). This agreement, however, only shows that there is consistency of interpretation between these two similar models in the study of different characteristics of the same data, but it does not provide an independent support for the

TABLE VI

M_{min} and M_{max} Estimated from the Regression

Based on Equation (1)

Period T, sec	$\zeta = 0.0$		$\zeta = 0.02$		$\zeta = 0.05$		$\zeta = 0.10$		$\zeta = 0.20$	
	M_{min}^{*}	M_{max}^{**}	M_{min}	M_{max}	M_{min}	M_{max}	M_{min}	M_{max}	M_{min}	M_{max}
0.04	3.89	8.19	4.14	7.71	4.15	7.76	4.12	7.83	4.06	7.96
0.07	4.27	8.00	4.15	7.70	4.24	7.65	4.20	7.71	4.21	7.75
0.11	4.51	7.85	4.31	7.59	4.33	7.54	4.28	7.58	4.30	7.59
0.19	4.62	7.88	4.55	7.51	4.46	7.51	4.41	7.54	4.38	7.61
0.32	4.61	8.11	4.63	7.68	4.56	7.67	4.51	7.70	4.46	7.78
0.55	4.66	8.40	4.65	8.15	4.61	8.10	4.62	8.08	4.53	8.15
0.92	5.06	8.28	4.97	8.32	4.92	8.31	4.92	8.25	4.76	8.39
1.56	5.50	7.97	5.41	8.00	5.35	7.98	5.28	8.01	5.13	8.09
2.63	5.70	7.78	5.67	7.72	5.64	7.69	5.57	7.71	5.45	7.69
4.45	5.66	7.62	5.73	7.55	5.73	7.53	5.70	7.50	5.59	7.50
7.50	5.40	7.64	5.51	7.58	5.54	7.58	5.57	7.52	5.46	7.56

* $M_{min} = \frac{-b(T)}{2f(T)}$

** $M_{max} = \frac{1-b(T)}{2f(T)}$

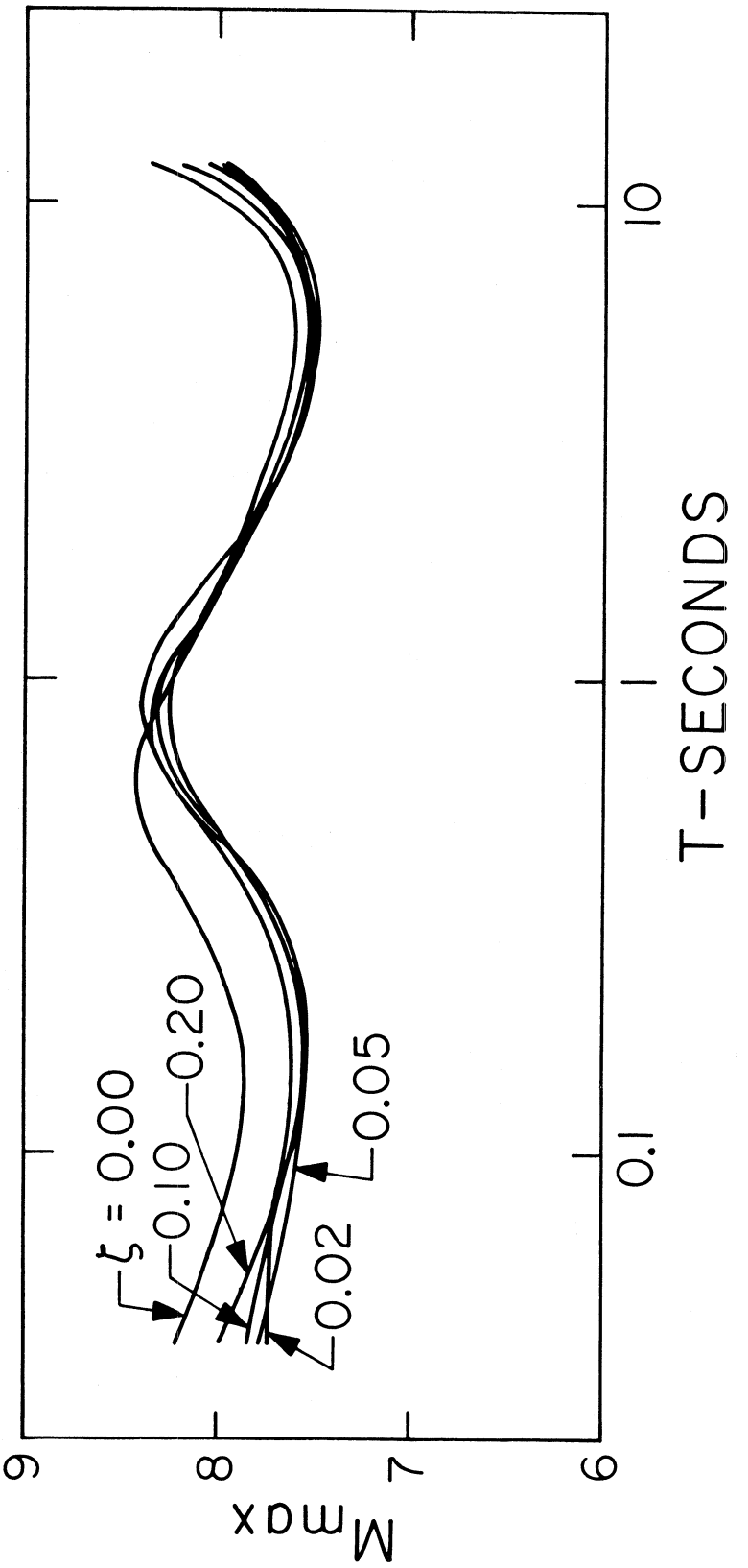

FIGURE 7

choice of these models or for the analysis which is based on these models. We are presenting the estimates of M_{min} and M_{max} in this report and discussing their possible physical meaning as it may relate to our present understanding of the earthquake source mechanism to show that the regression analysis in this report does not lead to unreasonable inferences when applied outside the range for which the data are now available. The final test, as well as the improvement of the model, can only come from numerous recordings of representative strong-motion records in the future.

The confidence level function a(T) decreases from about -1.0 for short periods to about -1.6 at periods of about 10.0 sec. This means that the spread of spectral amplitudes about the mean level is smallest close to the short periods equal to 0.04 sec and that it grows for longer periods to reach its maximum for $T \approx 10$ sec. The numerical values of a(T) are comparable to the corresponding coefficients in similar correlations of peak acceleration ($a \approx -0.9$), peak velocity ($a \approx -1.1$), and peak displacement ($a \approx -1.3$) (Trifunac, 1976a). This is as one might expect, since the peak acceleration is approached by the amplitudes of SA for $T \to 0$.

The amplitudes of the site dependent function d(T) are negative for periods shorter than about 0.2 sec. This means that the spectral amplitudes are, on the linear scale, up to about 20% greater at basement rock sites (s = 2) than on alluvium (s = 0). For periods greater than 0.2 sec d(T) becomes positive and reaches a nearly constant level equal to about 0.2 for periods greater than 1.0 sec. For these long periods equation (1) indicates that the spectral amplitudes

recorded on alluvium (s = 0) are on the average about 2.5 times greater than the average spectral amplitudes recorded on basement rock sites (s = 2). It is interesting to observe that the corresponding d coefficients for peak displacements (Trifunac, 1976a) and Fourier spectrum amplitudes (Trifunac, 1976b) are 0.2 as well.

In the high frequency range d(T) is slightly negative ($-0.06 \lesssim d(T) \lesssim -0.02$). This compares favorably with Trifunac (1976a), who found d to be 0.06 in the regression of peak acceleration. This confirms the observation that currently available data on peak accelerations when correlated with M and Δ is not very sensitive to site conditions.

Function e(T) in Figure 6 shows that for frequencies greater than about 5 cps, the amplitudes of SA spectra of vertical acceleration and for small ζ approach the corresponding SA amplitudes of horizontal accelerations. The amplitudes of e(T) for periods longer than about 0.2 sec are farily consistent with similar estimates of coefficient e for peak velocity ($e \approx 0.34$), and peak displacement ($e \approx 0.24$) (Trifunac, 1976a).

The amplitudes of g(T) are small and vary from about -0.0003 to about -0.0012 throughout the period range from 0.04 sec to 12 sec (Figure 6). This means that for a typical distance, say R = 100 km, the correction term g(T)R in equation (1) contributes at most 0.12 on the logarithmic scale, i.e., by a factor of 1.3 on the linear amplitude scale. Considering the spread of spectral amplitudes for a fixed set of parameters and the values of a(T), it appears that g(T)R represents only a minor correction to the overall average scaling of amplitudes versus distance in terms of $\log_{10} A_o(R)$ function. Therefore,

$\log_{10}A_o(R)$ + R/1000 would represent a good approximation for scaling SA amplitudes for all periods between 0.04 and 12 seconds.

b. Characteristics of the Model

Figures 8 through 17 show the SA spectra for horizontal and vertical ground motion at R = 0, for magnitudes M = 4.5, 5.5, 6.5, 7.5 and 8.5, for the approximate linearized 50 percent confidence level (p = 0.50) and for ζ = 0.0, 0.02, 0.05, 0.10 and 0.20. The average and the average plus one standard deviation of the smoothed spectra that would result from digitization noise and for the record durations equal to 15, 30, 60 and 100 seconds are also shown. The shape of the digitization noise spectra depends on damping as well as duration.

Formally, equation (1) implies that the spectra SA(T) computed at R = 0 represent the maximum spectral amplitudes for all other parameters held constant. Since an adequate number of SA spectra computed from recorded strong-motion accelerograms is available only for a distance range between about 20 km and 250 km and because the $\log_{10}A_o(R)$ curve may not be the best representation for the amplitude variation with distance for R less than about 10 to 20 km for all magnitudes (e.g., Trifunac, 1976a, b), the spectra in Figures 8 through 17 only represent extrapolations based on equation (1) and at this time cannot be tested by the recorded strong-motion data. However, because the g(T)R term contributes a negligible amount to spectral amplitudes at distances less than 20 km, the shape of the SA spectra at say R = 20 km and at R = 0 km is very similar. Because in previous discussions we examined some spectral characteristics at R = 0 km (Trifunac, 1976a,

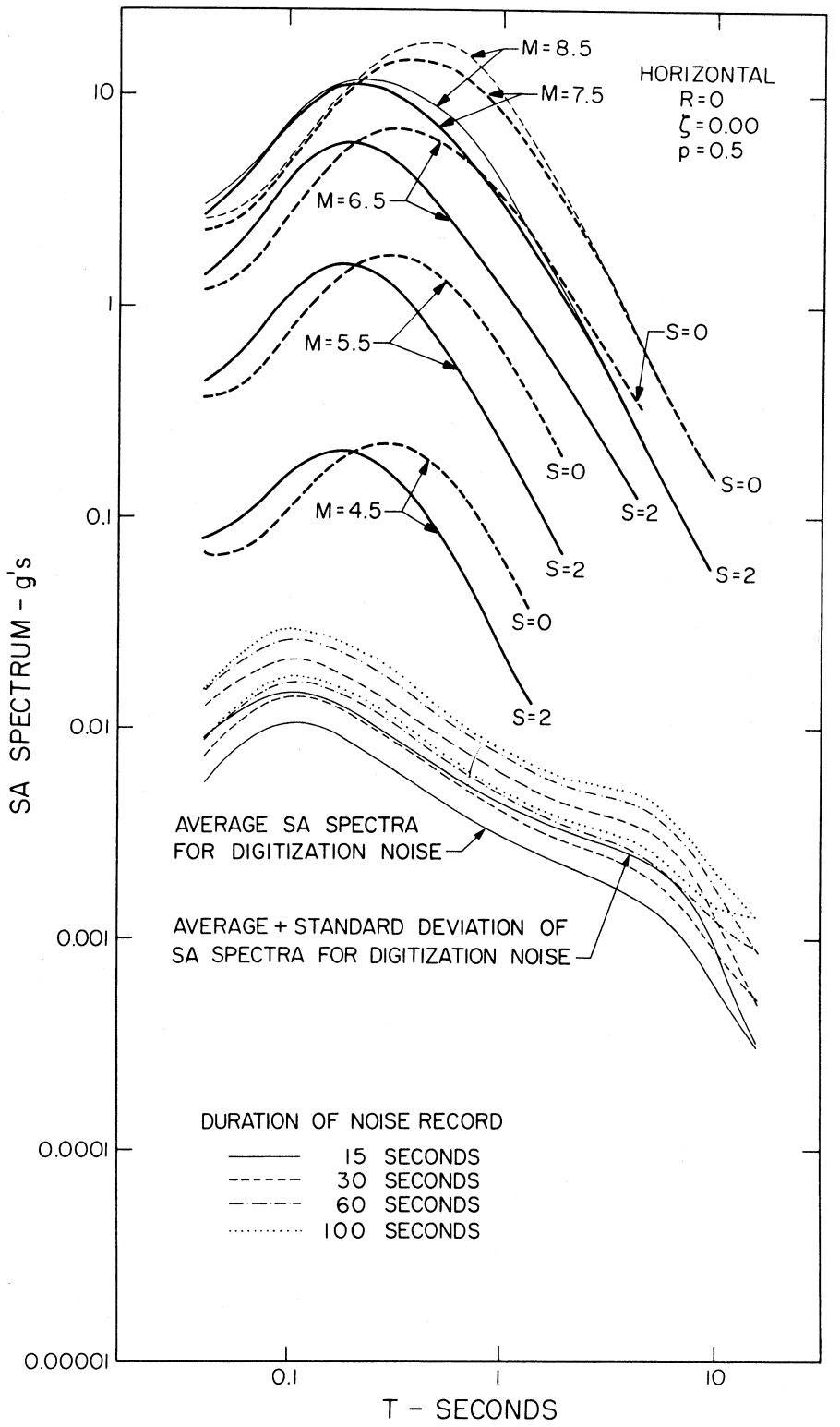
M=8.5
M=7.5
M=6.5
M=5.5
M=4.5
HORIZONTAL
R=0
ζ=0.00
p=0.5
S=0
S=2
AVERAGE SA SPECTRA
FOR DIGITIZATION NOISE
AVERAGE + STANDARD DEVIATION OF
SA SPECTRA FOR DIGITIZATION NOISE
DURATION OF NOISE RECORD
15 SECONDS
30 SECONDS
60 SECONDS
100 SECONDS
SA SPECTRUM - g's
T - SECONDS
10
1
0.1
0.01
0.001
0.0001
0.00001
0.1
1
10

FIGURE 8

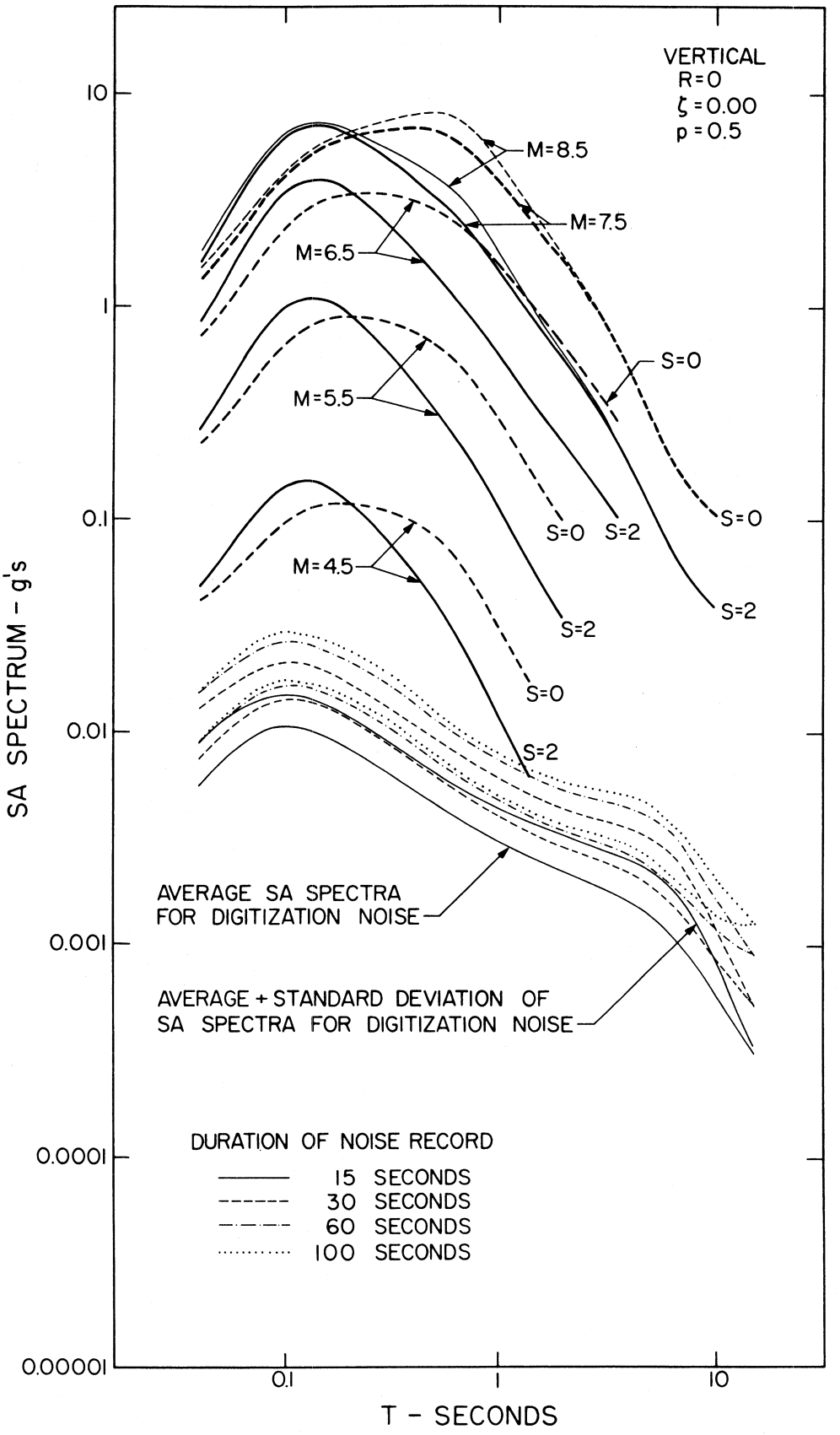
VERTICAL
R=0
ζ=0.00
p=0.5
M=8.5
M=7.5
M=6.5
M=5.5
M=4.5
S=0
S=2
AVERAGE SA SPECTRA FOR DIGITIZATION NOISE
AVERAGE + STANDARD DEVIATION OF SA SPECTRA FOR DIGITIZATION NOISE
DURATION OF NOISE RECORD
15 SECONDS
30 SECONDS
60 SECONDS
100 SECONDS
SA SPECTRUM - g's
T - SECONDS
10
1
0.1
0.01
0.001
0.0001
0.00001
0.1
1
10

FIGURE 9

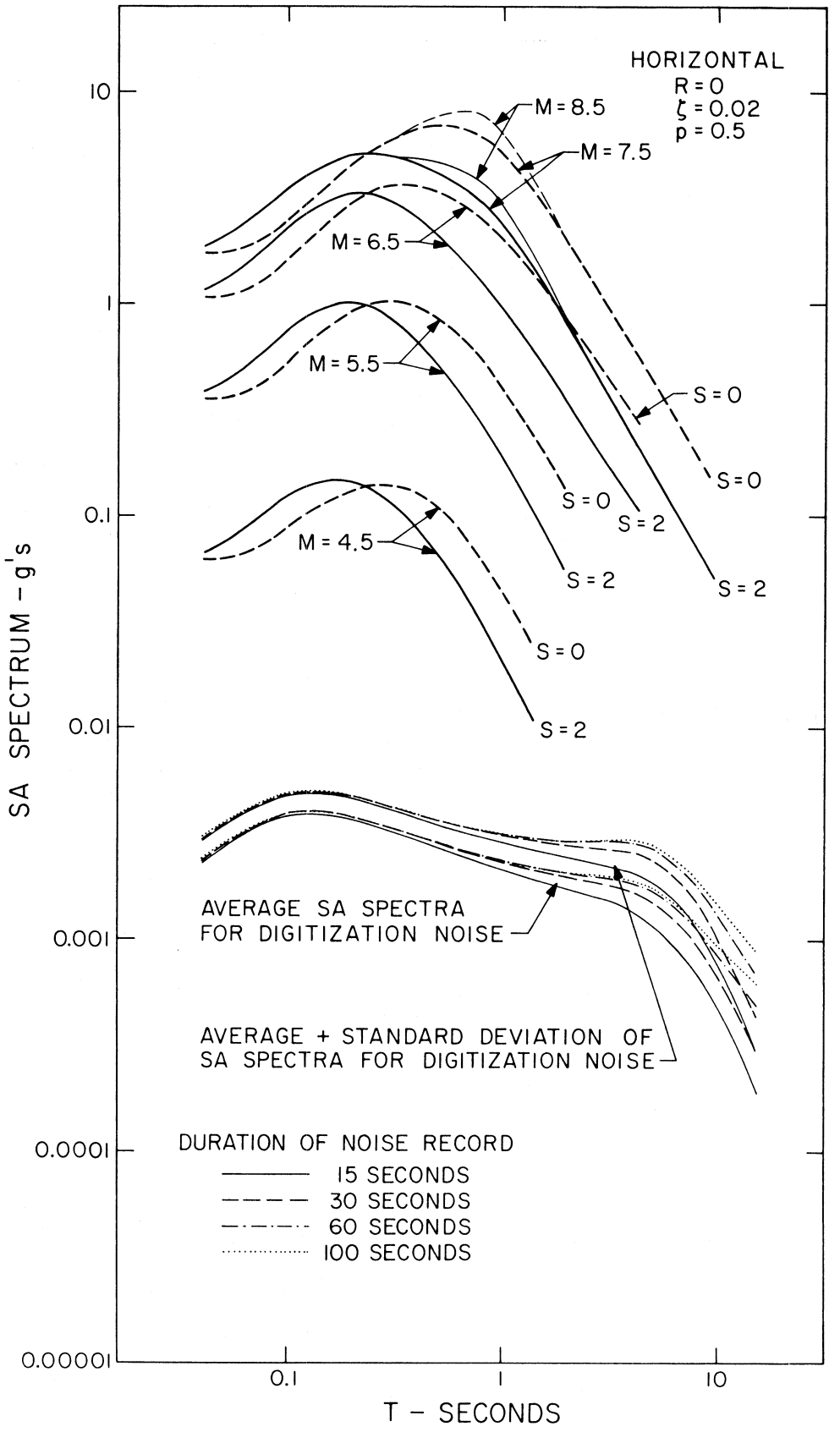
HORIZONTAL
R = 0
ζ = 0.02
p = 0.5
M = 8.5
M = 7.5
M = 6.5
M = 5.5
M = 4.5
S = 0
S = 2
AVERAGE SA SPECTRA
FOR DIGITIZATION NOISE
AVERAGE + STANDARD DEVIATION OF
SA SPECTRA FOR DIGITIZATION NOISE
DURATION OF NOISE RECORD
15 SECONDS
30 SECONDS
60 SECONDS
100 SECONDS
SA SPECTRUM - g's
T - SECONDS
10
1
0.1
0.01
0.001
0.0001
0.00001
0.1
1
10

FIGURE 10

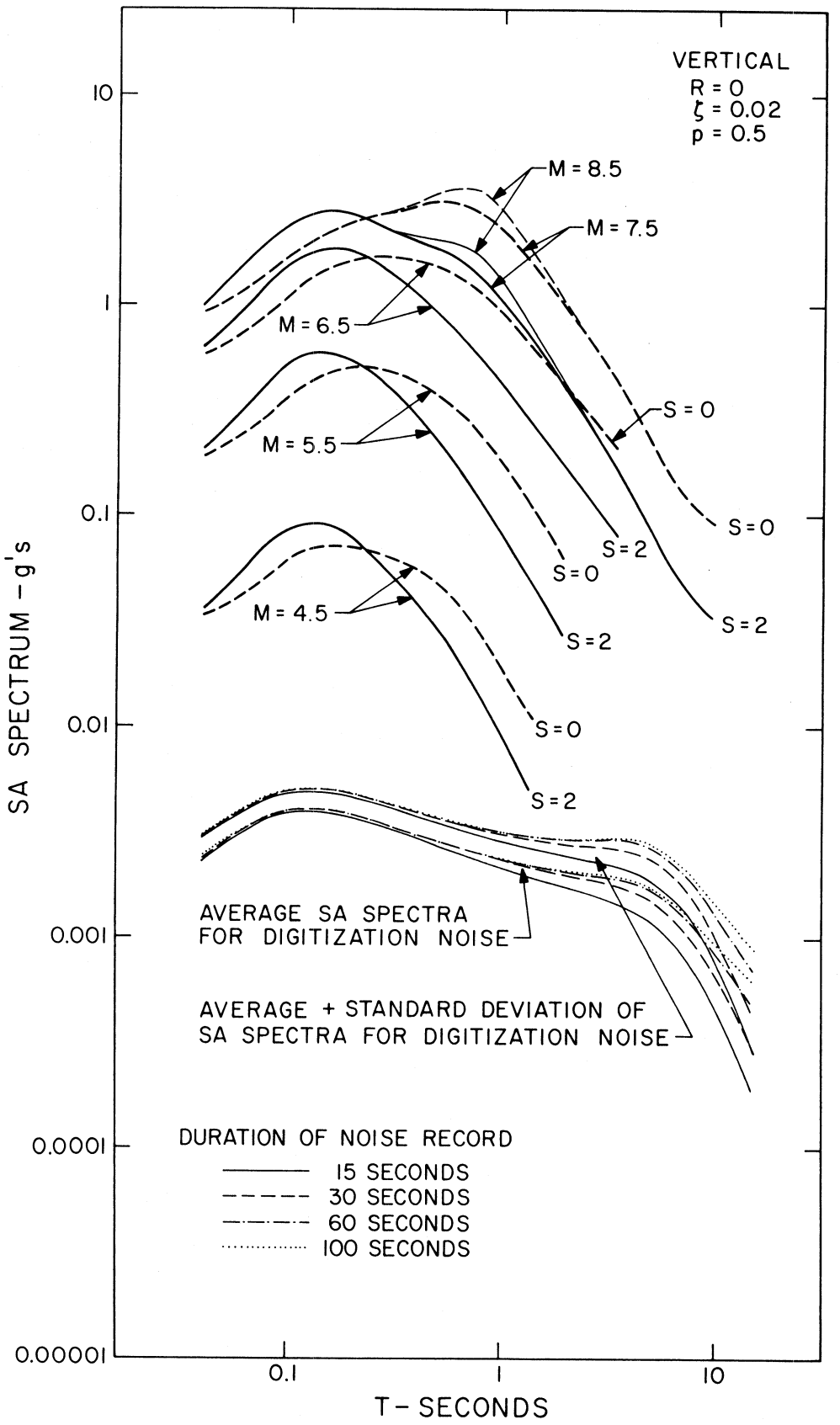
VERTICAL
R = 0
ζ = 0.02
p = 0.5
M = 8.5
M = 7.5
M = 6.5
M = 5.5
M = 4.5
S = 0
S = 2
AVERAGE SA SPECTRA FOR DIGITIZATION NOISE
AVERAGE + STANDARD DEVIATION OF SA SPECTRA FOR DIGITIZATION NOISE
DURATION OF NOISE RECORD
15 SECONDS
30 SECONDS
60 SECONDS
100 SECONDS
SA SPECTRUM - g's
T - SECONDS
10
1
0.1
0.01
0.001
0.0001
0.00001
0.1
1
10

FIGURE 11

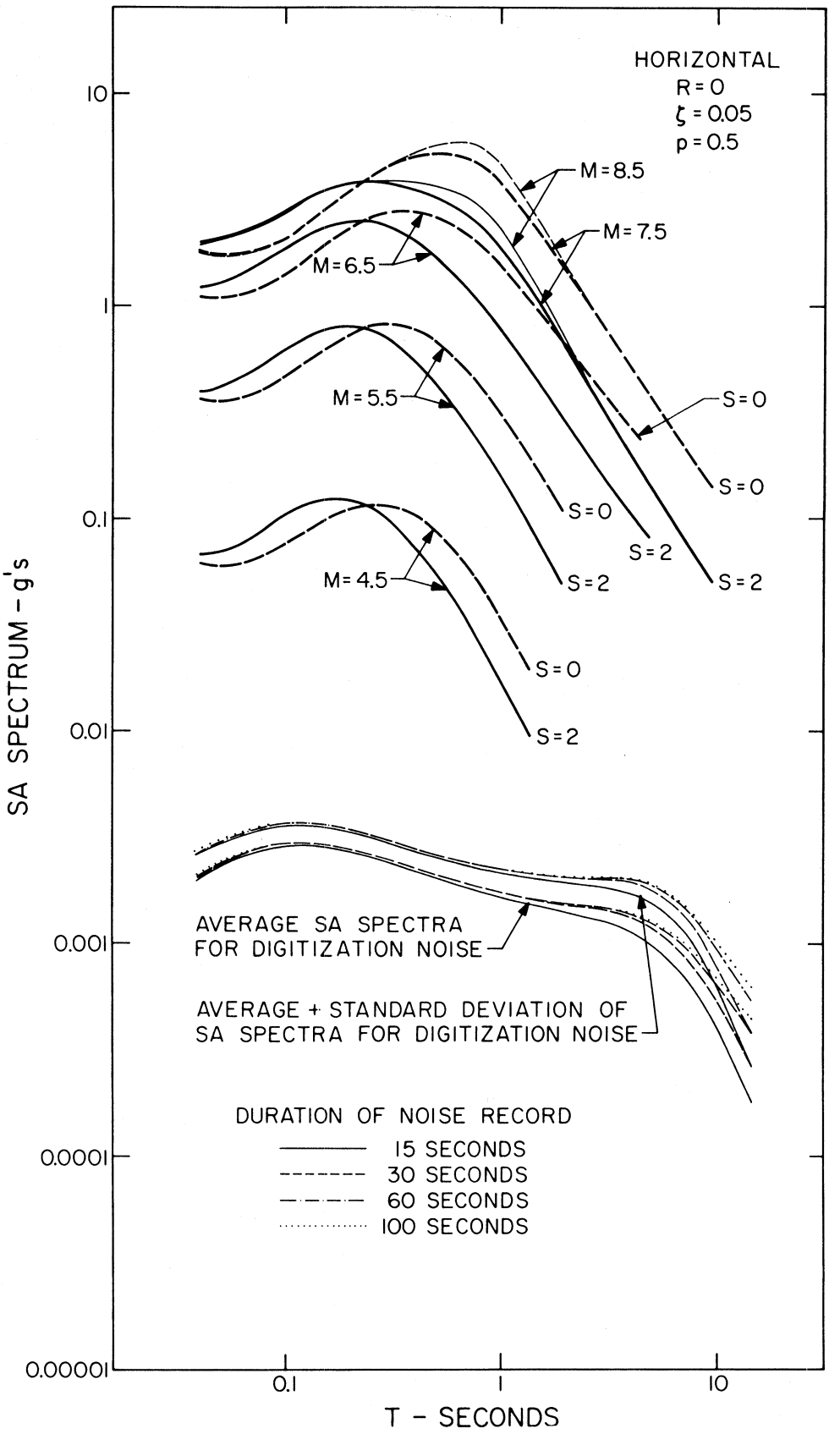
HORIZONTAL
R = 0
ζ = 0.05
p = 0.5
M = 8.5
M = 7.5
M = 6.5
M = 5.5
M = 4.5
S = 0
S = 2
AVERAGE SA SPECTRA
FOR DIGITIZATION NOISE
AVERAGE + STANDARD DEVIATION OF
SA SPECTRA FOR DIGITIZATION NOISE
DURATION OF NOISE RECORD
15 SECONDS
30 SECONDS
60 SECONDS
100 SECONDS
SA SPECTRUM - g's
10
1
0.1
0.01
0.001
0.0001
0.00001
0.1
1
10
T - SECONDS

FIGURE 12

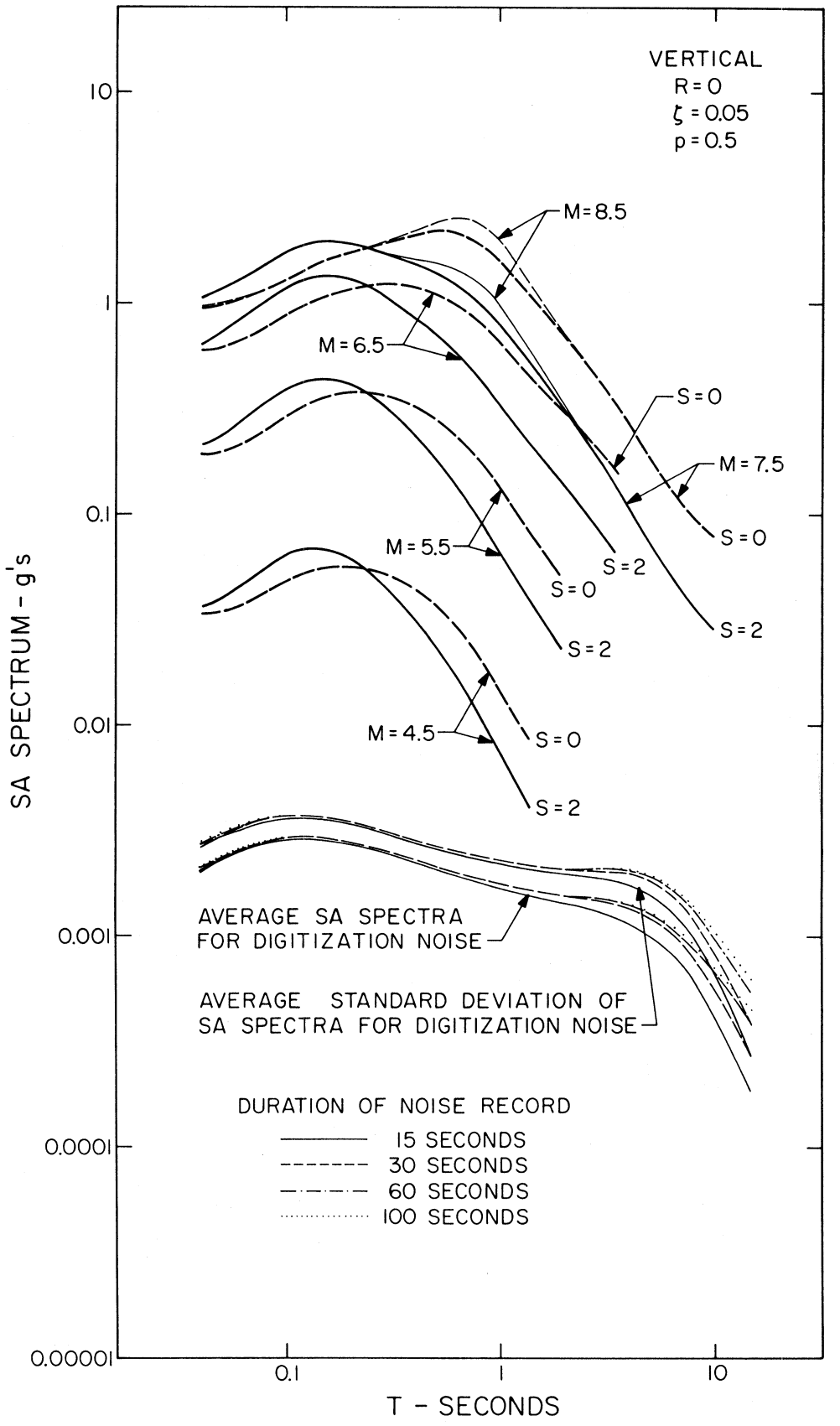
VERTICAL
R = 0
ζ = 0.05
p = 0.5
M=8.5
M=6.5
S=0
M=7.5
S=0
M=5.5
S=2
S=0
S=2
S=2
M=4.5
S=0
S=2
AVERAGE SA SPECTRA
FOR DIGITIZATION NOISE
AVERAGE STANDARD DEVIATION OF
SA SPECTRA FOR DIGITIZATION NOISE
DURATION OF NOISE RECORD
15 SECONDS
30 SECONDS
60 SECONDS
100 SECONDS
SA SPECTRUM - g's
10
1
0.1
0.01
0.001
0.0001
0.00001
0.1
1
10
T - SECONDS

FIGURE 13

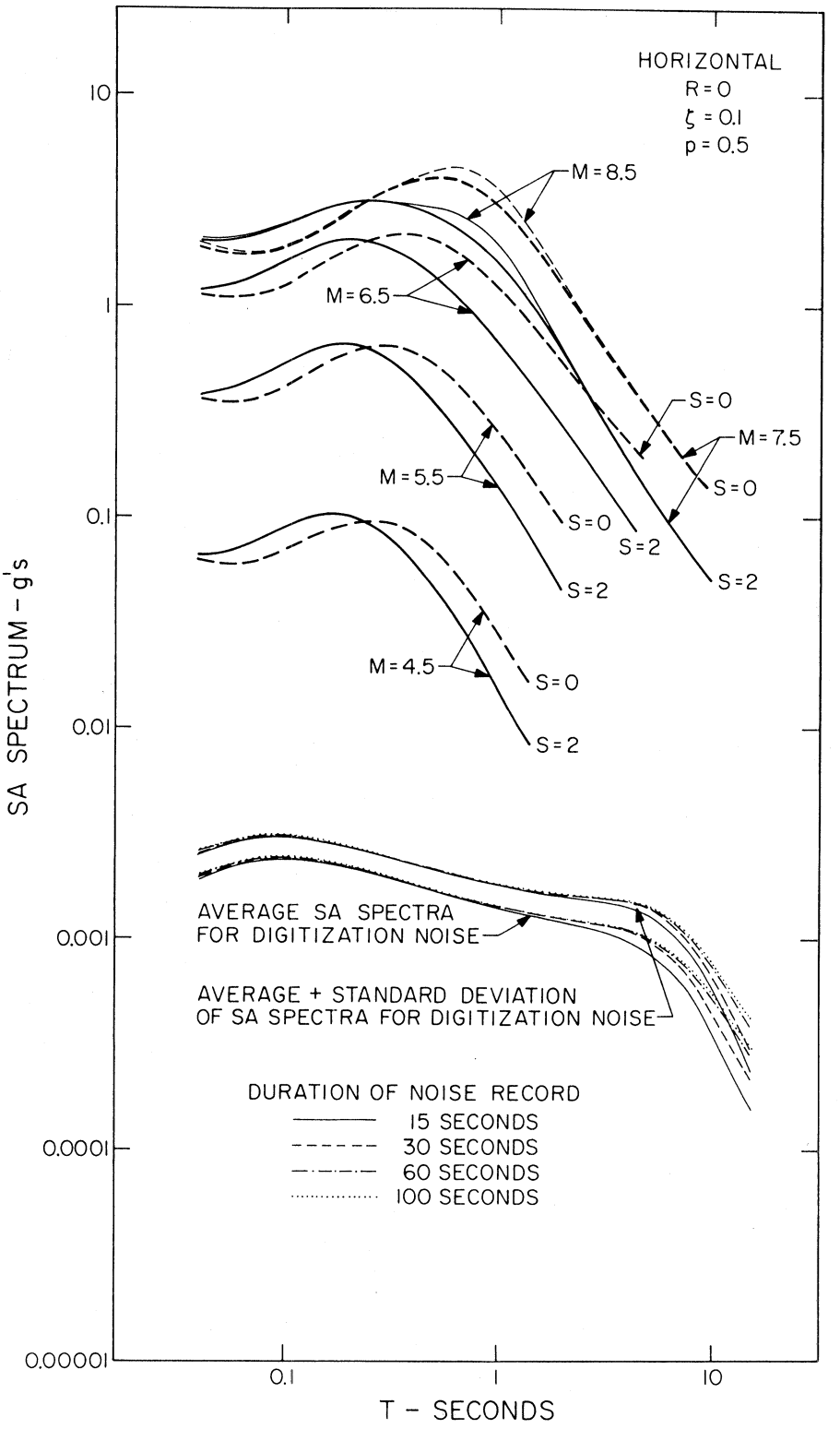
HORIZONTAL
R = 0
ζ = 0.1
p = 0.5
M = 8.5
M = 6.5
M = 5.5
M = 4.5
M = 7.5
S = 0
S = 2
AVERAGE SA SPECTRA
FOR DIGITIZATION NOISE
AVERAGE + STANDARD DEVIATION
OF SA SPECTRA FOR DIGITIZATION NOISE
DURATION OF NOISE RECORD
15 SECONDS
30 SECONDS
60 SECONDS
100 SECONDS
SA SPECTRUM - g's
T - SECONDS
10
1
0.1
0.01
0.001
0.0001
0.00001
0.1
1
10

FIGURE 14

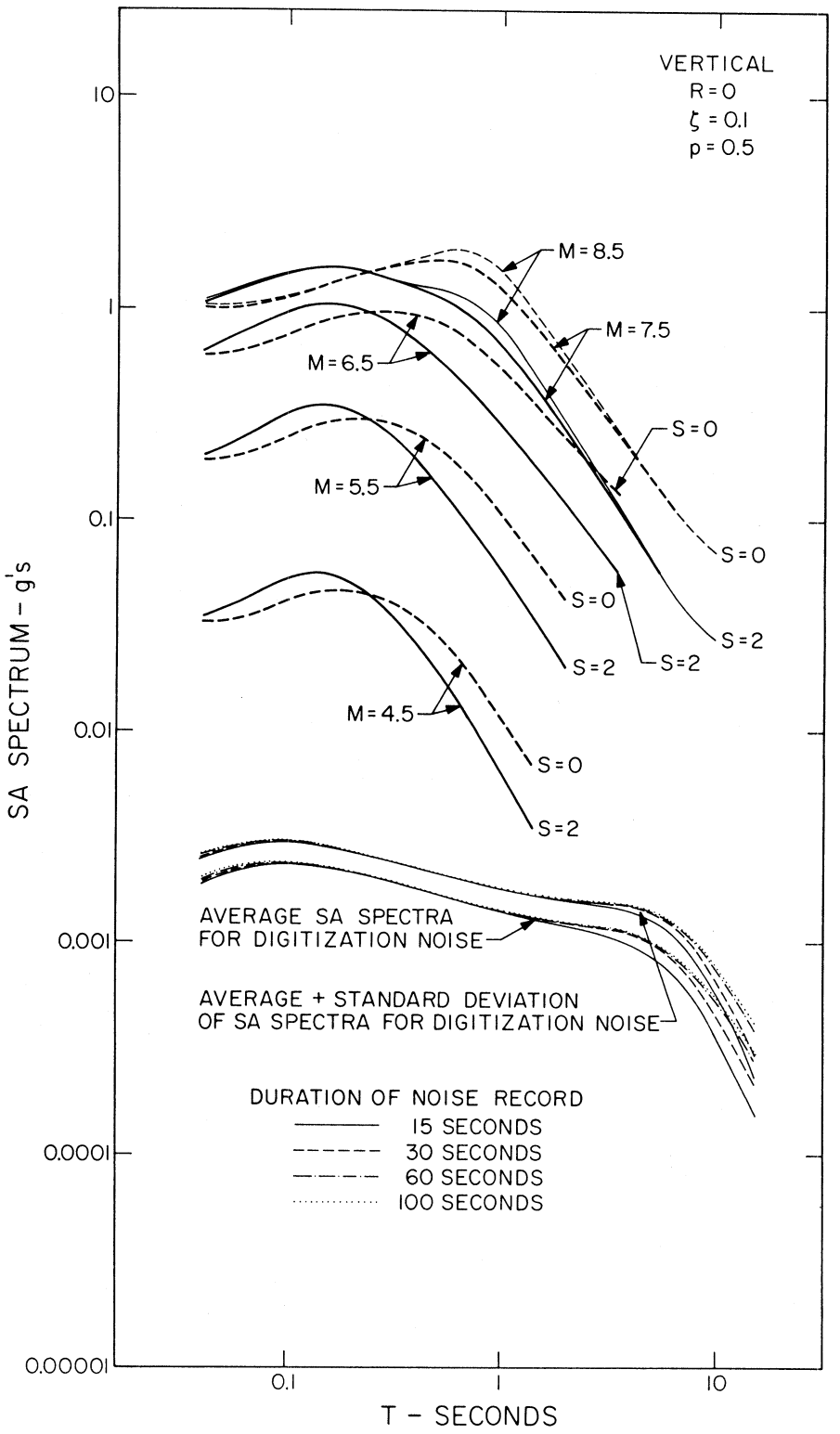
VERTICAL
R = 0
ζ = 0.1
p = 0.5
M = 8.5
M = 7.5
M = 6.5
M = 5.5
M = 4.5
S = 0
S = 2
AVERAGE SA SPECTRA
FOR DIGITIZATION NOISE
AVERAGE + STANDARD DEVIATION
OF SA SPECTRA FOR DIGITIZATION NOISE
DURATION OF NOISE RECORD
15 SECONDS
30 SECONDS
60 SECONDS
100 SECONDS
SA SPECTRUM - g's
T - SECONDS
10
1
0.1
0.01
0.001
0.0001
0.00001
0.1
1
10

FIGURE 15

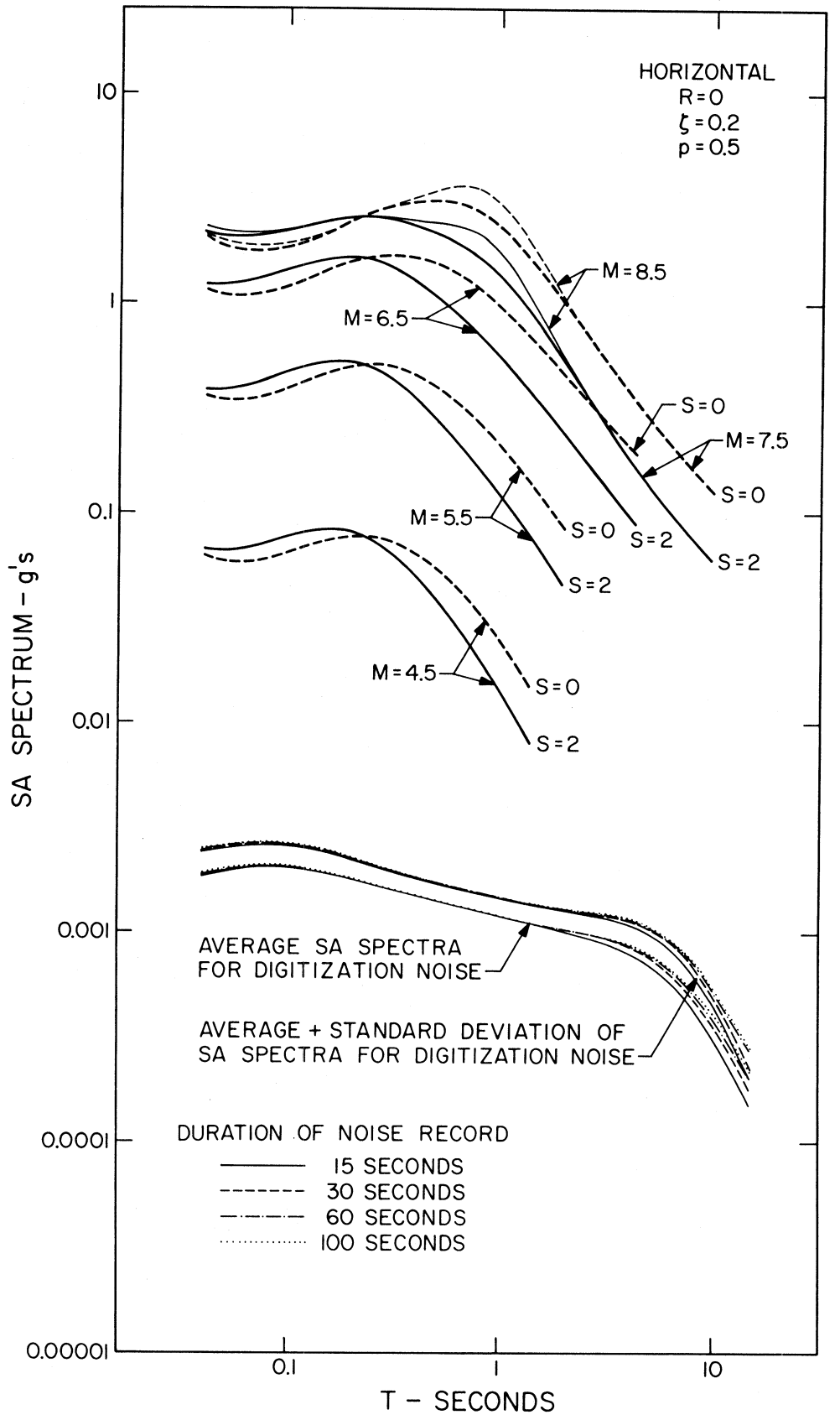
HORIZONTAL
R=0
ζ=0.2
p=0.5
M=8.5
M=6.5
S=0
M=7.5
S=0
M=5.5
S=0
S=2
S=2
S=2
M=4.5
S=0
S=2
AVERAGE SA SPECTRA
FOR DIGITIZATION NOISE
AVERAGE + STANDARD DEVIATION OF
SA SPECTRA FOR DIGITIZATION NOISE
DURATION OF NOISE RECORD
15 SECONDS
30 SECONDS
60 SECONDS
100 SECONDS
SA SPECTRUM - g's
10
1
0.1
0.01
0.001
0.0001
0.00001
0.1
1
10
T - SECONDS

FIGURE 16

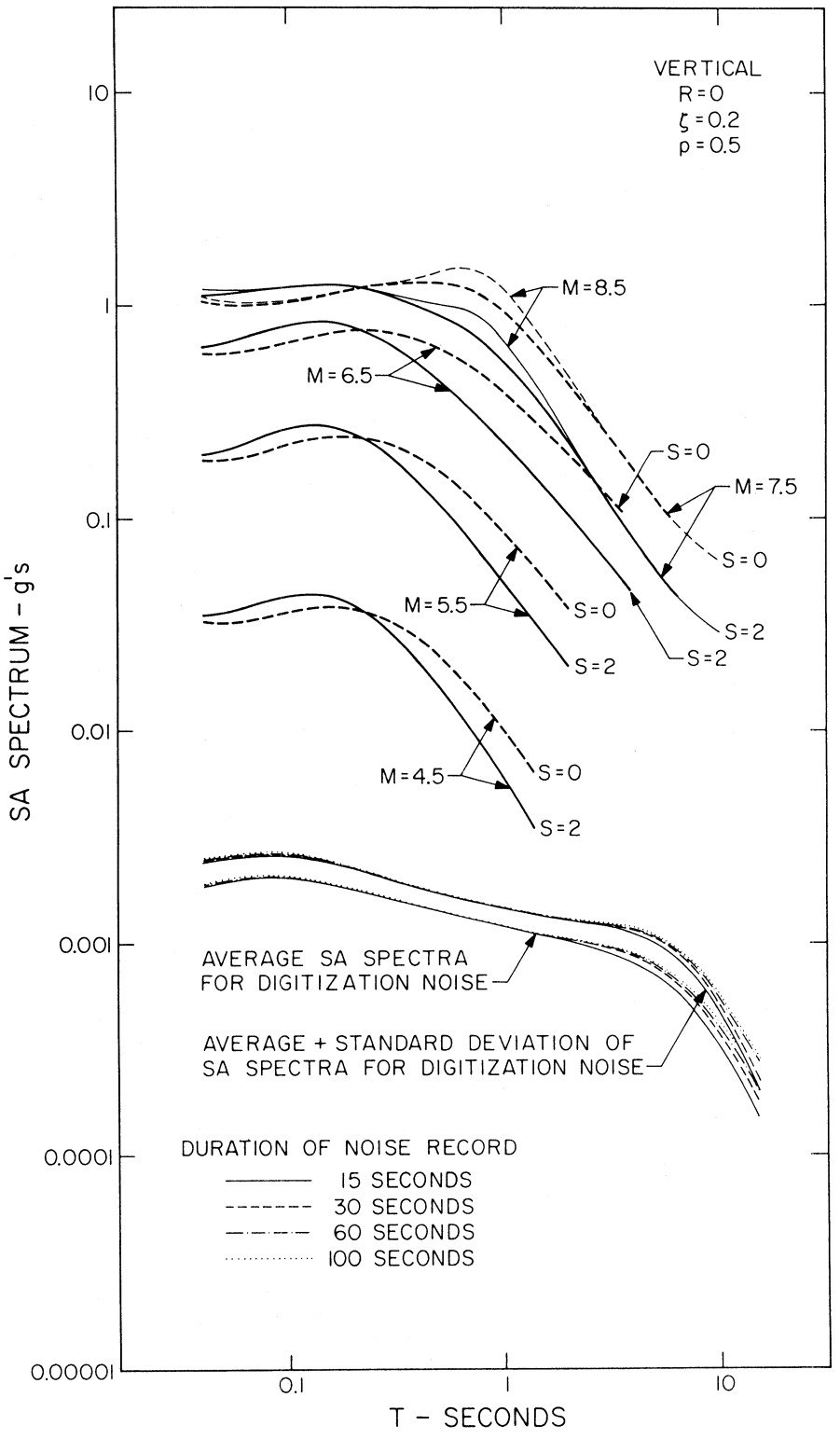
VERTICAL
R=0
ζ=0.2
ρ=0.5
M=8.5
M=6.5
M=7.5
M=5.5
M=4.5
S=0
S=2
AVERAGE SA SPECTRA
FOR DIGITIZATION NOISE
AVERAGE + STANDARD DEVIATION OF
SA SPECTRA FOR DIGITIZATION NOISE
DURATION OF NOISE RECORD
15 SECONDS
30 SECONDS
60 SECONDS
100 SECONDS
SA SPECTRUM - g's
T - SECONDS
10
1
0.1
0.01
0.001
0.0001
0.00001
0.1
1
10

FIGURE 17

b), which are based on the properties of shallow and surface earthquake sources, to enable comparison and consistency checks we chose to present the spectra in Figures 8 through 17 for epicentral distance R = 0.

The expected value of the SA spectrum amplitudes computed from digitization noise (Figures 8 through 17) had been subtracted from the SA amplitude spectra of the digitized accelerograms before the regression analysis was carried out. However, because this noise subtraction scheme is approximate, it does not eliminate all the long period errors in the computed absolute acceleration spectra (Trifunac et al., 1973). Furthermore, to maintain as many spectra as possible for all periods which were considered in the regression analysis, we did not eliminate all those spectral amplitudes that were characterized by low signal-to-noise ratio. The consequence of this has been that the functions b(T), c(T) and f(T) still reflect considerable noise content in the raw data for periods longer than 1 to 2 seconds for magnitudes close to 4.5 and for periods longer than 6 to 8 seconds for magnitudes close to 7.5. Thus, the spectra that would be obtained from equation (1) are not accurate for the periods and magnitudes greater than those just indicated. This limitation is also reflected in some of the Figures 8 through 17 where we terminated the spectra in this long period range. The long period cut-off points in those figures have been selected at periods where spectra computed from equation (1) begin to deviate appreciably from a constant slope and start to approach a constant level.

Further corrections and improvements of the functions a(T), c(T)

and f(T) so that they do not depend on contributions from processing and digitization noise, are, of course, possible. One possible procedure would be to apply an optimum band-pass filter for each of the 546 accelerograms used in this study. The filter could be designed in such a way that only selected frequency bands remain so that all data have better than some predetermined signal-to-noise ratio. However, we did not carry out such correction procedures in this work because many data points would have been eliminated from an analysis that already has only a marginal number of representative accelerograms. Furthermore, such correction procedures would require separate extensive and costly analysis of each accelerogram and would only contribute to better accuracy of b(T), c(T) and f(T) in the frequency range where the overall trends of spectral amplitudes may be inferred from other theoretical and/or observational analyses (Trifunac, 1976b). For these reasons, it was decided to postpone this noise elimination scheme for a later time when more strong-motion accelerograms become available.

In the short period range for small magnitudes (Figures 8 through 17) the signal-to-noise ratio also becomes small. However, because the strong-motion data for all recordings employed in this paper are proportional to acceleration, the noise and the recorded spectra tend to be roughly parallel in the high-frequency range so that poor signal accuracy can be expected only for small and/or distant earthquakes and for very high frequencies. Therefore, the high-frequency noise contributions to digitized accelerograms represent less of a problem than the long period noise.

As it can be seen from equation (1), the terms $\log_{10}A_o(R)$ and $g(T)R$ govern the changes of SA amplitudes with distance. The term $\log_{10}A_o(R)$ leads to overall amplitude variations which are frequency independent, while the term $g(T)R$ is negative for all frequencies ($f = 1/T$), and acts to increase SA(T) amplitudes with distance. Because, on the whole, the absolute value of g(T) is smaller for intermediate-frequencies and larger for high and low-frequencies, the net effect of $g(T)R$ is to attenuate the intermediate-frequency waves somewhat faster than the high and low-frequency waves.

Figures 8 through 17 show SA spectra for M = 4.5, 5.5, 6.5, and 7.5 plotted with heavy lines and the spectra for M = 8.5 plotted with light lines. This was done to emphasize that the spectra for M = 8.5 are well beyond the magnitude range for which the data is currently available and thus represent extrapolations based on equation (1). Though all our previous work (e.g., Trifunac, 1976a, b) also suggests that the spectral amplitudes should cease to grow for M in the range from 6.5 to 7.5 the check on the validity of this extrapolation must await the critical tests in terms of actual strong motion data.

Equation (1) can be utilized to study the relationships between the fixed shape spectra shown in Figures 1, 2, 3 and 4 and the spectra which depend on M, R, s, v and p. A convenient format for such a comparison consists of forming [normalized SA(T)] = SA(T)/SA(0.04). Such normalization is approximately equivalent to normalizing all SA spectra by the respective peak accelerations prior to carrying out the regression analysis for a(T), b(T), ..., and g(T). The shape of the resulting spectra would, of course, still depend on M, R, s, v and p.

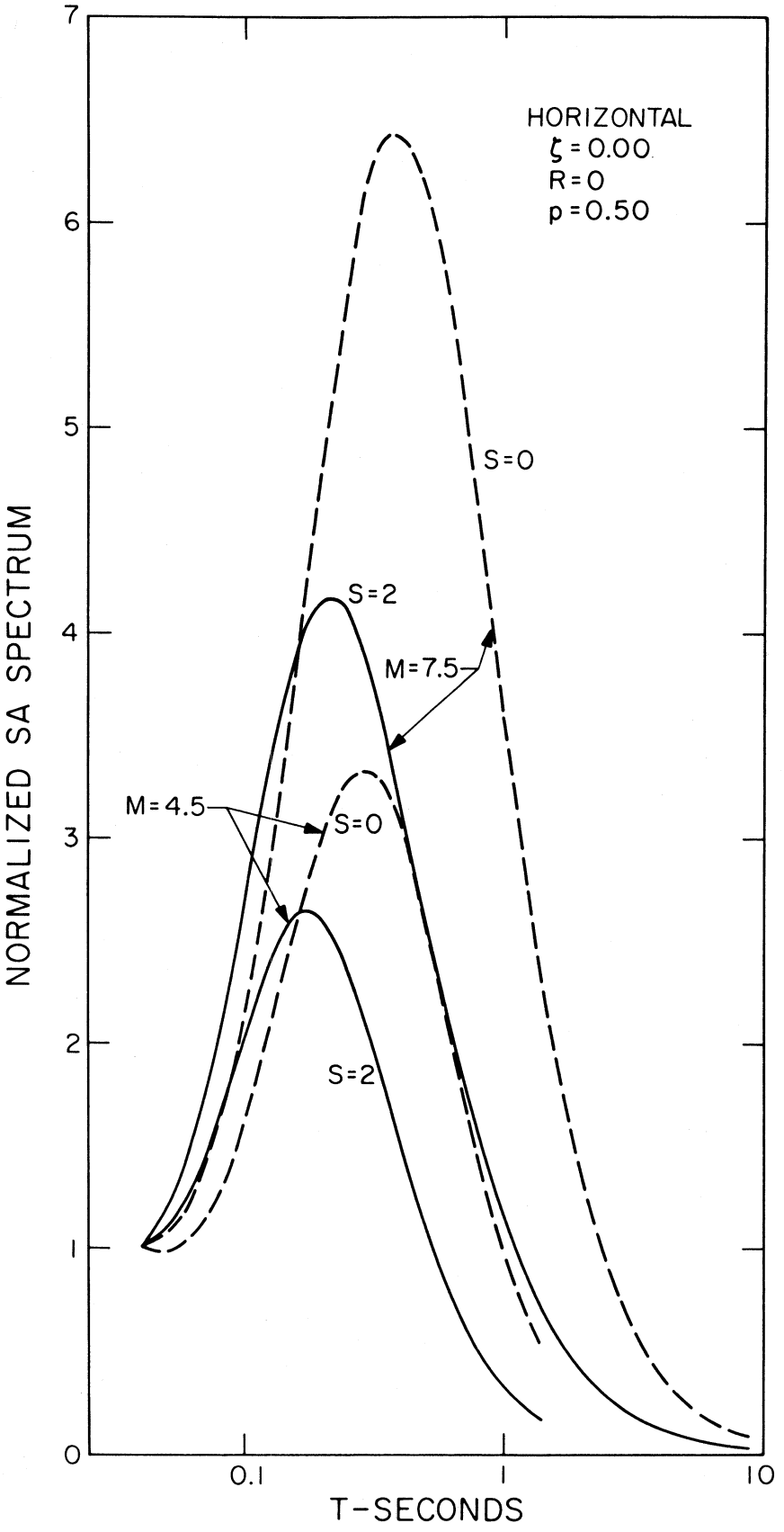
HORIZONTAL
ζ = 0.00
R = 0
p = 0.50
S=0
S=2
M=7.5
M=4.5
S=0
S=2
NORMALIZED SA SPECTRUM
T-SECONDS
0
1
2
3
4
5
6
7
0.1
1
10

FIGURE 18

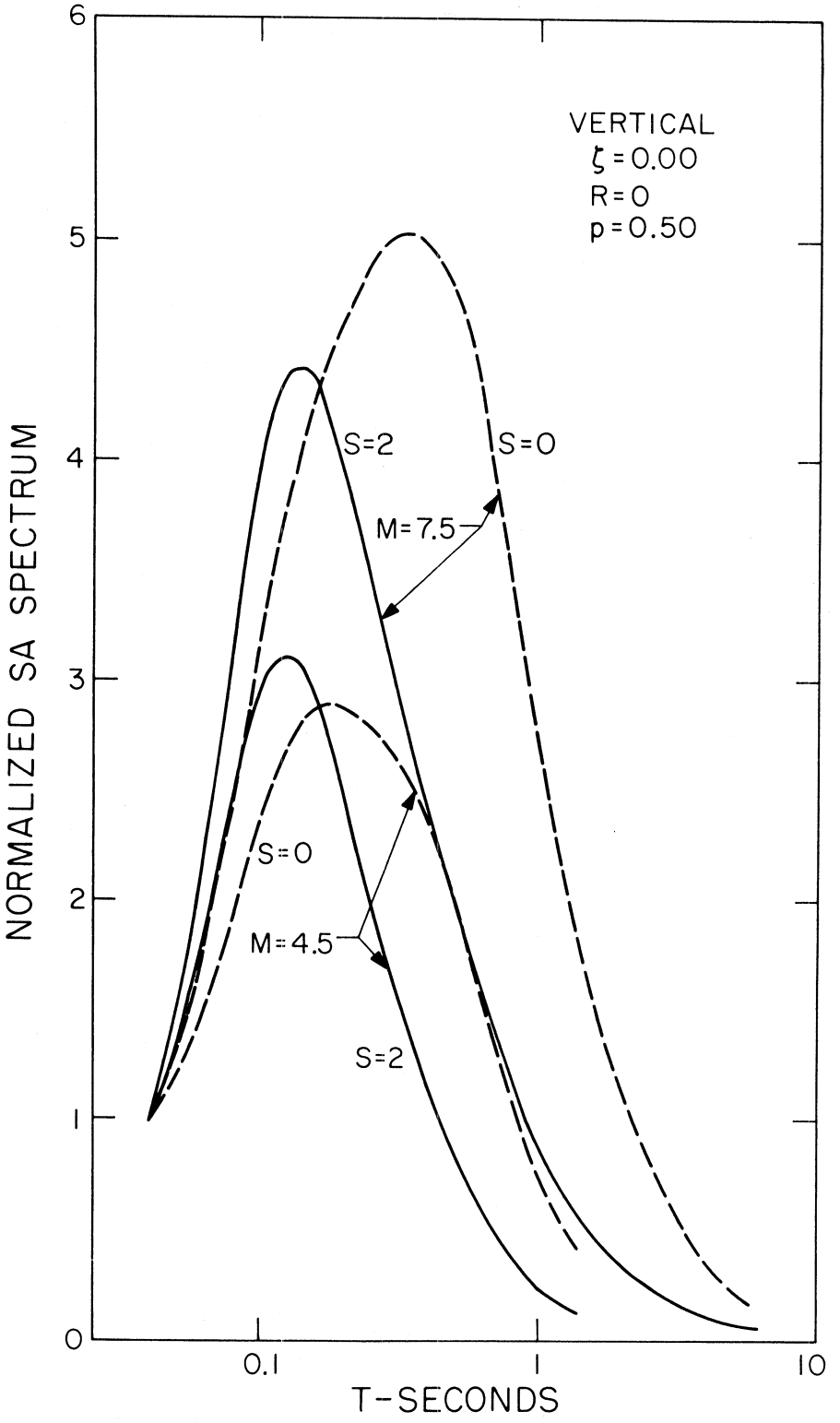
VERTICAL
ζ = 0.00
R = 0
p = 0.50
S=2
S=0
M=7.5
S=0
M=4.5
S=2
NORMALIZED SA SPECTRUM
T-SECONDS
0
1
2
3
4
5
6
0.1
1
10

FIGURE 19

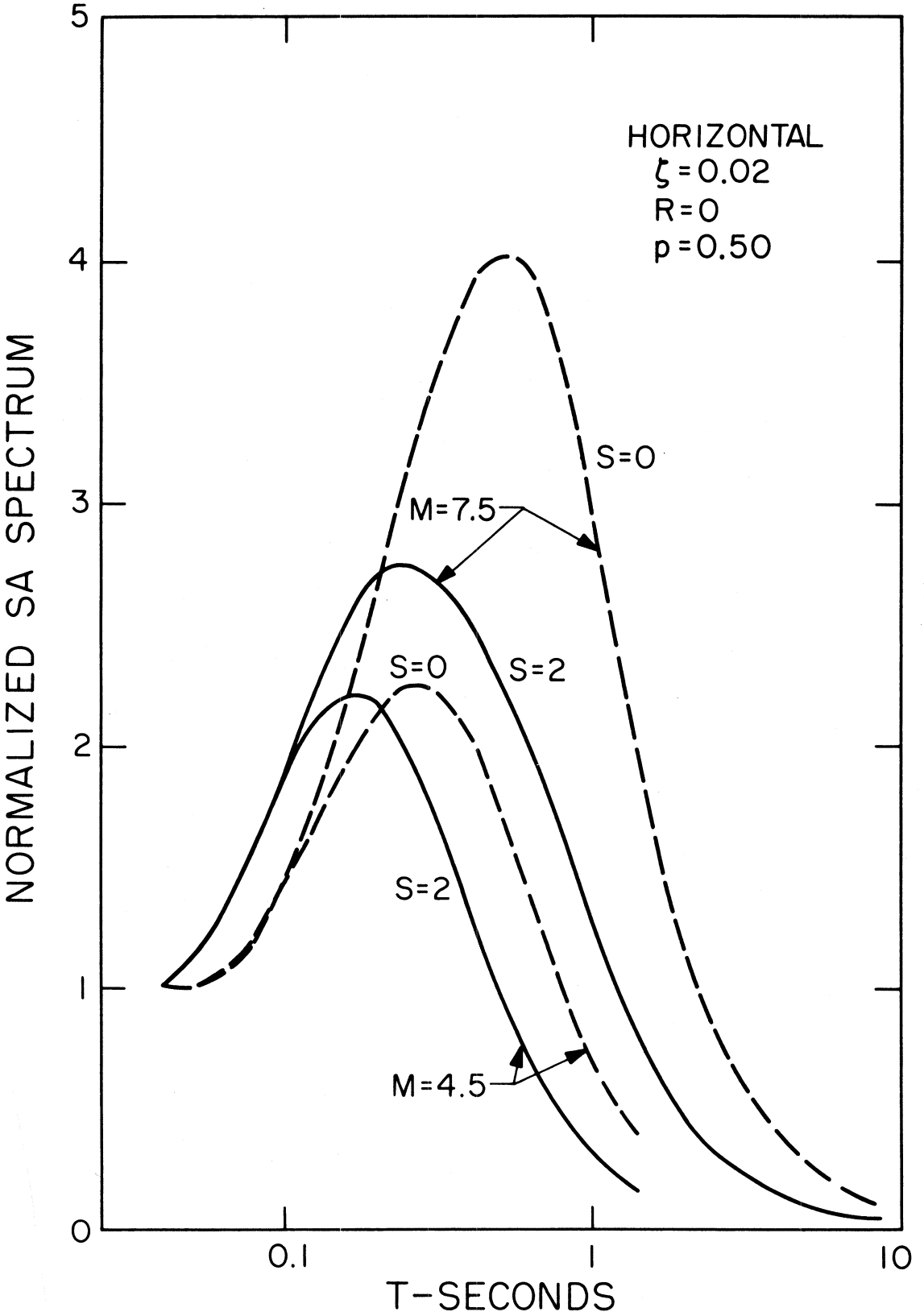
HORIZONTAL
ζ = 0.02
R = 0
p = 0.50
S=0
M=7.5
S=0
S=2
S=2
M=4.5
NORMALIZED SA SPECTRUM
T-SECONDS
0
1
2
3
4
5
0.1
1
10

FIGURE 20

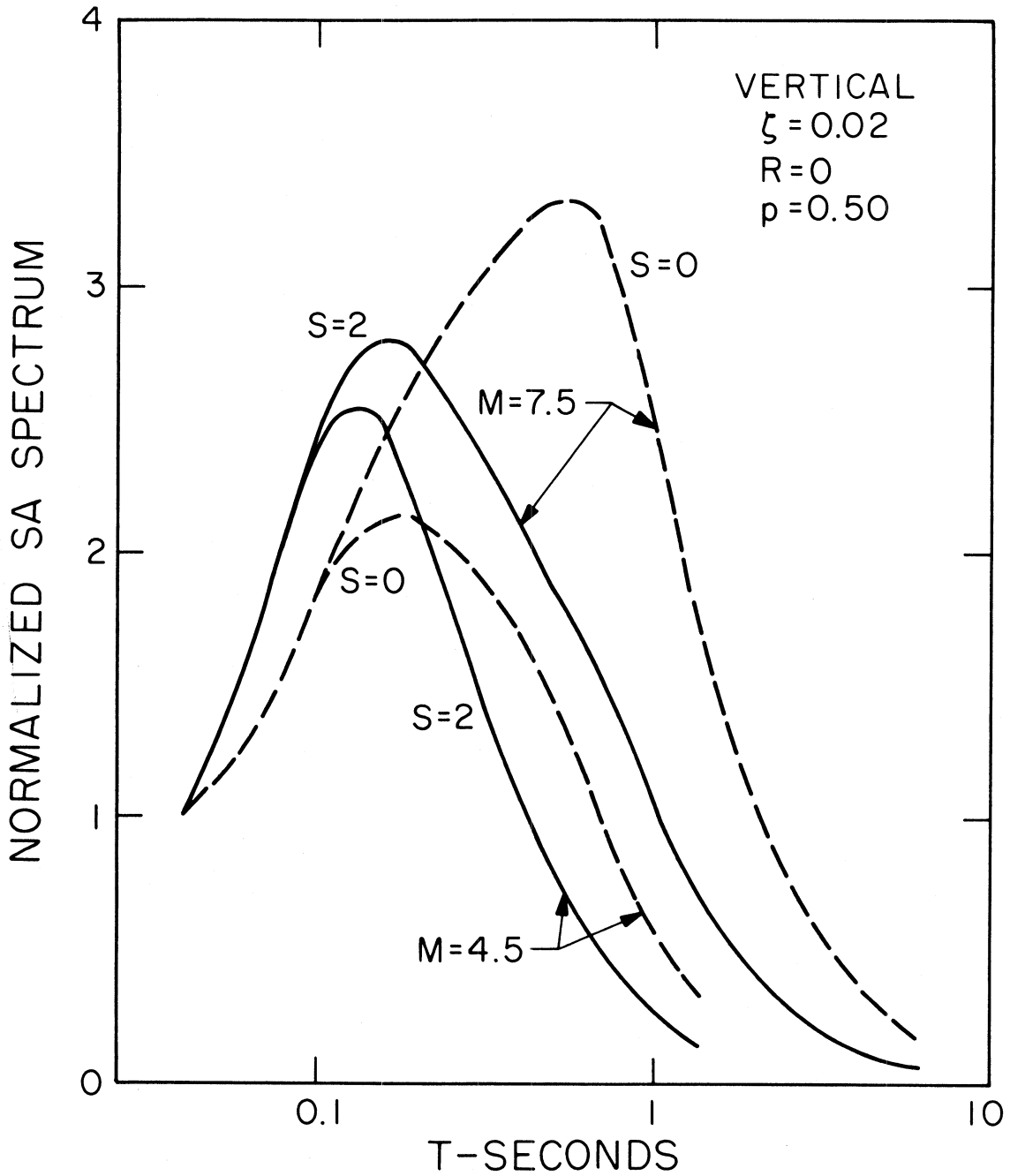
VERTICAL
ζ = 0.02
R = 0
p = 0.50
S=0
S=2
M=7.5
S=0
S=2
M=4.5
NORMALIZED SA SPECTRUM
T-SECONDS
0
1
2
3
4
0.1
1
10

FIGURE 21

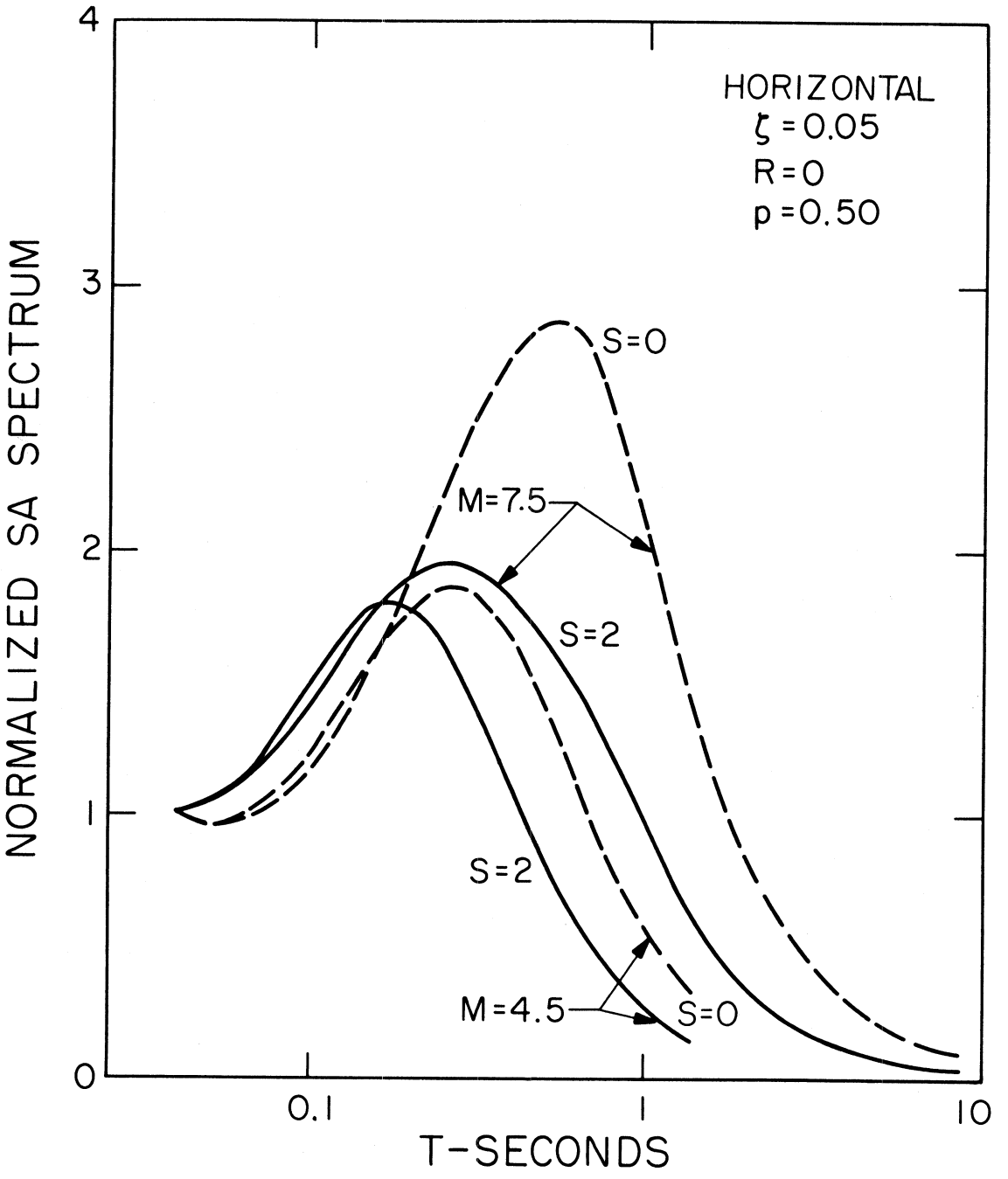
HORIZONTAL
ζ = 0.05
R = 0
p = 0.50
S=0
M=7.5
S=2
S=2
M=4.5
S=0
NORMALIZED SA SPECTRUM
T-SECONDS
0
1
2
3
4
0.1
1
10

FIGURE 22

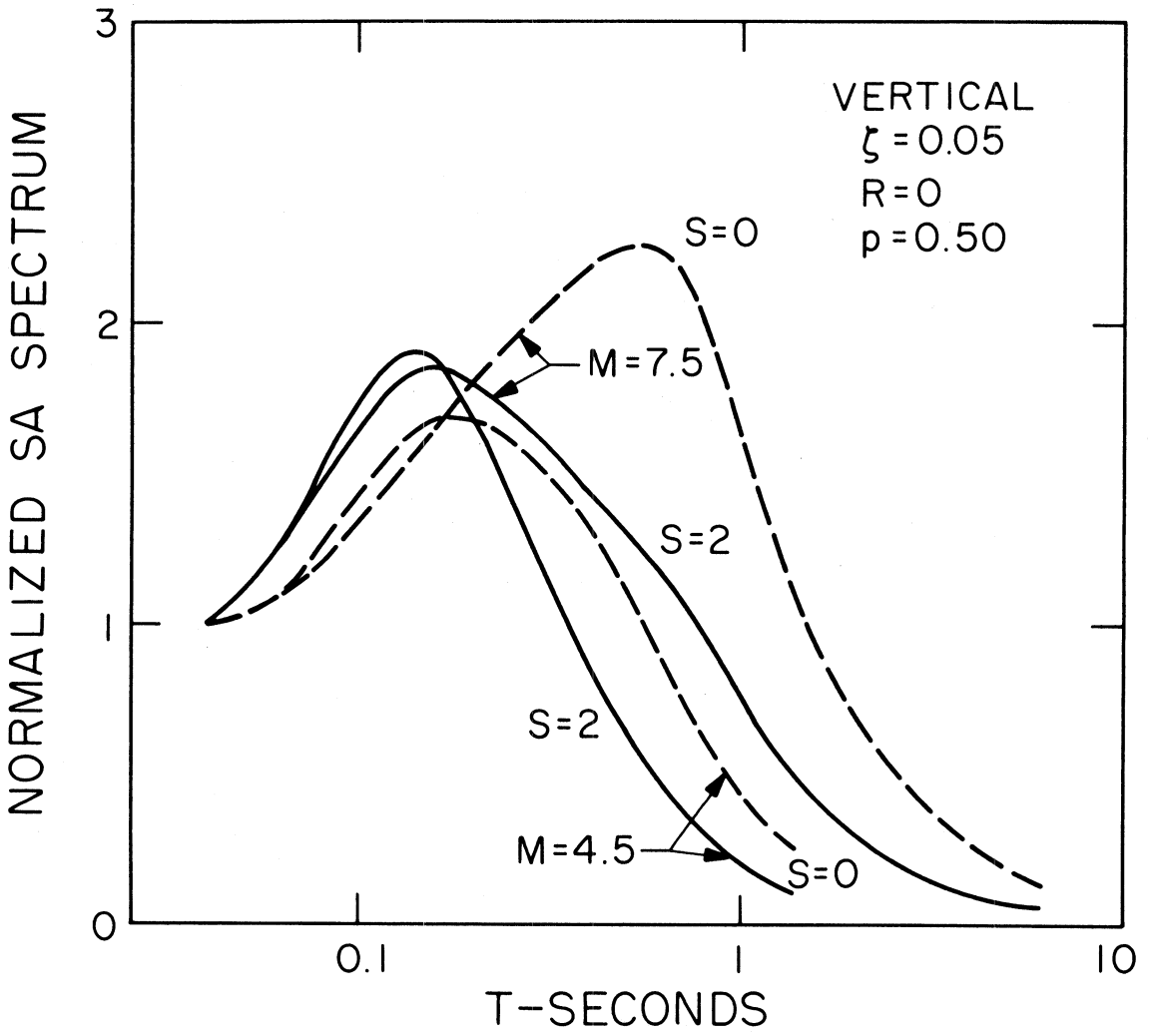
NORMALIZED SA SPECTRUM
T-SECONDS
VERTICAL
ζ = 0.05
R = 0
p = 0.50
S=0
M=7.5
S=2
S=2
M=4.5
S=0
0
1
2
3
0.1
1
10

FIGURE 23

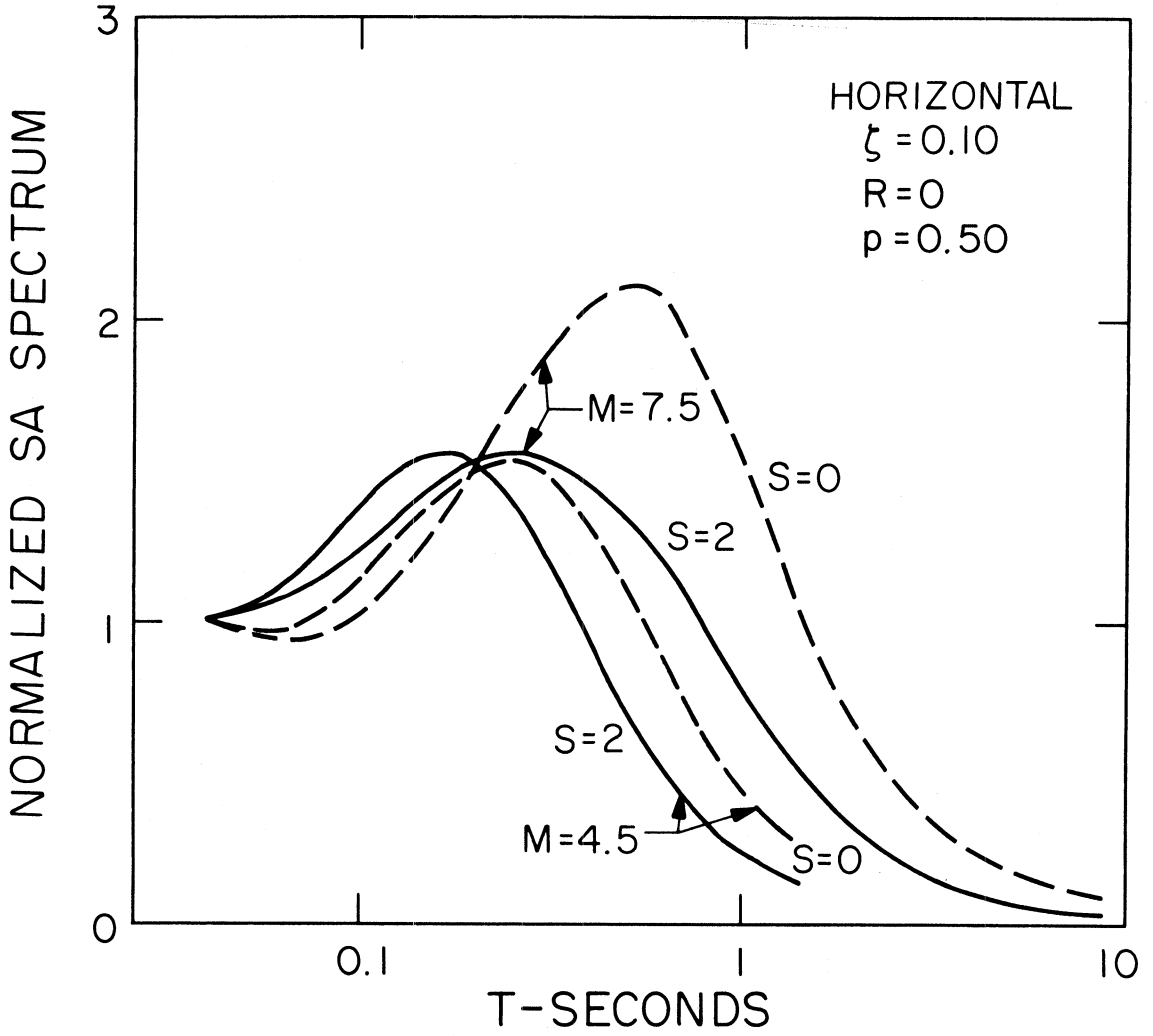
HORIZONTAL
ζ = 0.10
R = 0
p = 0.50
M=7.5
S=0
S=2
S=2
M=4.5
S=0
NORMALIZED SA SPECTRUM
T-SECONDS
0
1
2
3
0.1
1
10

FIGURE 24

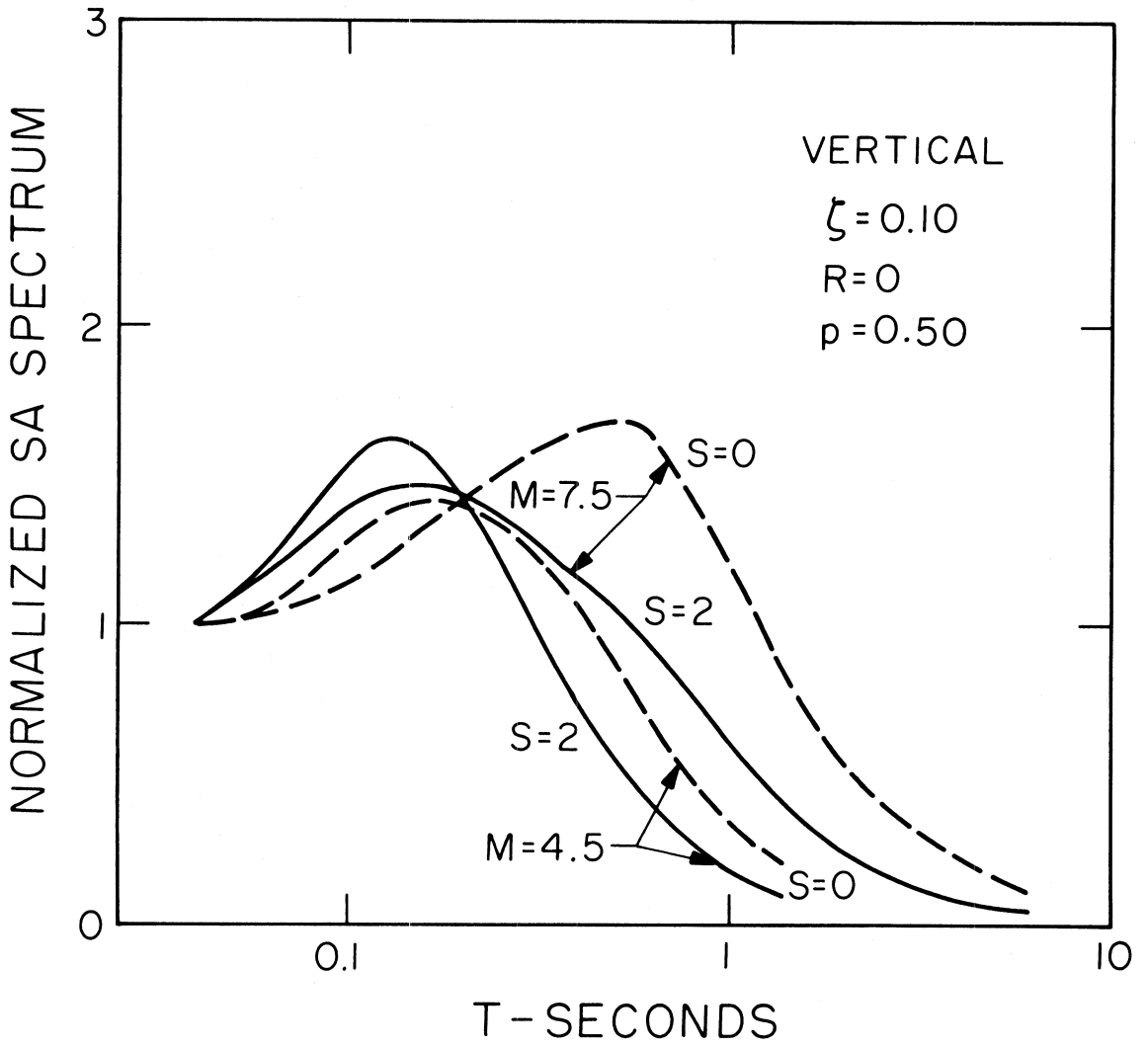
NORMALIZED SA SPECTRUM
3
2
1
0
VERTICAL
ζ = 0.10
R = 0
p = 0.50
S=0
M=7.5
S=2
S=2
M=4.5
S=0
0.1
1
10
T - SECONDS

FIGURE 25

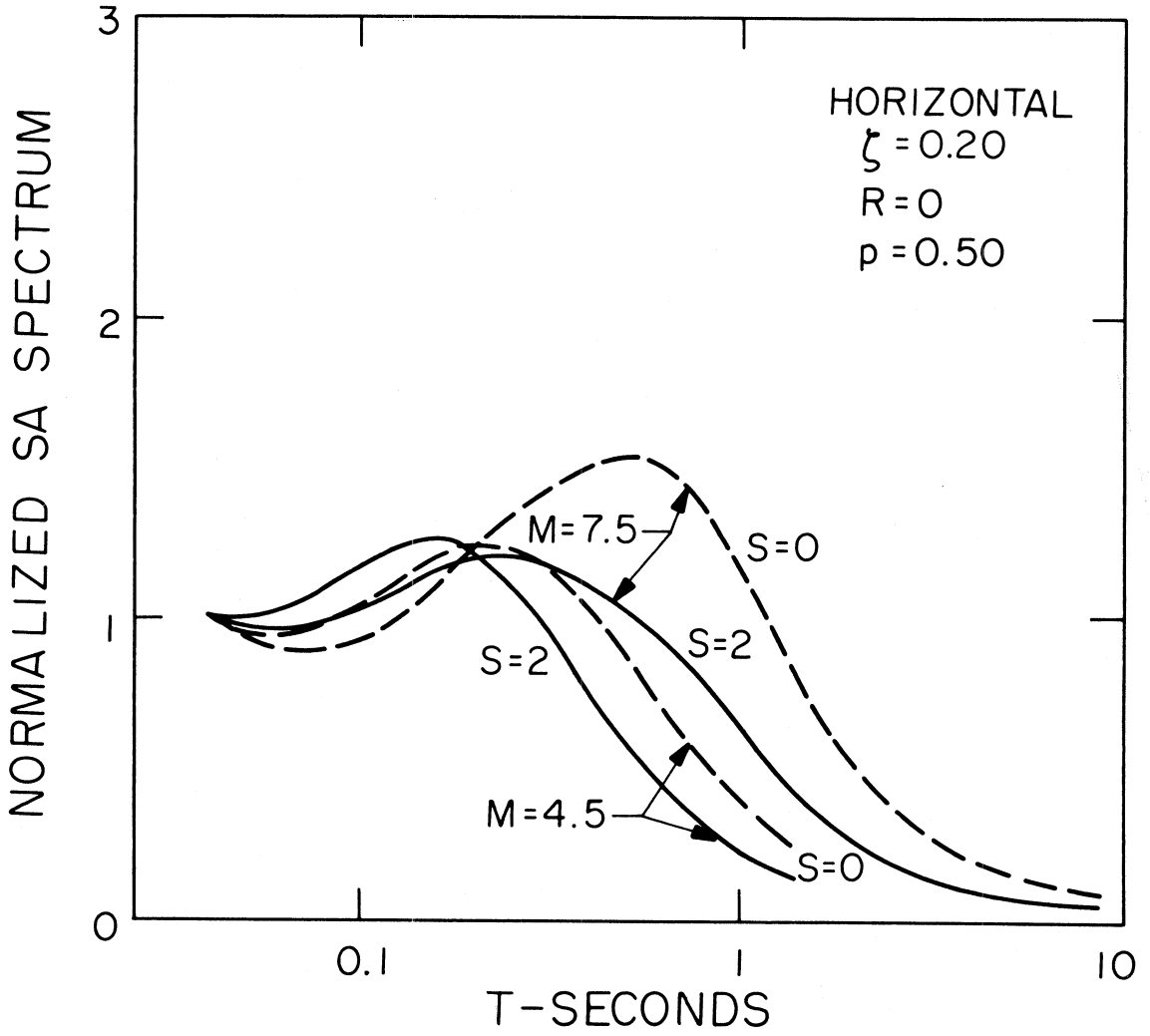
HORIZONTAL
ζ = 0.20
R = 0
p = 0.50
M=7.5
S=0
S=2
S=2
M=4.5
S=0
NORMALIZED SA SPECTRUM
T-SECONDS
0
1
2
3
0.1
1
10

FIGURE 26

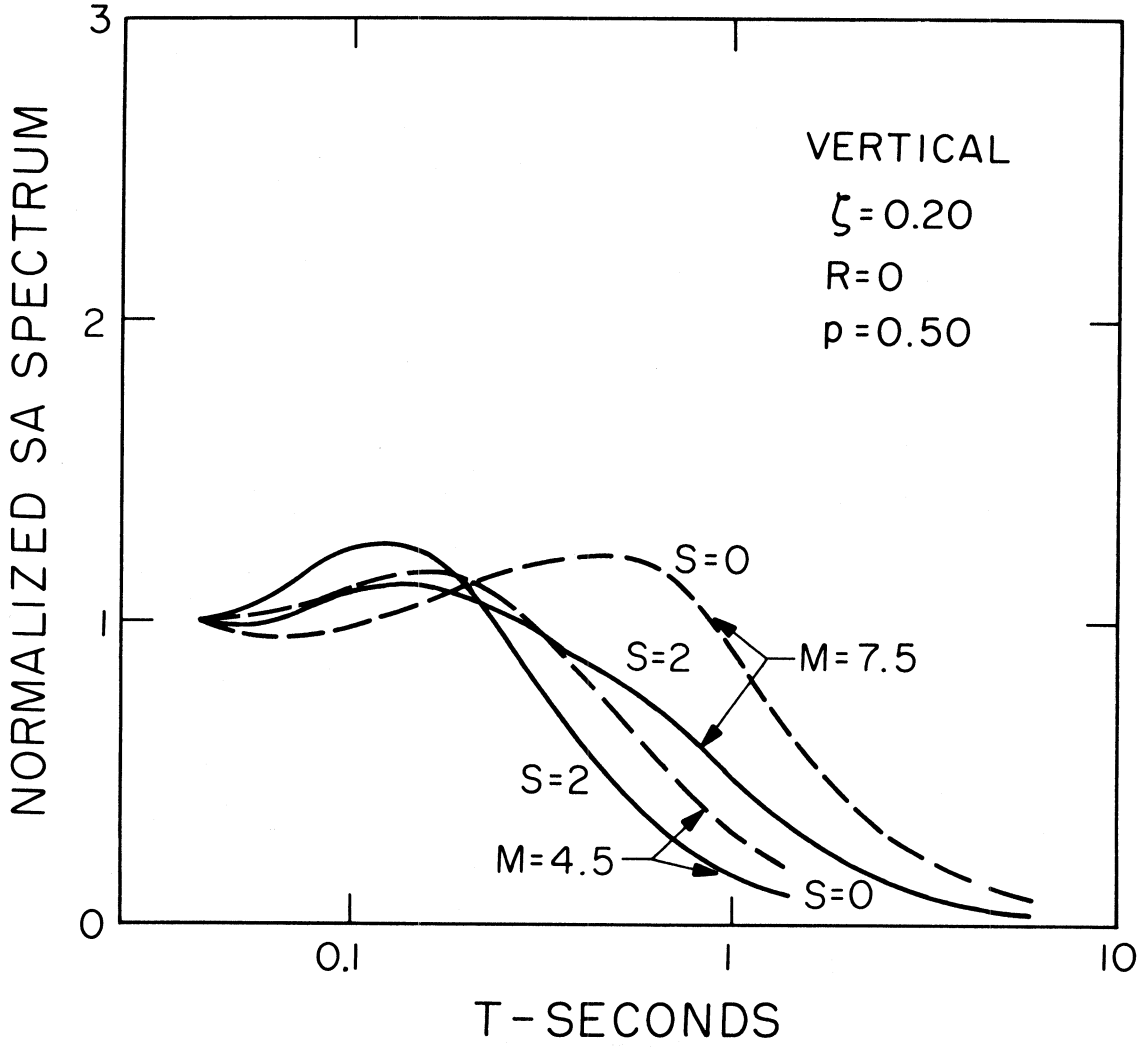
NORMALIZED SA SPECTRUM
3
2
1
0
VERTICAL
ζ = 0.20
R = 0
p = 0.50
S=0
S=2
M=7.5
S=2
M=4.5
S=0
0.1
1
10
T-SECONDS

FIGURE 27

Examples of the normalized SA spectra for M = 4.5 and 7.5, for s = 0 and 2, for R = 0, p = 0.5 and for ζ = 0.00, 0.02, 0.05, 0.10 and 0.20 are shown in Figures 18 through 27. To avoid cluttering of curves each figure shows only four spectral shapes for M = 4.5 and 7.5 and for s = 0 and 2. p = 0.5 was selected to illustrate the "average" shapes. Additional figures to illustrate the dependence of spectra on R were omitted because g(T) is small and influences the spectral amplitudes only for large R. A dependence of spectral shapes on s is as expected from the behavior of d(T) shown in Figure 6. However, the periods where the spectra for s = 0 cross the spectra for s = 2 are affected by the above normalization procedure. The dependence of spectral shapes on magnitudes is in agreement with the expectations based on the source mechanism theory which requires larger energy content in the long period range for larger earthquakes (e.g., Trifunac, 1976b). Examination of the Figures 18 through 27 shows the limitations of the fixed shape SA spectra and the degree to which such spectra may underestimate or overestimate SA amplitudes for given M, R, s, v and p. In Figures 22 through 27, the appearance of larger amplitudes for a magnitude 4.5 event than a magnitude 7.5 event is a consequence of the normalization and the differing frequency content of radiation from large and small events.

Figures 28, 29 and 30 show examples of how horizontal and vertical spectra computed from equation (1) compare with the acceleration spectra for the three components of strong-motion recorded at the Pacoima Dam site during the San Fernando, California, earthquake of February 9, 1971. In these figures, $SA(T)_p$ spectra were computed for p = 0.1, and 0.9 and

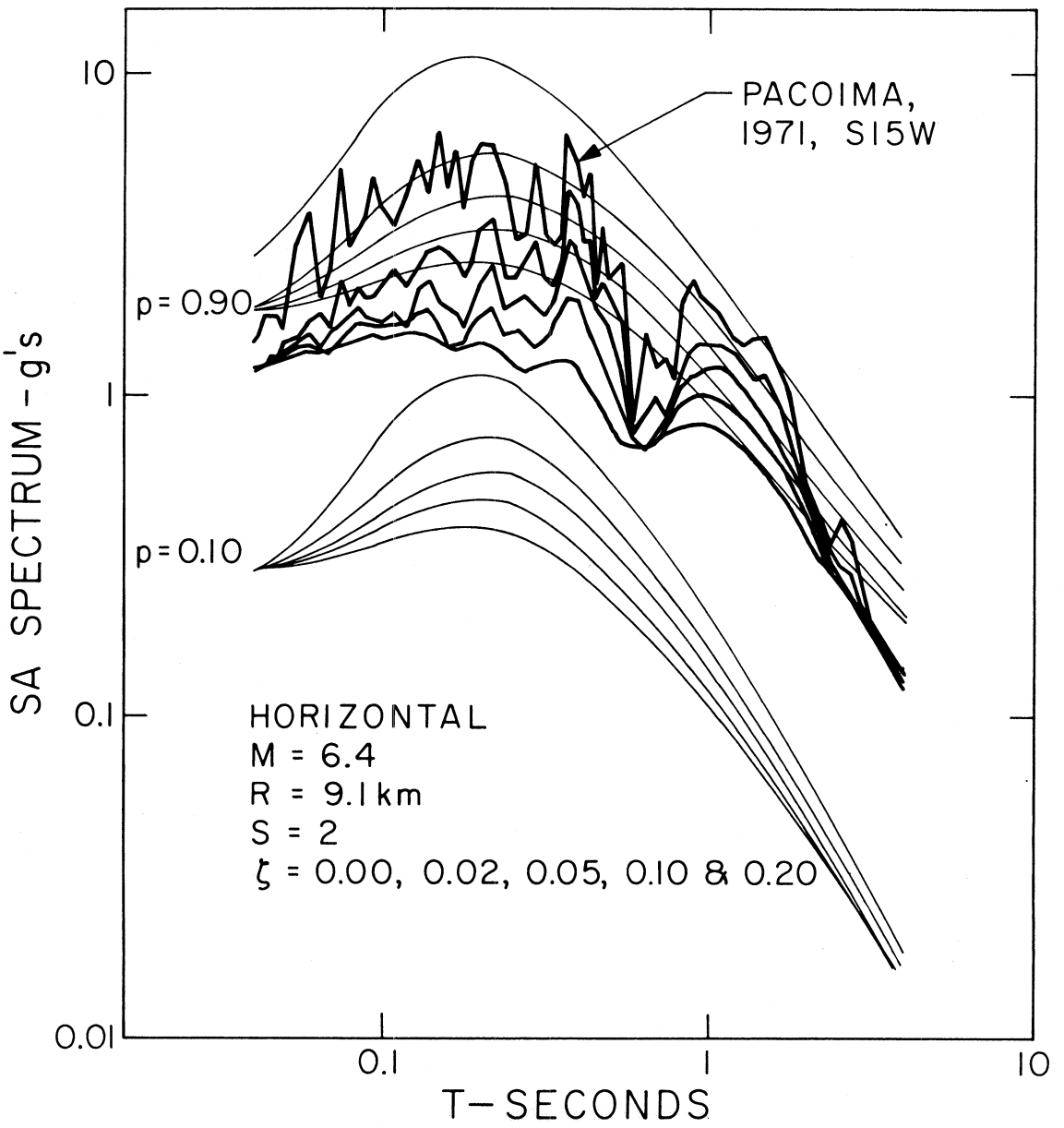
10
1
0.1
0.01
SA SPECTRUM - g's
PACOIMA,
1971, S15W
p = 0.90
p = 0.10
HORIZONTAL
M = 6.4
R = 9.1 km
S = 2
ζ = 0.00, 0.02, 0.05, 0.10 & 0.20
0.1
1
10
T-SECONDS

FIGURE 28

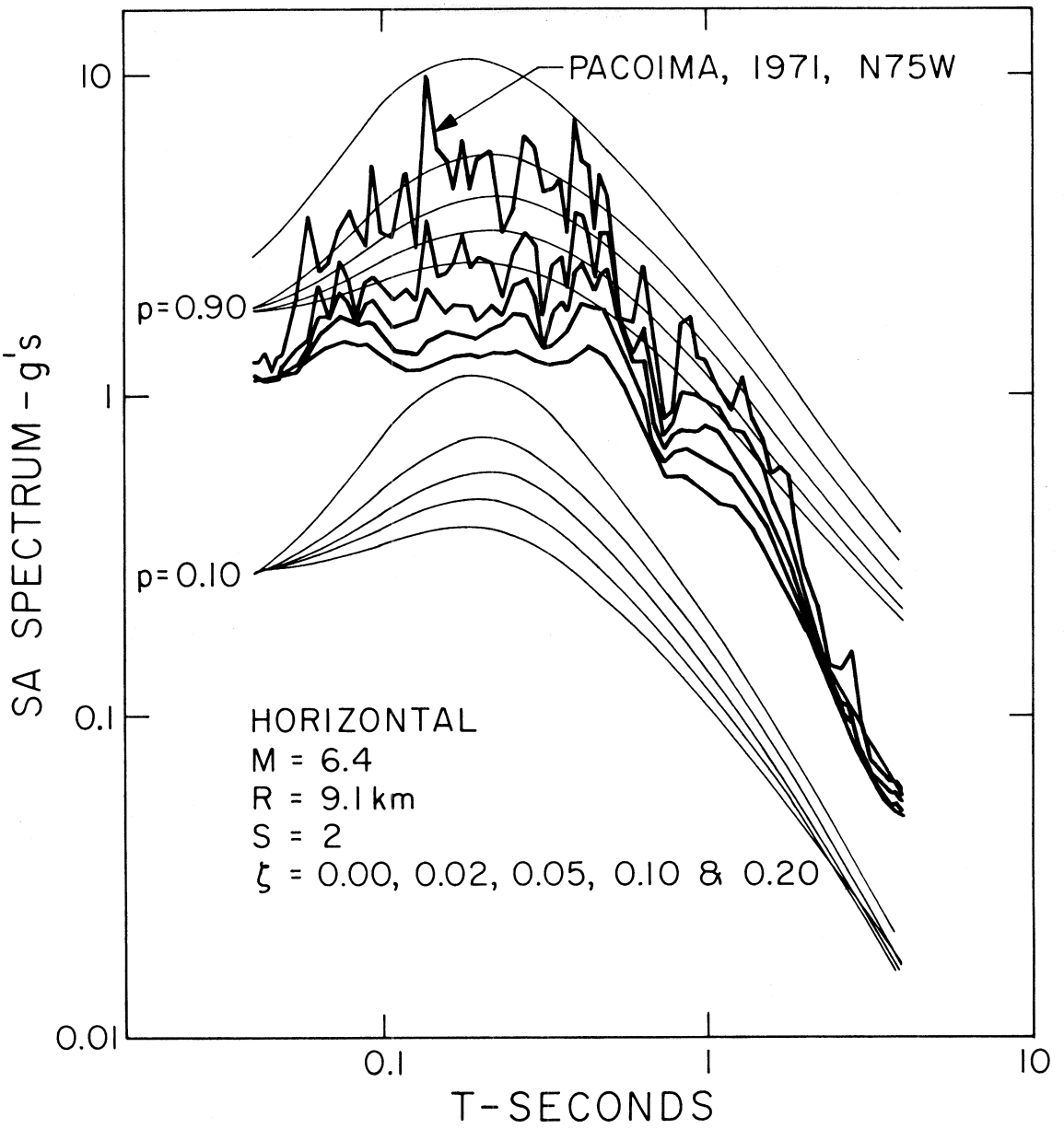
PACOIMA, 1971, N75W
p=0.90
p=0.10
HORIZONTAL
M = 6.4
R = 9.1 km
S = 2
ζ = 0.00, 0.02, 0.05, 0.10 & 0.20
SA SPECTRUM - g's
T-SECONDS
10
1
0.1
0.01
0.1
1
10

FIGURE 29

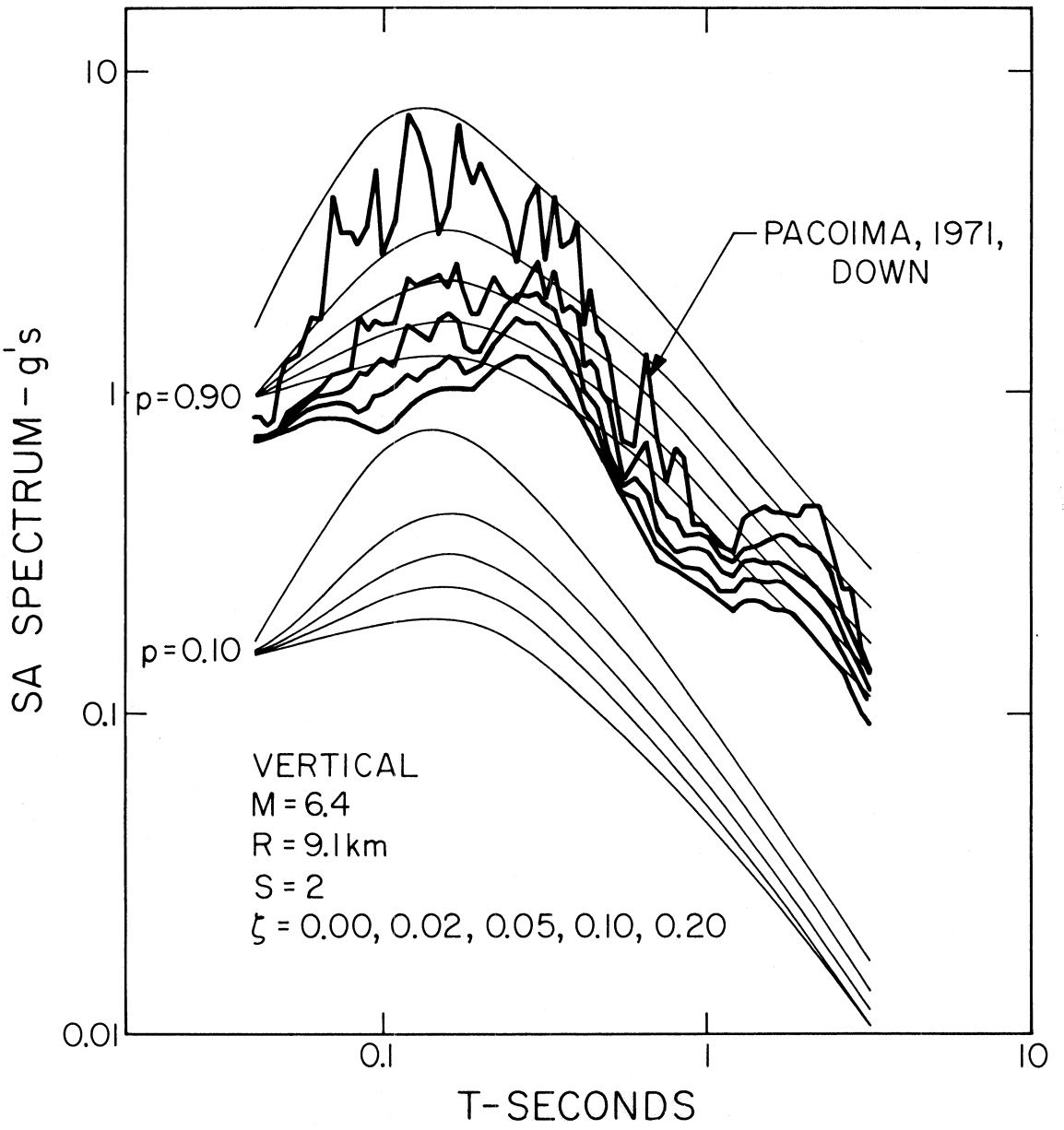
10
1
0.1
0.01
SA SPECTRUM - g's
p=0.90
p=0.10
PACOIMA, 1971,
DOWN
VERTICAL
M = 6.4
R = 9.1km
S = 2
ζ = 0.00, 0.02, 0.05, 0.10, 0.20
0.1
1
10
T-SECONDS

FIGURE 30

for ζ = 0.0, 0.02, 0.05, 0.10 and 0.20 so that the interval between the spectra for p = 0.1 and p = 0.9 represents an estimate of the 80 percent confidence interval. As may be seen from these figures, the agreement between the recorded and empirically predicted spectra in this case is good. The spectra for p = 0.1 and p = 0.9 do not only envelope the spectra of recorded accelerograms but also follow the overall amplitude and shape trends well. This type of agreement between empirically predicted and actually recorded spectra, however, is probably better than what might be expected in an average case.

An example of worse than average fit is illustrated in Figures 31, 32 and 33 for the spectra of strong-motion accelerograms recorded in El Centro during the Imperial Valley, California, earthquake of 1940. This relatively poor agreement represents one good example of why the function a(T) has such large amplitudes, implying about an order of magnitude scatter at the 80% confidence interval.

The differences between computed and observed spectra in Figures 31, 32 and 33 clearly show that the scaling of spectral characteristics of strong earthquake ground motion in terms of earthquake magnitude alone cannot be expected to yeild satisfactory answers in all cases, especially for complex earthquake mechanisms. Introduction of additional parameters into the empirical scaling functions could reduce the observed differences. The additional parameters could specify the relative source-to-station geometrical position more precisely than is now done by epicentral distance alone and could describe such properties of the earthquake sources as radiation pattern and the direction and velocity of the propagating dislocation. The compilation of these additional parameters could be carried out during detailed source

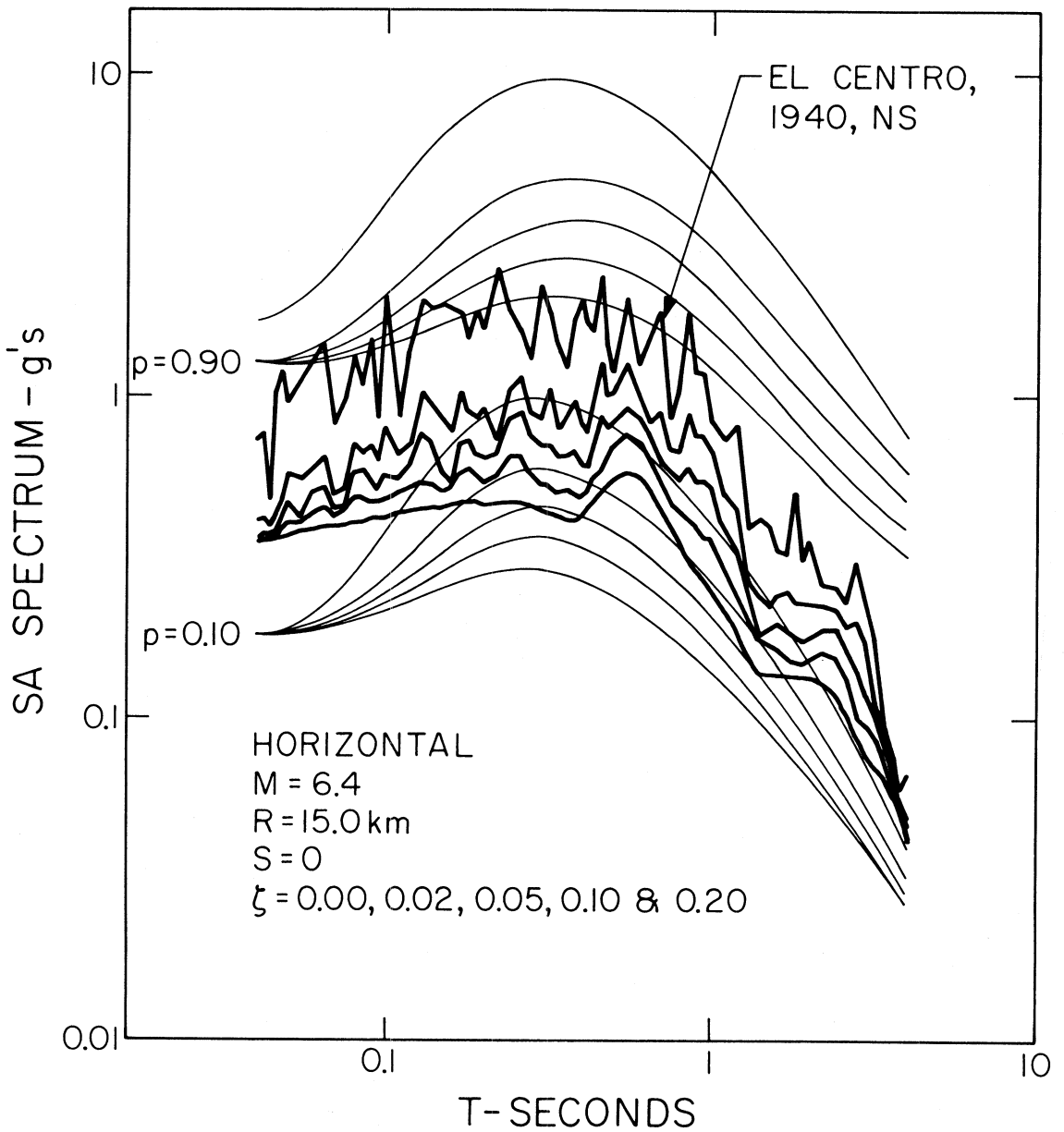
EL CENTRO,
1940, NS
p=0.90
p=0.10
HORIZONTAL
M = 6.4
R = 15.0 km
S = 0
ζ = 0.00, 0.02, 0.05, 0.10 & 0.20
SA SPECTRUM - g's
T-SECONDS
10
1
0.1
0.01
0.1
1
10

FIGURE 31

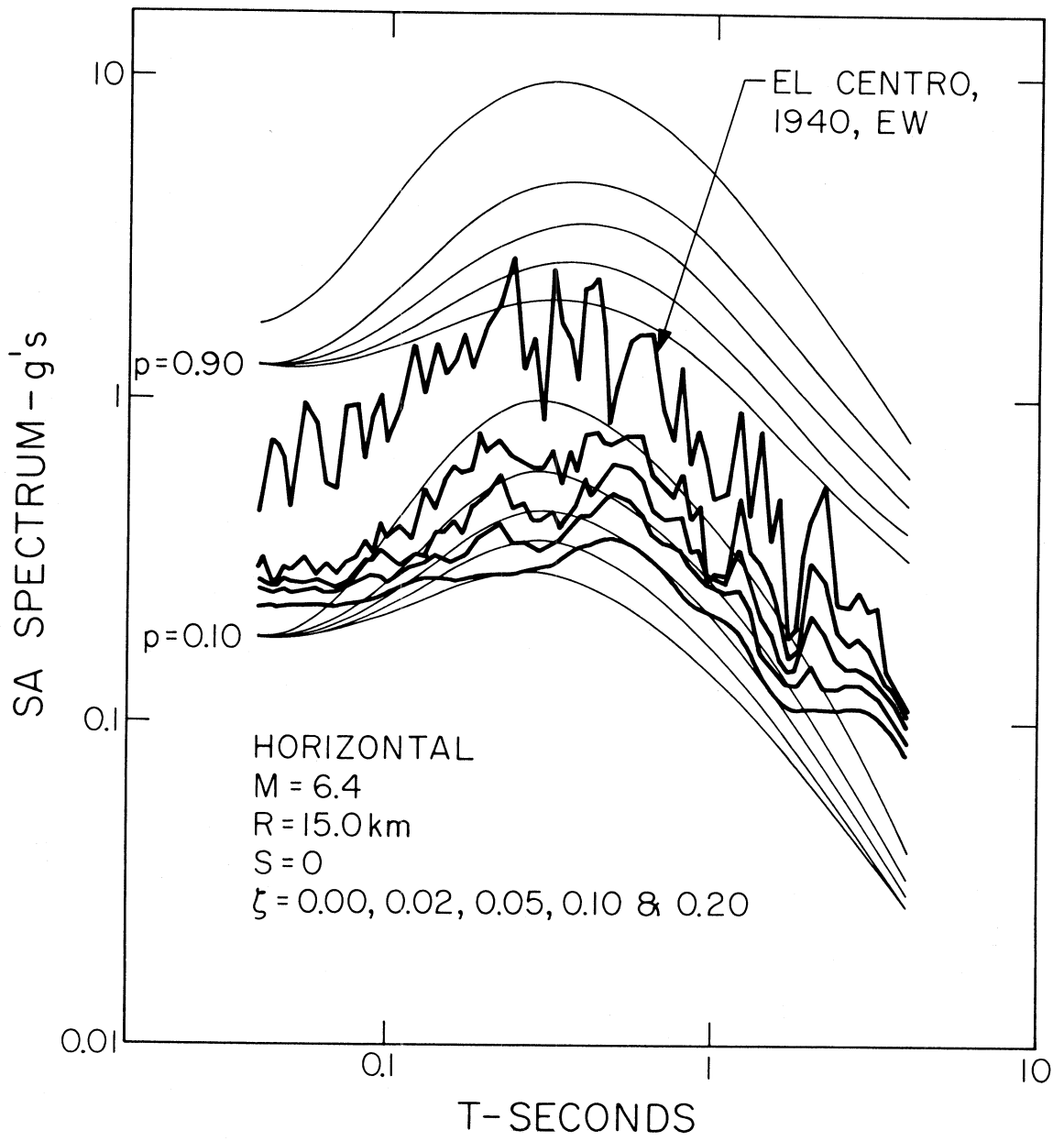
EL CENTRO,
1940, EW
p=0.90
p=0.10
HORIZONTAL
M = 6.4
R = 15.0 km
S = 0
ζ = 0.00, 0.02, 0.05, 0.10 & 0.20
SA SPECTRUM - g's
T - SECONDS
10
1
0.1
0.01
0.1
1
10

FIGURE 32

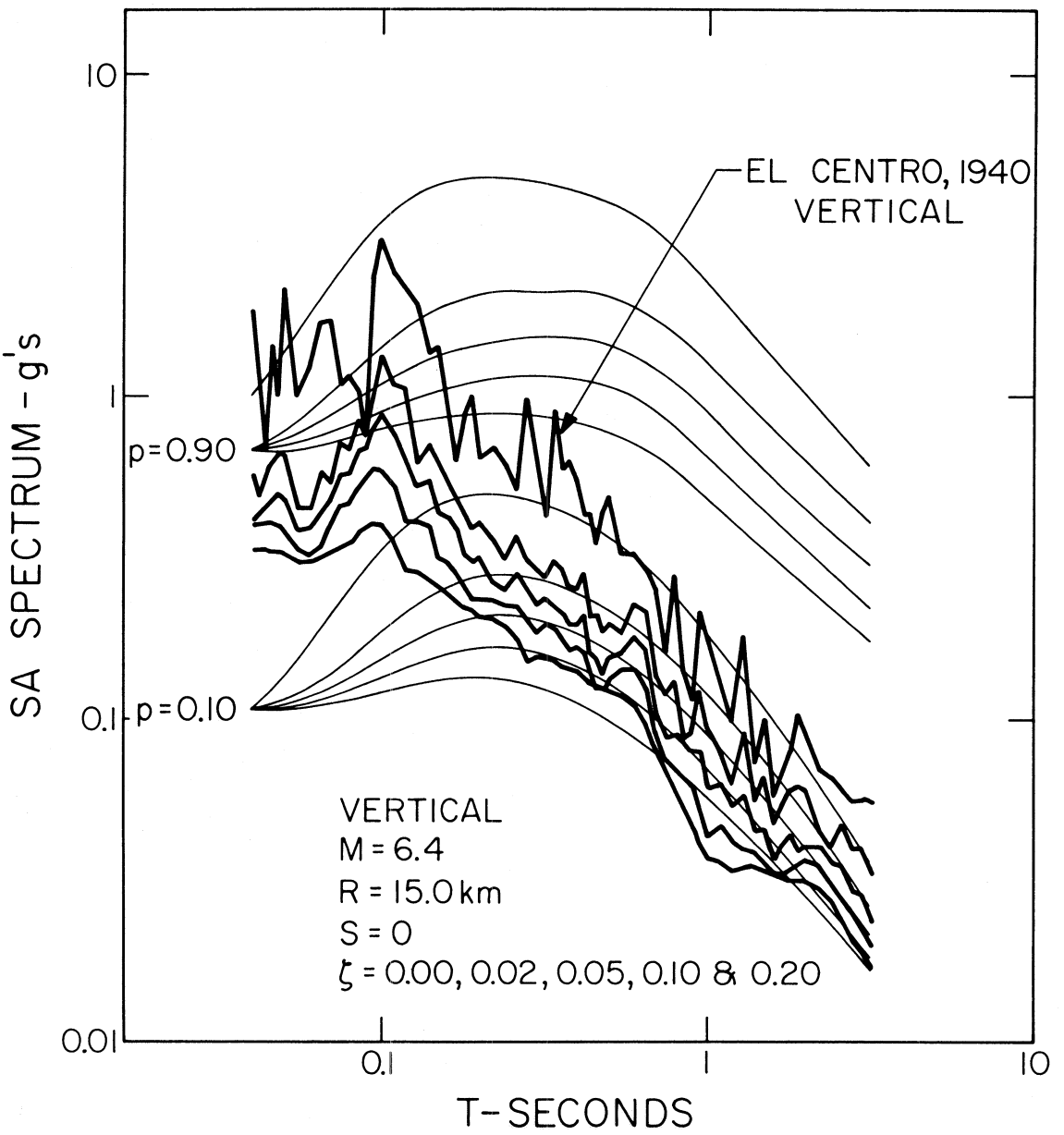
10
1
0.1
0.01
SA SPECTRUM - g's
p=0.90
p=0.10
EL CENTRO, 1940
VERTICAL
VERTICAL
M = 6.4
R = 15.0 km
S = 0
ζ = 0.00, 0.02, 0.05, 0.10 & 0.20
0.1
1
10
T-SECONDS

FIGURE 33

mechanism studies. Such studies have now been carried out for several earthquakes that lead to the data base which is used in this paper (e.g., Trifunac and Brune, 1970; Trifunac, 1972a; Trifunac, 1972b; Trifunac, 1974; Trifunac and Udwadia, 1974). While such a posteriori refinements of the empirical models will, no doubt, become possible when more data becomes available for well documented and carefully studied earthquakes, the practical question still remains: How detailed characterization of possible future earthquakes will it be feasible to obtain a priori? Detailed investigations may enable one to estimate the possible location and probable size (e.g., magnitude and/or fault length) of a future earthquake; if this earthquake is predicted to occur on the existing fault, the relative position of the fault to the station may also be known. However, such details as the stress-drop, the direction and the velocity with which dislocation will propagate, and the possible multiplicity of the source appear to be quite difficult to predict at this time. Therefore, for practical earthquake engineering applications, it may be desirable to work with empirical scaling functions which are purposely not more detailed than equation (1), for example, so that the empirical models themselves do not imply smaller uncertainties than those which have to be associated with the input parameters.

c. Correlations in Terms of I_{MM}, p, s and v

Figure 34 and Table VII present the results of least squares fitting of equation (2) to the SA data. The estimates of a(T), b(T), ..., and e(T) for ζ = 0.0, 0.02, 0.05, 0.10 and 0.20 have been smoothed by low-pass filtering the data with an Ormsby filter along the $\log_{10}T$ axis.

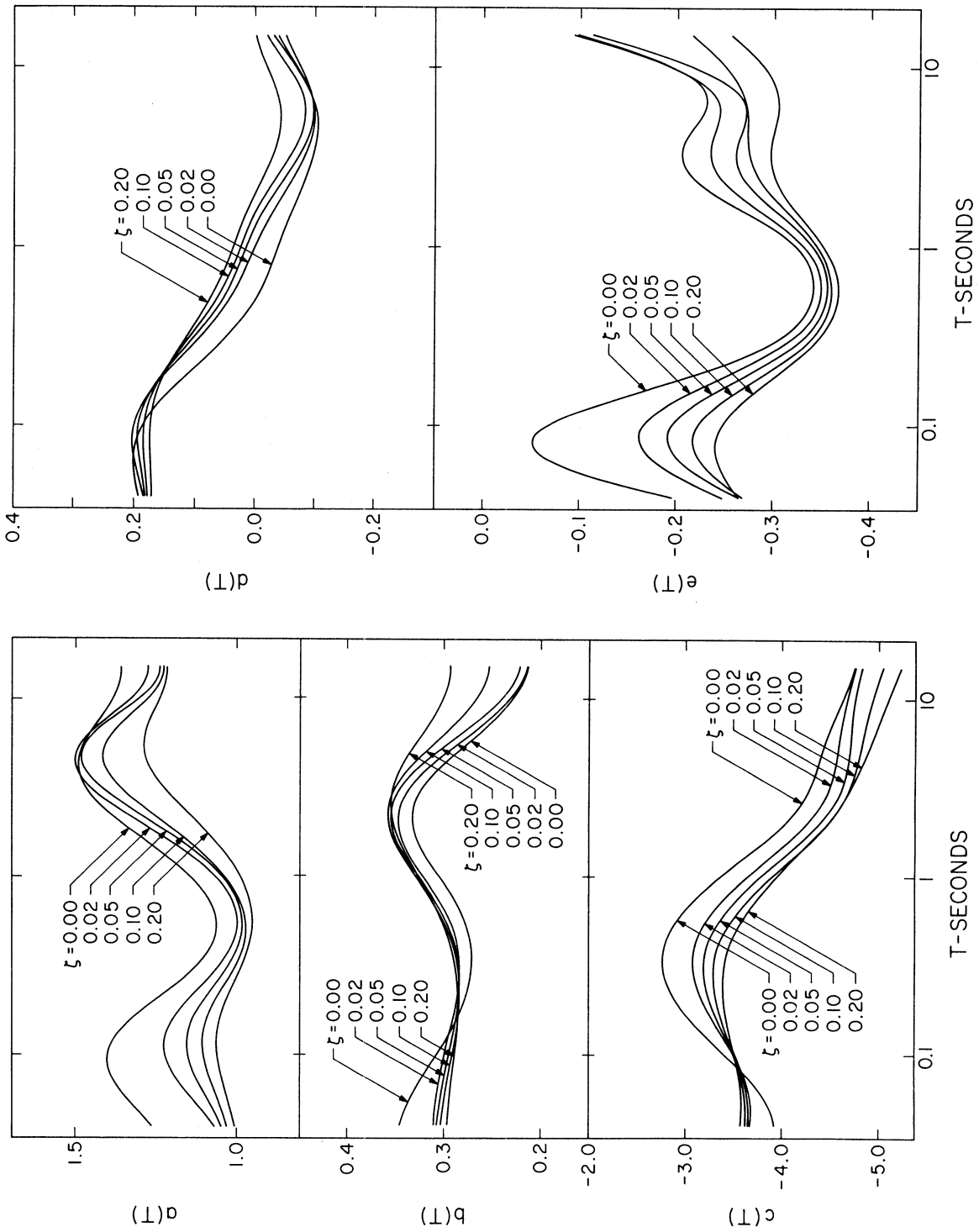
a(T)
b(T)
c(T)
d(T)
e(T)
T-SECONDS
T-SECONDS
ζ=0.00
0.02
0.05
0.10
0.20
ζ=0.20
0.10
0.05
0.02
0.00

FIGURE 34

TABLE VII

Regression Parameters for Equation (2) and $\alpha(T)$, $\beta(T)$ and $N(T)^*$ at Eleven Selected Periods

logT(sec)	-1.398	-1.171	-0.943	-0.716	-0.489	-0.261	-0.034	0.193	0.420	0.648	0.875
ζ = 0.0											
a(T)	1.262	1.370	1.389	1.268	1.119	1.061	1.124	1.270	1.428	1.490	1.428
b(T)	0.345	0.327	0.301	0.279	0.271	0.278	0.300	0.326	0.329	0.295	0.248
c(T)	-3.923	-3.718	-3.302	-2.920	-2.766	-2.896	-3.289	-3.810	-4.209	-4.391	-4.533
d(T)	0.192	0.201	0.176	0.113	0.044	-0.007	-0.034	-0.060	-0.089	-0.105	-0.093
e(T)	-0.197	-0.064	-0.089	-0.217	-0.312	-0.341	-0.331	-0.275	-0.212	-0.215	-0.228
$\alpha(T)$	2.639	2.542	2.528	2.599	2.640	3.886	3.861	3.776	3.558	3.398	3.457
$\beta(T)$	-1.169	-1.137	-1.143	-1.178	-1.186	-2.456	-2.458	-2.452	-2.360	-2.268	-2.282
N(T)	2	2	2	2	2	1	1	1	1	1	1
ζ = 0.02											
a(T)	1.067	1.170	1.224	1.161	1.050	0.995	1.046	1.194	1.394	1.499	1.412
b(T)	0.310	0.305	0.296	0.287	0.283	0.293	0.317	0.342	0.343	0.307	0.254
c(T)	-3.672	-3.636	-3.436	-3.192	-3.077	-3.204	-3.574	-4.056	-4.423	-4.568	-4.629
d(T)	0.184	0.200	0.194	0.149	0.087	0.036	0.004	-0.029	-0.069	-0.097	-0.091
e(T)	-0.249	-0.173	-0.176	-0.251	-0.324	-0.350	-0.338	-0.290	-0.241	-0.240	-0.234
$\alpha(T)$	2.609	2.559	2.560	2.626	2.649	3.842	3.771	3.707	3.551	3.414	3.423
$\beta(T)$	-1.164	-1.147	-1.161	-1.203	-1.204	-2.444	-2.418	-2.423	-2.363	-2.278	-2.256
N(T)	2	2	2	2	2	1	1	1	1	1	1
ζ = 0.05											
a(T)	1.045	1.111	1.154	1.109	1.021	0.979	1.028	1.161	1.357	1.479	1.396
b(T)	0.307	0.301	0.292	0.285	0.284	0.296	0.322	0.348	0.351	0.317	0.264
c(T)	-3.652	-3.616	-3.452	-3.263	-3.192	-3.342	-3.714	-4.186	-4.550	-4.694	-4.731
d(T)	0.181	0.191	0.189	0.153	0.097	0.048	0.019	-0.012	-0.056	-0.092	-0.092
e(T)	-0.266	-0.201	-0.204	-0.271	-0.334	-0.356	-0.346	-0.306	-0.265	-0.267	-0.260
$\alpha(T)$	2.613	2.568	2.569	2.626	2.655	3.863	3.786	3.696	3.553	3.437	3.417
$\beta(T)$	-1.170	-1.152	-1.164	-1.201	-1.207	-2.458	-2.426	-2.413	-2.358	-2.288	-2.256
N(T)	2	2	2	2	2	1	1	1	1	1	1

TABLE VII

(Continued)

$\zeta = 0.10$

a(T)	1.028	1.073	1.104	1.070	0.997	0.968	1.020	1.142	1.308	1.412	1.348
b(T)	0.303	0.297	0.289	0.284	0.286	0.299	0.324	0.350	0.355	0.328	0.284
c(T)	-3.621	-3.594	-3.463	-3.324	-3.295	-3.463	-3.829	-4.282	-4.632	-4.793	-4.881
d(T)	0.177	0.183	0.181	0.152	0.104	0.058	0.028	-0.001	-0.041	-0.079	-0.077
e(T)	-0.270	-0.223	-0.231	-0.289	-0.343	-0.360	-0.350	-0.317	-0.281	-0.273	-0.266
α(T)	2.612	2.572	2.570	2.619	2.648	3.872	3.801	3.705	3.547	3.416	3.406
β(T)	-1.171	-1.150	-1.158	-1.192	-1.201	-2.463	-2.436	-2.414	-2.344	-2.267	-2.248
N(T)	2	2	2	2	2	1	1	1	1	1	1

$\zeta = 0.20$

a(T)	1.005	1.038	1.061	1.035	0.979	0.949	0.976	1.059	1.182	1.278	1.270
b(T)	0.296	0.292	0.287	0.285	0.288	0.301	0.322	0.345	0.354	0.340	0.312
c(T)	-3.571	-3.569	-3.483	-3.399	-3.409	-3.571	-3.888	-4.286	-4.631	-4.853	-5.015
d(T)	0.170	0.173	0.170	0.149	0.111	0.070	0.040	0.015	-0.017	-0.041	-0.034
e(T)	-0.266	-0.242	-0.256	-0.303	-0.350	-0.367	-0.357	-0.326	-0.299	-0.300	-0.303
α(T)	2.596	2.581	2.583	2.619	2.639	3.865	3.784	3.685	3.558	3.455	3.429
β(T)	-1.164	-1.160	-1.168	-1.193	-1.201	-2.463	-2.420	-2.388	-2.340	-2.292	-2.277
N(T)	2	2	2	2	2	1	1	1	1	1	1

---

* See section entitled "Distribution of Spectral Amplitudes for Definition of α(T), β(T) and N(T).

For selected values of T, p, s and v equation (2) represents a straight line with respect to I_{MM}. Here I_{MM} represents numerical values ranging from 1 to 12 and corresponding to the descriptive Modified Mercalli Intensity (M.M.I.) levels I through XII. This simplistic linear assignment of numerical values to a qualitative M.M.I. scale has been discussed elsewhere and need not be repeated here in detail (e.g., Trifunac, 1976c). It is only useful to note here that between the levels IV and VIII on the M.M.I. scale the linear form of equation (2) appears to be adequate for this preliminary scaling of the absolute acceleration spectra. We will discuss this point again in connection with the comparison of equations (1) and (2) for the largest levels of shaking.

The confidence level function a(T), shown in Figure 34, fluctuates between 1 and 1.5 and has the overall trend of increasing from short periods towards longer periods. This again implies that there is about an order of magnitude difference between the 0.1 and 0.9 confidence levels for a single earthquake. The smallest amplitudes of a(T) are found in the period range between about 0.2 and 1.0 seconds. In the corresponding correlations which dealt with peak acceleration (Trifunac, 1976c) we found the coefficient a to be 0.94. Since the absolute acceleration spectra, SA, tend towards the absolute peak acceleration for $T \to 0$ we would expect essentially all the coefficients found in our previous study for scaling of peak accelerations to agree approximately with the amplitudes of a(T), b(T), d(T) and e(T). The coefficient c in the correlation of peak accelerations with M.M.I. (Trifunac, 1976c) is larger than c(T) for $T \to 0$ in this study by a factor approximately equal to 3.00. This is caused by different normalizations used

in these two papers (in our previous work we used the units of cm and sec while in this paper we are using g = 981 cm/sec^2).

Function b(T) (Figure 34) fluctuates between 0.3 and 0.35 for intermediate and short periods and then decreases towards 0.2 for long periods. This means that for each additional level of I_{MM} the SA spectral amplitudes approximately double. We found the same rate of growth with respect to I_{MM} in the correlations with peak acceleration using linear regression (Trifunac, 1976c).

The amplitudes of the site dependent function d(T) are positive for periods shorter than about 1 sec and negative for longer periods. These amplitudes decrease from about 0.18 near T = 0.04 sec. to zero near T = 1 sec. and towards 0.0 to -0.05 for T = 10 sec., depending on the fraction of critical damping ζ. Again, for T = 0.04 sec, the amplitudes of about 0.17 are in fair agreement with d = 0.14 computed for the linear regression analysis of peak accelerations with I_{MM} (Trifunac, 1976c). This trend of d(T) implies that the amplitude of the absolute acceleration spectra on hard basement rock (s = 2) are about twice as large as the spectral amplitudes recorded on alluvium (s = 0) for the same level of shaking as qualitatively described by I_{MM}.

Finally the function e(T) fluctuates between -0.1 and -0.35. Its largest amplitudes are attained for T$\sim$0.1 sec and for ζ = 0.00. This shows that for short periods and small damping vertical absolute acceleration spectra are nearly as large as the horizontal spectra. This overall trend of e(T) in Figure 34 is in good agreement with the trend of e(T) in the correlations of the Fourier

amplitude spectra with M, R, s and v (Trifunac, 1976b) and with I_{MM}, s and v (in preparation). In this study, however, for periods shorter than about 0.1 sec. e(T) ceases to grow and converges to the range of amplitudes between -0.2 and -0.28 depending on the values of ζ. It is noted that we found e = -0.27 in our previous work (Trifunac, 1976c).

It is instructive to compare certain characteristics of the two models portrayed by equations (1) and (2). In both of these models, functions a(T), b(T), ..., and e(T) describe the analogous type of dependence on the scaling parameters p, M or I_{MM}, s and v. Function a(T), for example, describes the scatter of spectra with respect to the average spectral amplitudes for $p \approx 0.5$ (see one of the later sections of this report for a more precise discussion of this distribution). By comparing the absolute values of these functions in Figures 6 and 34, it is possible to compare approximately the expected scatter of the observed spectral amplitudes with respect to equations (1) and (2). Detailed analysis of these two figures will show that with the exception of several isolated periods $|a(T)|$ in Figure 34 is smaller than $|a(T)|$ in Figure 6. This means that the model (2) appears to predict SA amplitudes with somewhat smaller uncertainty than the model (1). This provides a check on our previous findings (Trifunac, 1976c) which lead to the conclusion that the quality of scaling of strong ground motion by Modified Mercalli Intensity is better than might have been expected.

Functions d(T) in Figures 6 and 34 are in qualitative agreement showing that spectral amplitudes tend to be larger on hard basement rock than on alluvium sites for $T \to 0$, with the reversed trend for $T \to 10$ sec, but differ in the overall level. $|d(T)|$ in equation (1) is

larger for long periods and tends toward 0.2 depending on ζ. Its absolute values at T $\sim$ 10 sec in Figure 34 are only about 0.05 to 0.10. The consequence of this is that the period where the spectra for s = 0 cross the spectra for s = 2 is shifted towards longer periods for correlations based on (2) relative to the correlations based on (1). These differences may be related to the distribution of the available data with respect to magnitude, M, epicentral distance, R, and the Modified Mercalli Intensities at the recording stations as well as to the nature of the attenuation with distance.

d. Characteristics of the Model

Figures 35 through 44 show the SA spectra for horizontal and vertical ground motion for M.M.I. levels IV, VI and VIII, for 50% confidence level (p = 0.5) for site conditions s = 0 and 2 and for ζ = 0.00, 0.02, 0.05, 0.10 and 0.20. The spectral amplitudes for the range of M.M.I. between IV and VIII are shown in heavy lines to remind the reader of the range where most strong-motion records are available. To illustrate the trends implied by equation (2), but outside the range where equation (2) applies, the SA spectra for M.M.I. levels equal to X and XII have also been plotted using light lines. The average and average plus one standard deviation of the smooth SA spectra of digitization noise and for record durations equal to 15, 30, 60 and 100 seconds are also shown in these figures.

The expected values of the SA spectral amplitudes computed from the digitization noise (Figures 35 through 44) have been subtracted from SA spectral amplitudes prior to the regression analysis. However, for the reasons already discussed in section b of this report, not all

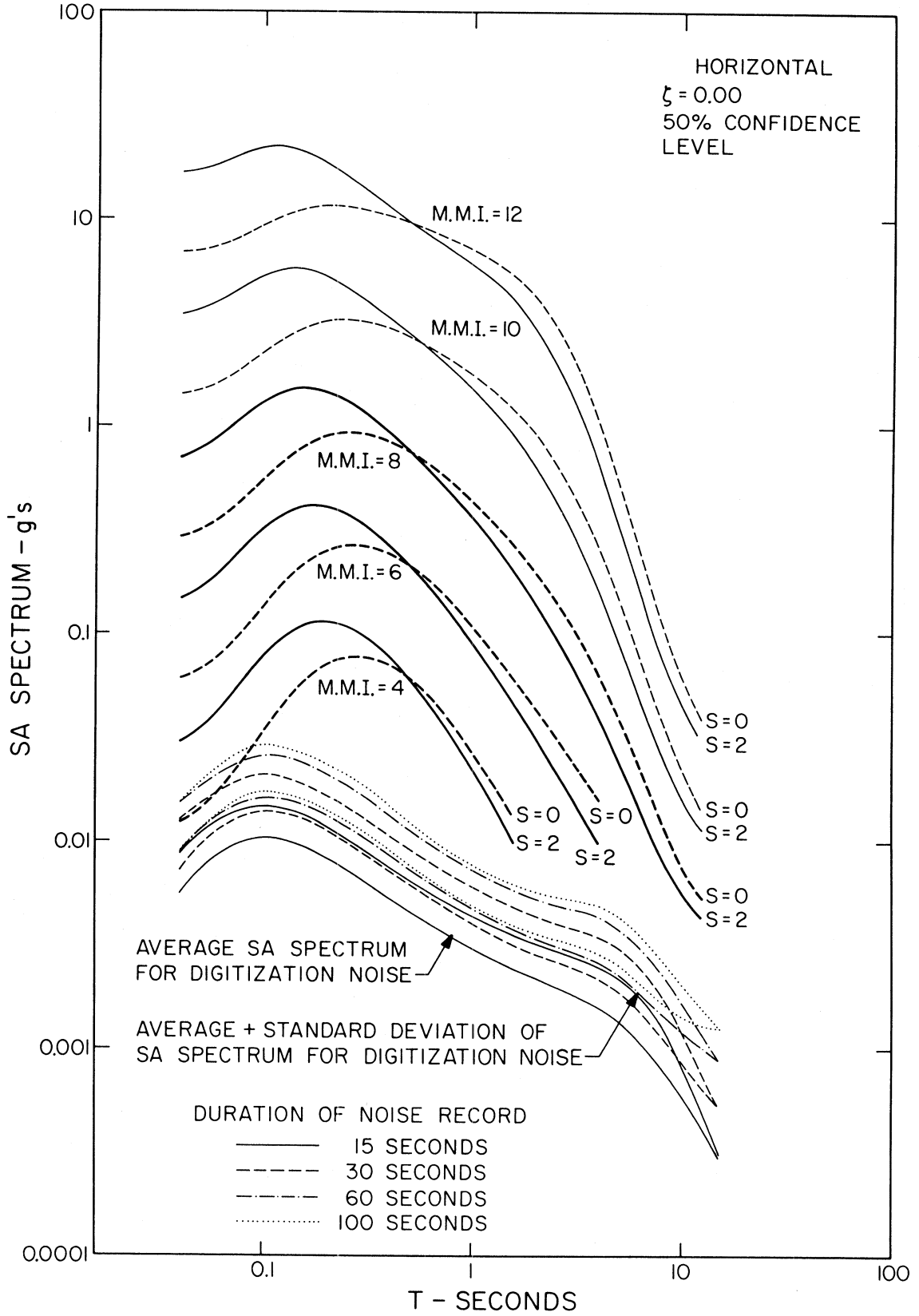
HORIZONTAL
ζ = 0.00
50% CONFIDENCE
LEVEL
M.M.I. = 12
M.M.I. = 10
M.M.I. = 8
M.M.I. = 6
M.M.I. = 4
S = 0
S = 2
AVERAGE SA SPECTRUM
FOR DIGITIZATION NOISE
AVERAGE + STANDARD DEVIATION OF
SA SPECTRUM FOR DIGITIZATION NOISE
DURATION OF NOISE RECORD
15 SECONDS
30 SECONDS
60 SECONDS
100 SECONDS
SA SPECTRUM - g's
T - SECONDS
100
10
1
0.1
0.01
0.001
0.0001
0.1
1
10
100

FIGURE 35

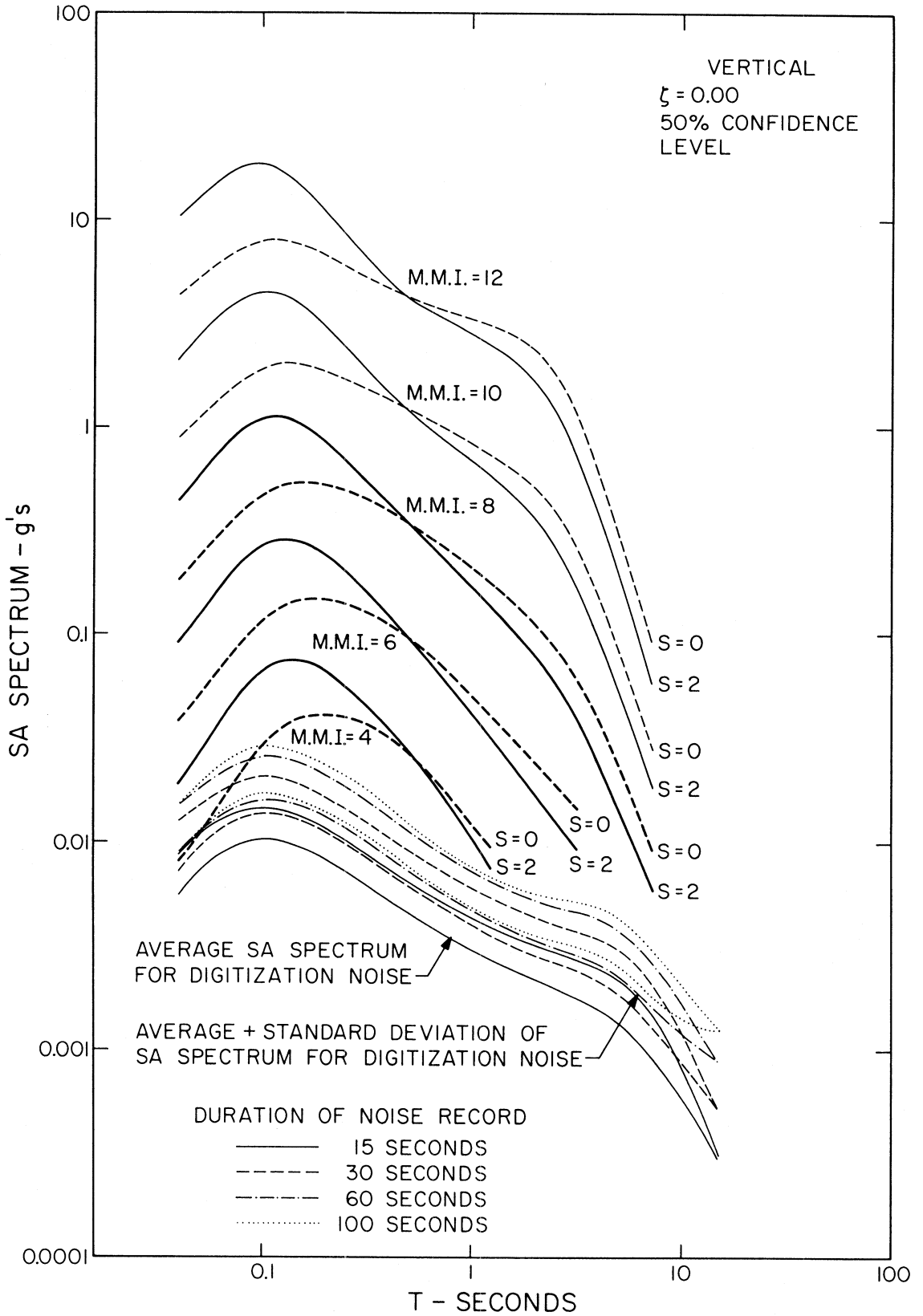
VERTICAL
ζ = 0.00
50% CONFIDENCE
LEVEL
M.M.I. = 12
M.M.I. = 10
M.M.I. = 8
M.M.I. = 6
M.M.I. = 4
S = 0
S = 2
AVERAGE SA SPECTRUM
FOR DIGITIZATION NOISE
AVERAGE + STANDARD DEVIATION OF
SA SPECTRUM FOR DIGITIZATION NOISE
DURATION OF NOISE RECORD
15 SECONDS
30 SECONDS
60 SECONDS
100 SECONDS
SA SPECTRUM - g's
T - SECONDS
100
10
1
0.1
0.01
0.001
0.0001
0.1
1
10
100

FIGURE 36

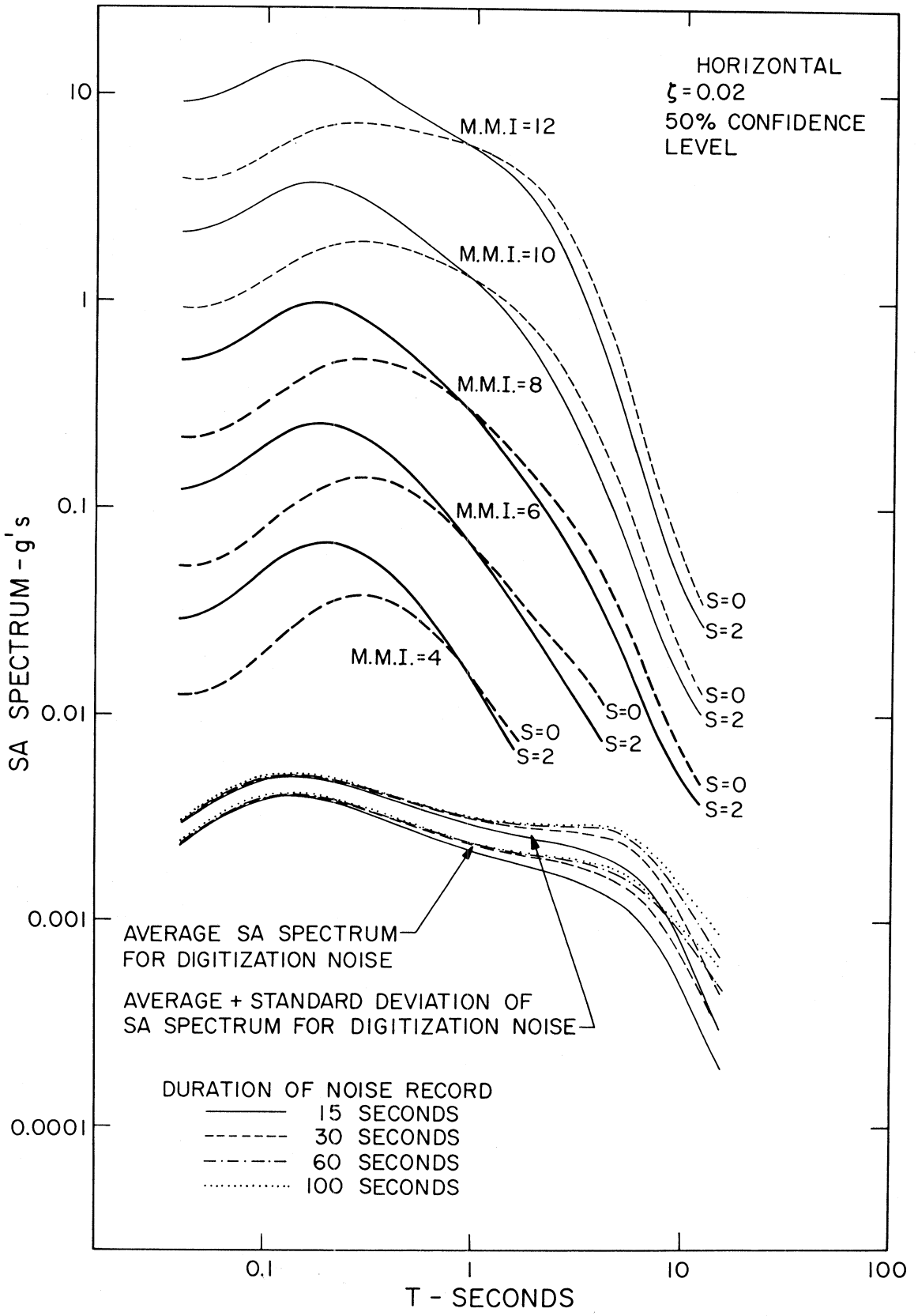
HORIZONTAL
ζ = 0.02
50% CONFIDENCE LEVEL
M.M.I=12
M.M.I.=10
M.M.I.=8
M.M.I.=6
M.M.I.=4
S=0
S=2
AVERAGE SA SPECTRUM FOR DIGITIZATION NOISE
AVERAGE + STANDARD DEVIATION OF SA SPECTRUM FOR DIGITIZATION NOISE
DURATION OF NOISE RECORD
15 SECONDS
30 SECONDS
60 SECONDS
100 SECONDS
SA SPECTRUM - g's
T - SECONDS
10
1
0.1
0.01
0.001
0.0001
0.1
1
10
100

FIGURE 37

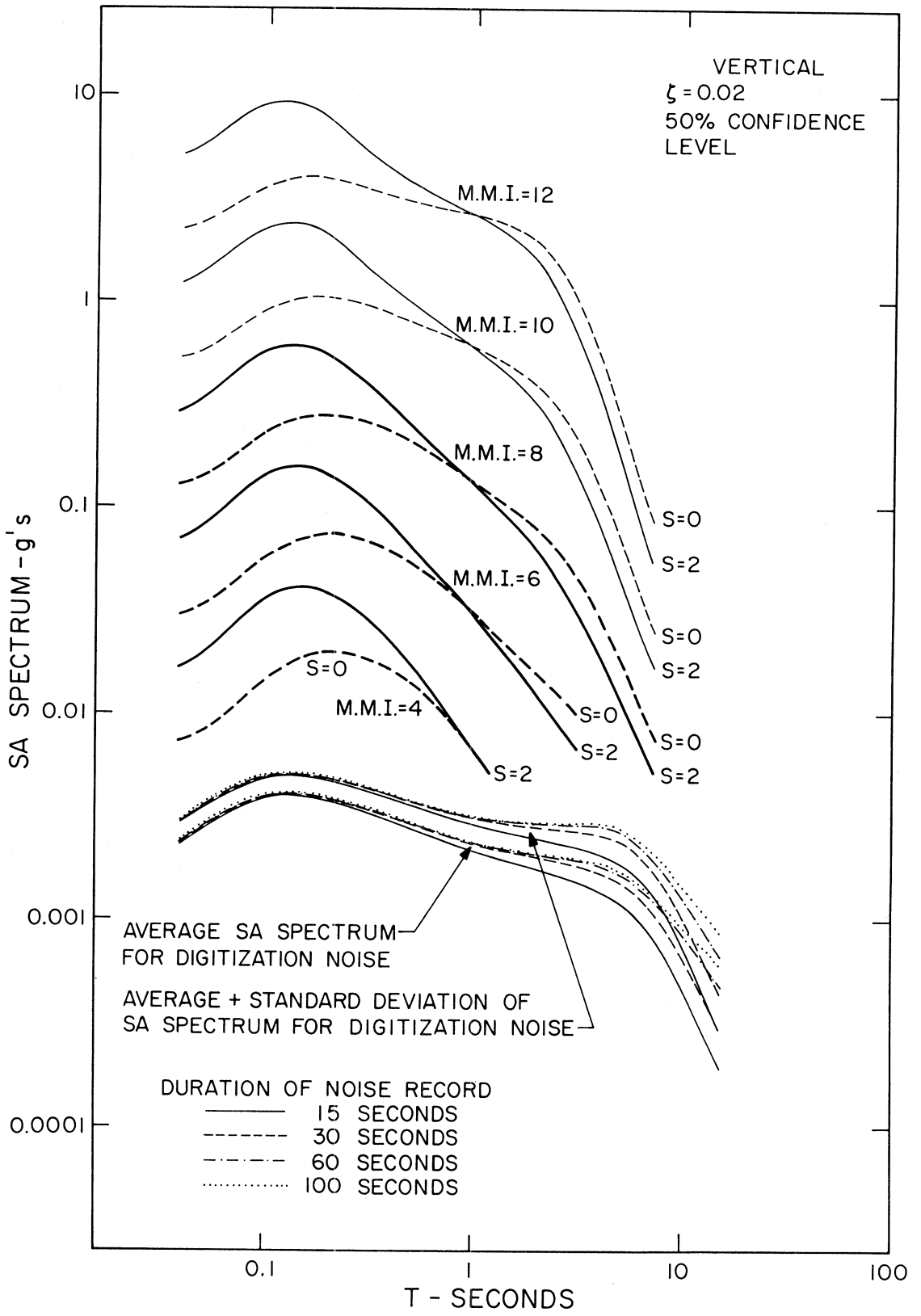
VERTICAL
ζ = 0.02
50% CONFIDENCE
LEVEL
M.M.I.=12
M.M.I.=10
M.M.I.=8
M.M.I.=6
M.M.I.=4
S=0
S=2
S=0
S=2
S=0
S=2
S=0
S=2
S=0
S=2
AVERAGE SA SPECTRUM
FOR DIGITIZATION NOISE
AVERAGE + STANDARD DEVIATION OF
SA SPECTRUM FOR DIGITIZATION NOISE
DURATION OF NOISE RECORD
15 SECONDS
30 SECONDS
60 SECONDS
100 SECONDS
SA SPECTRUM - g's
10
1
0.1
0.01
0.001
0.0001
0.1
1
10
100
T - SECONDS

FIGURE 38

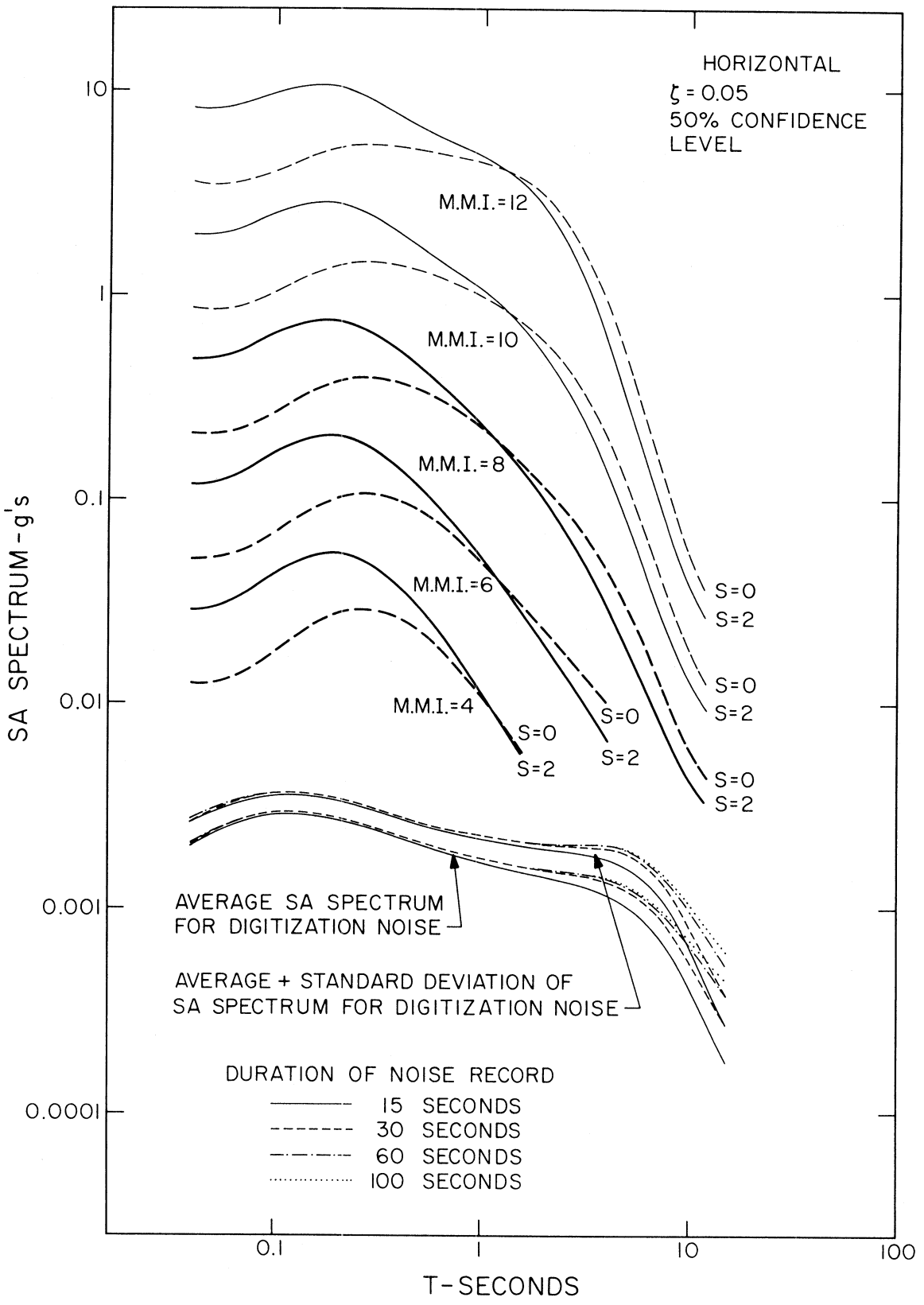
HORIZONTAL
ζ = 0.05
50% CONFIDENCE
LEVEL
M.M.I.=12
M.M.I.=10
M.M.I.=8
M.M.I.=6
M.M.I.=4
S=0
S=2
S=0
S=2
S=0
S=2
S=0
S=2
S=0
S=2
AVERAGE SA SPECTRUM
FOR DIGITIZATION NOISE
AVERAGE + STANDARD DEVIATION OF
SA SPECTRUM FOR DIGITIZATION NOISE
DURATION OF NOISE RECORD
15 SECONDS
30 SECONDS
60 SECONDS
100 SECONDS
SA SPECTRUM-g's
10
1
0.1
0.01
0.001
0.0001
0.1
1
10
100
T-SECONDS

FIGURE 39

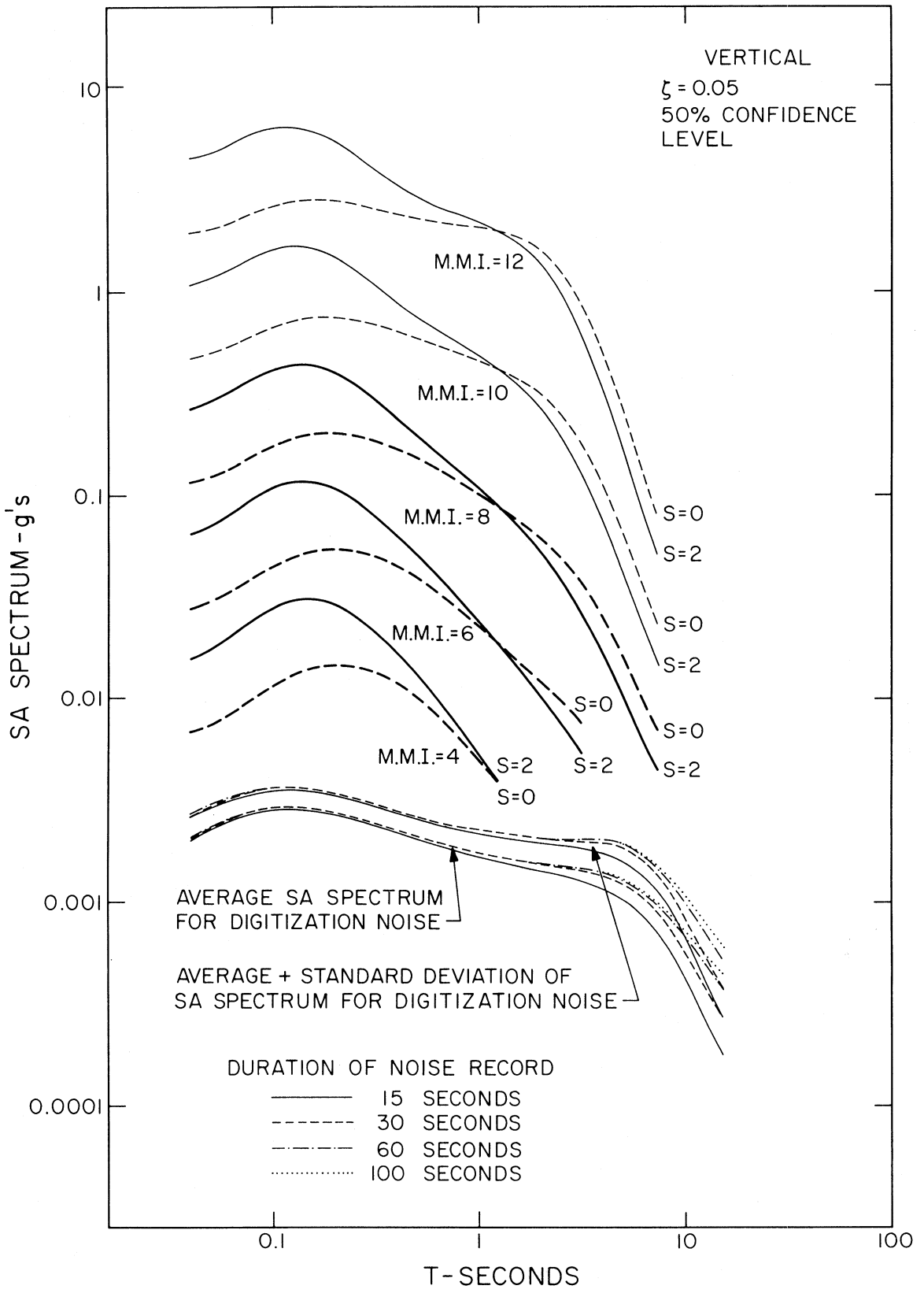
VERTICAL
ζ = 0.05
50% CONFIDENCE
LEVEL
M.M.I.=12
M.M.I.=10
M.M.I.=8
M.M.I.=6
M.M.I.=4
S=0
S=2
AVERAGE SA SPECTRUM
FOR DIGITIZATION NOISE
AVERAGE + STANDARD DEVIATION OF
SA SPECTRUM FOR DIGITIZATION NOISE
DURATION OF NOISE RECORD
15 SECONDS
30 SECONDS
60 SECONDS
100 SECONDS
SA SPECTRUM - g's
T - SECONDS
10
1
0.1
0.01
0.001
0.0001
0.1
1
10
100

FIGURE 40

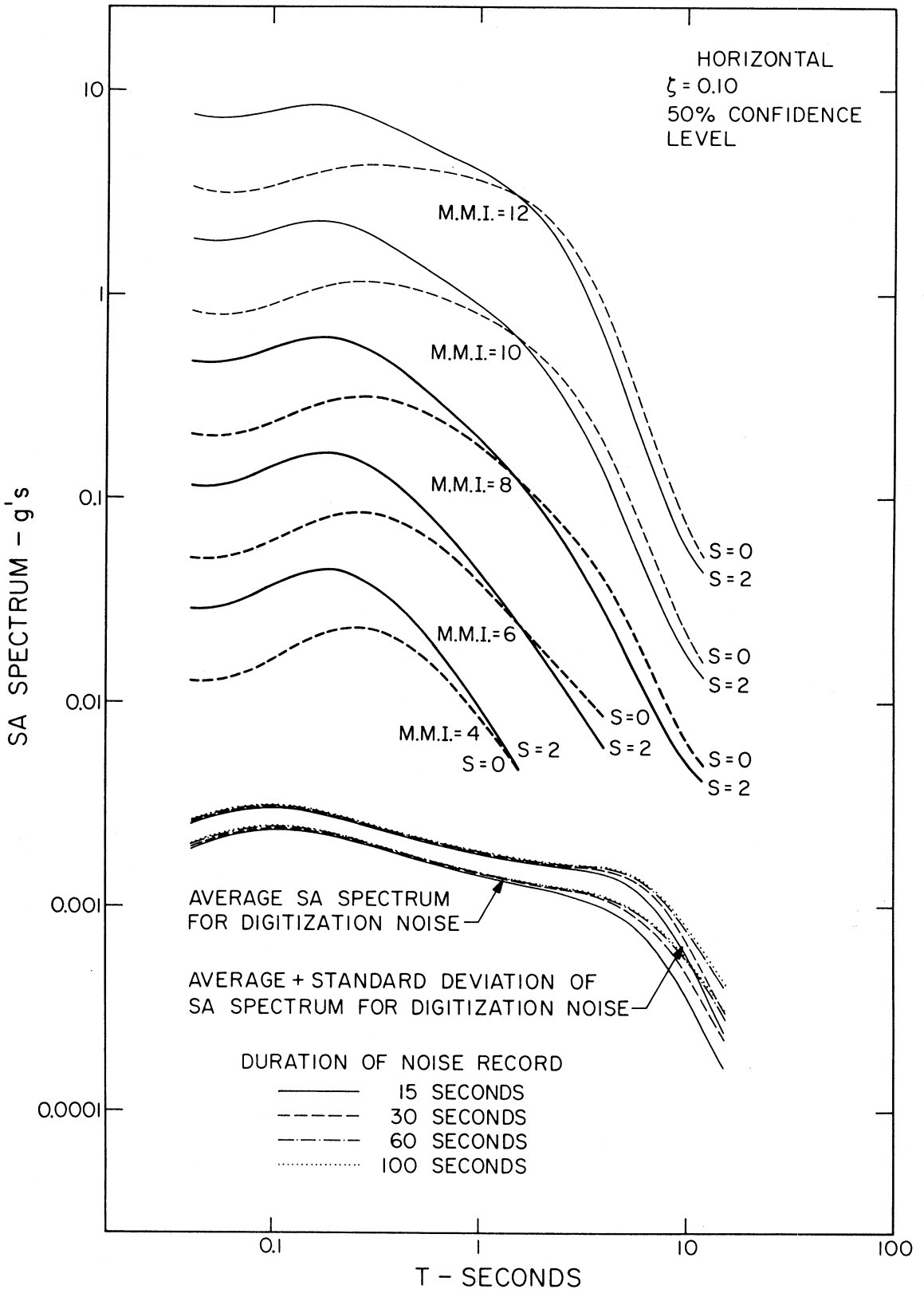
HORIZONTAL
ζ = 0.10
50% CONFIDENCE LEVEL
M.M.I. = 12
M.M.I. = 10
M.M.I. = 8
M.M.I. = 6
M.M.I. = 4
S = 0
S = 2
AVERAGE SA SPECTRUM FOR DIGITIZATION NOISE
AVERAGE + STANDARD DEVIATION OF SA SPECTRUM FOR DIGITIZATION NOISE
DURATION OF NOISE RECORD
15 SECONDS
30 SECONDS
60 SECONDS
100 SECONDS
SA SPECTRUM - g's
T - SECONDS
10
1
0.1
0.01
0.001
0.0001
0.1
1
10
100

FIGURE 41

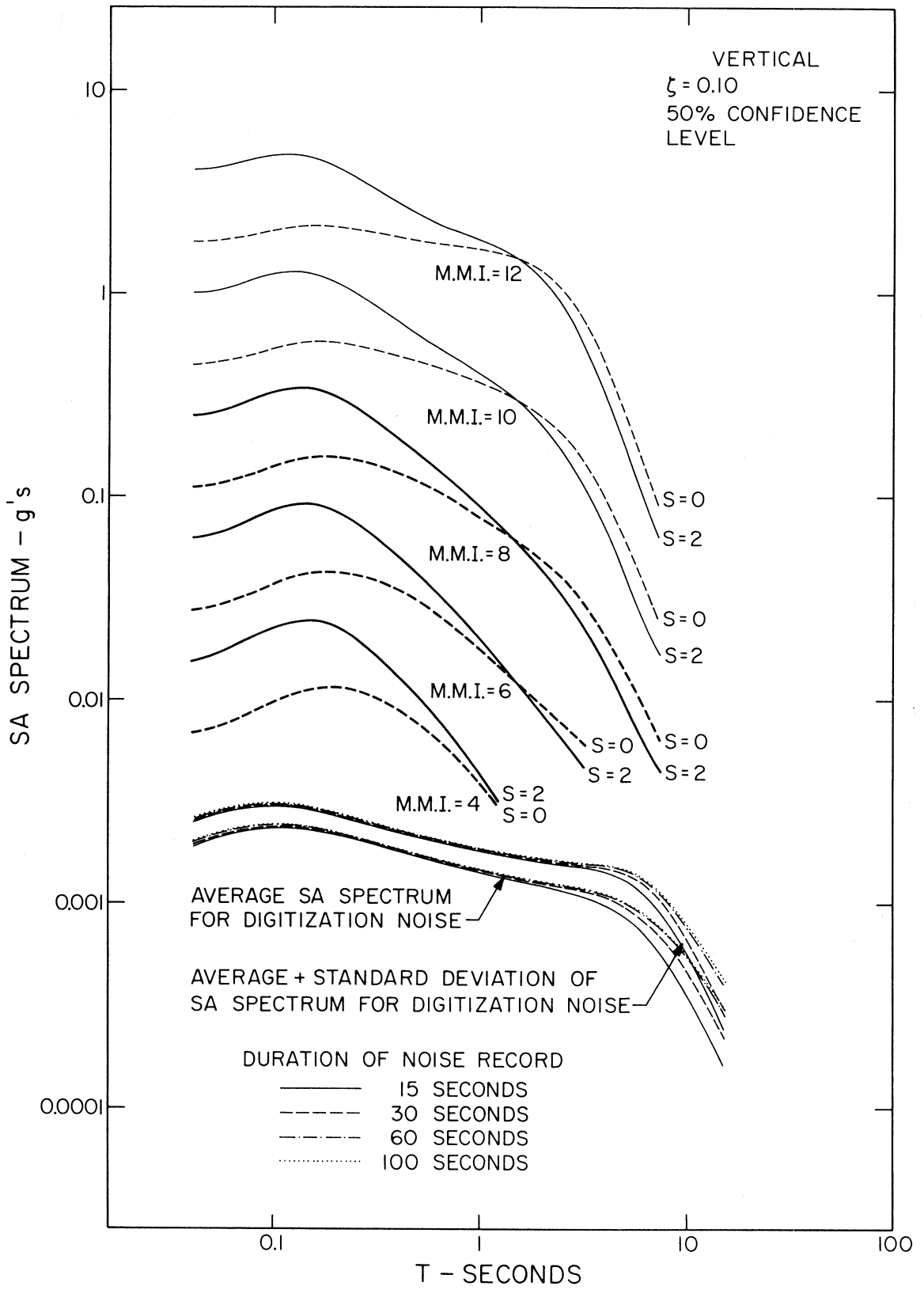
VERTICAL
ζ = 0.10
50% CONFIDENCE
LEVEL
M.M.I.= 12
M.M.I.= 10
M.M.I.= 8
M.M.I.= 6
M.M.I.= 4
S=0
S=2
S=0
S=2
S=0
S=2
S=0
S=2
S=2
S=0
AVERAGE SA SPECTRUM
FOR DIGITIZATION NOISE
AVERAGE + STANDARD DEVIATION OF
SA SPECTRUM FOR DIGITIZATION NOISE
DURATION OF NOISE RECORD
15 SECONDS
30 SECONDS
60 SECONDS
100 SECONDS
SA SPECTRUM - g's
10
1
0.1
0.01
0.001
0.0001
0.1
1
10
100
T - SECONDS

FIGURE 42

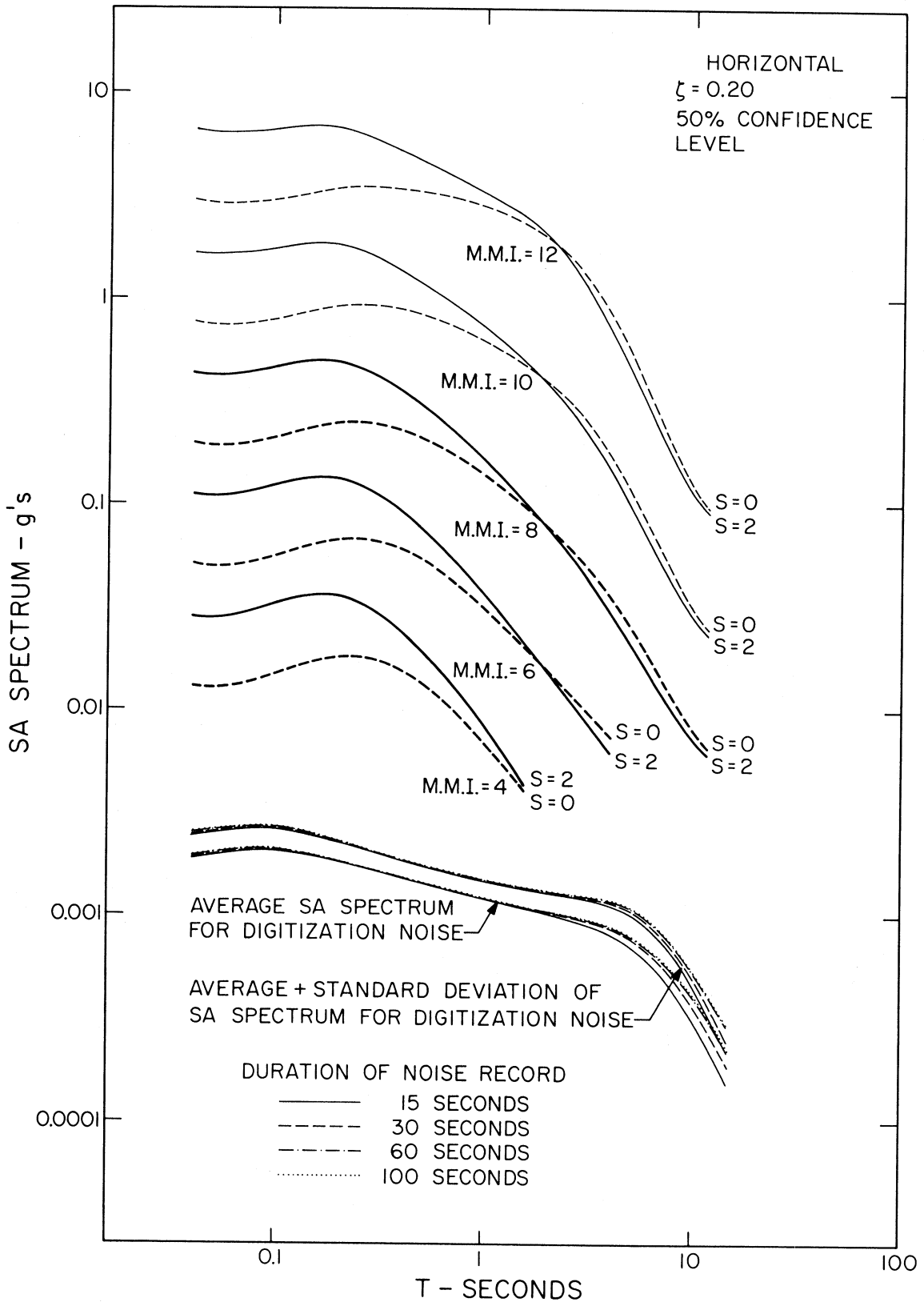
HORIZONTAL
ζ = 0.20
50% CONFIDENCE
LEVEL
M.M.I. = 12
M.M.I. = 10
M.M.I. = 8
M.M.I. = 6
M.M.I. = 4
S = 0
S = 2
S = 0
S = 2
S = 0
S = 2
S = 0
S = 2
S = 2
S = 0
AVERAGE SA SPECTRUM
FOR DIGITIZATION NOISE
AVERAGE + STANDARD DEVIATION OF
SA SPECTRUM FOR DIGITIZATION NOISE
DURATION OF NOISE RECORD
15 SECONDS
30 SECONDS
60 SECONDS
100 SECONDS
SA SPECTRUM - g's
10
1
0.1
0.01
0.001
0.0001
0.1
1
10
100
T - SECONDS

FIGURE 43

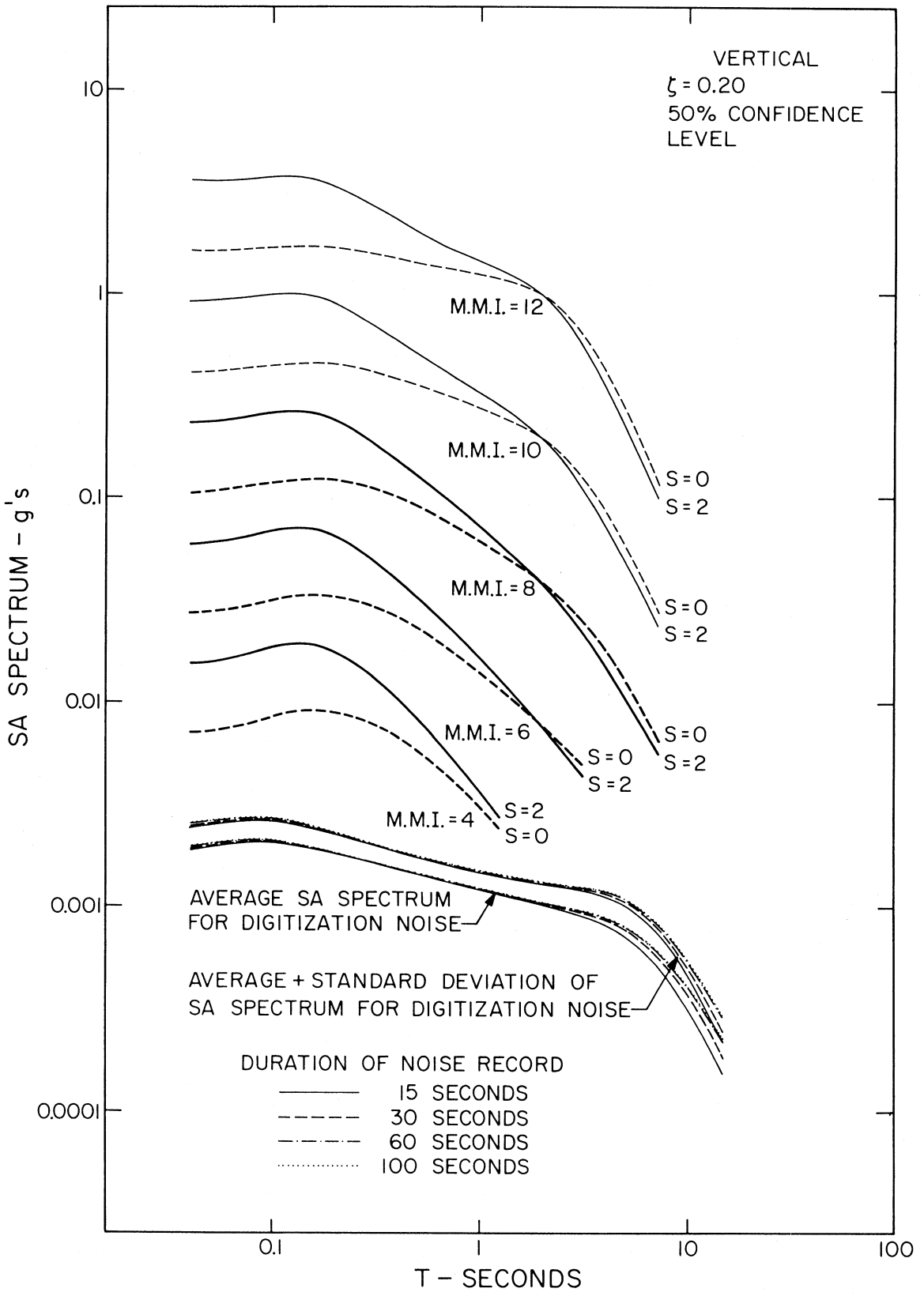
VERTICAL
ζ = 0.20
50% CONFIDENCE
LEVEL
M.M.I. = 12
M.M.I. = 10
M.M.I. = 8
M.M.I. = 6
M.M.I. = 4
S = 0
S = 2
AVERAGE SA SPECTRUM
FOR DIGITIZATION NOISE
AVERAGE + STANDARD DEVIATION OF
SA SPECTRUM FOR DIGITIZATION NOISE
DURATION OF NOISE RECORD
15 SECONDS
30 SECONDS
60 SECONDS
100 SECONDS
SA SPECTRUM - g's
10
1
0.1
0.01
0.001
0.0001
0.1
1
10
100
T - SECONDS

FIGURE 44

contributions of this noise could be eliminated from the data. Therefore, the functions b(T) and c(T), no doubt, reflect considerable noise content in the data for periods longer than about 8 seconds for M.M.I. near IV and greater. Other scaling functions a(T), d(T) and e(T) are also affected by the digitization noise but probably to a lesser degree than b(T) and c(T). Consequently, the spectra that can be computed from equation (2) and for a(T), b(T), ..., e(T) shown in Figure 34 are not accurate for the periods and intensities other than those shown in Figures 35 through 44.

Figures 45 through 50 show examples of how horizontal and vertical SA spectra computed from equation (2) compare with the spectra of recorded motions at the Pacoima Dam Site and in El Centro. These figures present SA spectra computed for p = 0.1 and 0.9, and for ζ = 0.0, 0.02, 0.05, 0.10 and 0.20. The agreement between the resulting 80 percent confidence interval and the spectra of recorded accelerograms is good at the Pacoima Dam site and worse than average for the El Centro accelerograms. Possible reasons for such discrepancies have been discussed by Trifunac (1976b).

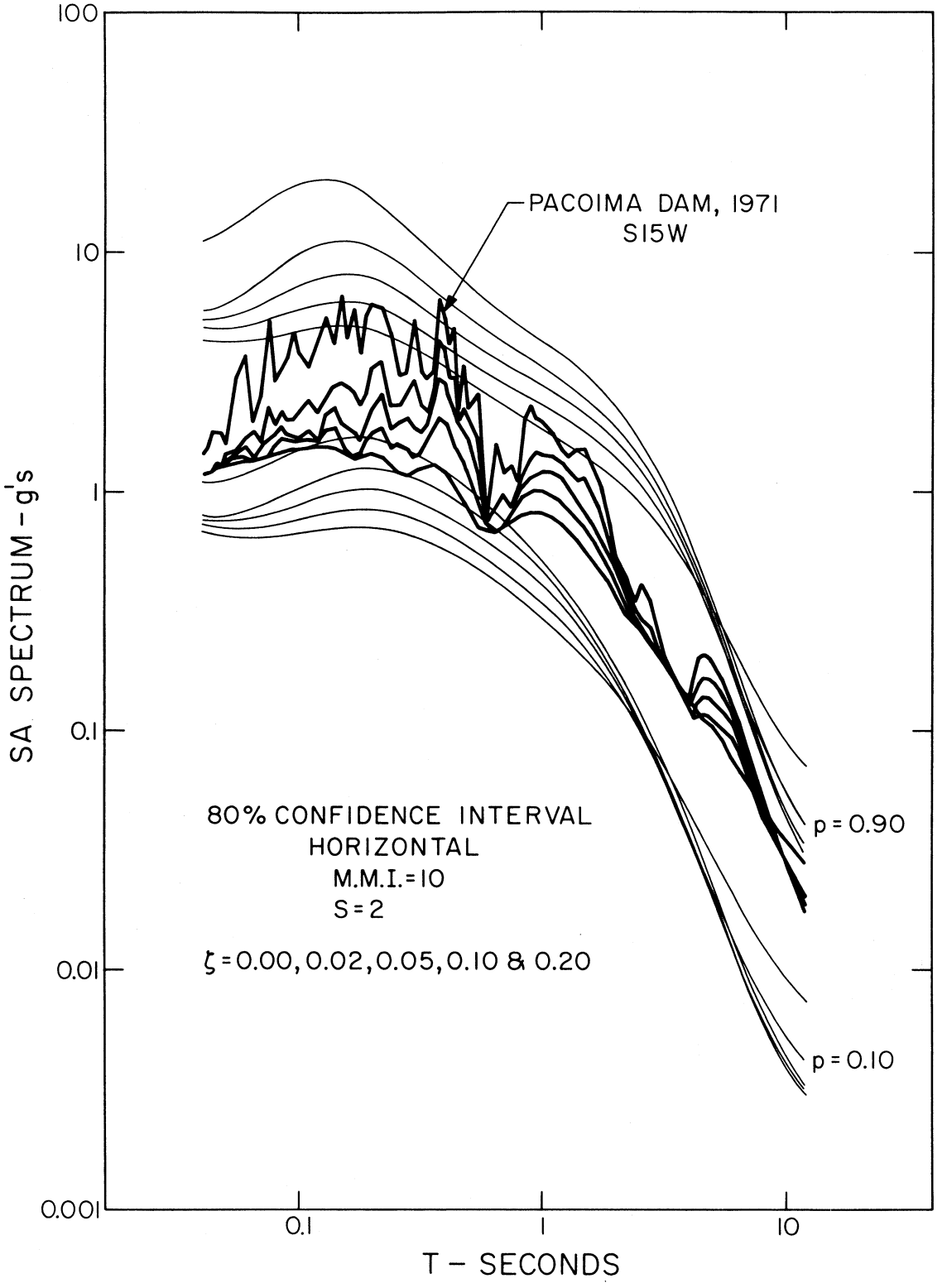
100
10
1
0.1
0.01
0.001
SA SPECTRUM - g's
PACOIMA DAM, 1971
S15W
80% CONFIDENCE INTERVAL
HORIZONTAL
M.M.I. = 10
S = 2
ζ = 0.00, 0.02, 0.05, 0.10 & 0.20
p = 0.90
p = 0.10
0.1
1
10
T - SECONDS

FIGURE 45

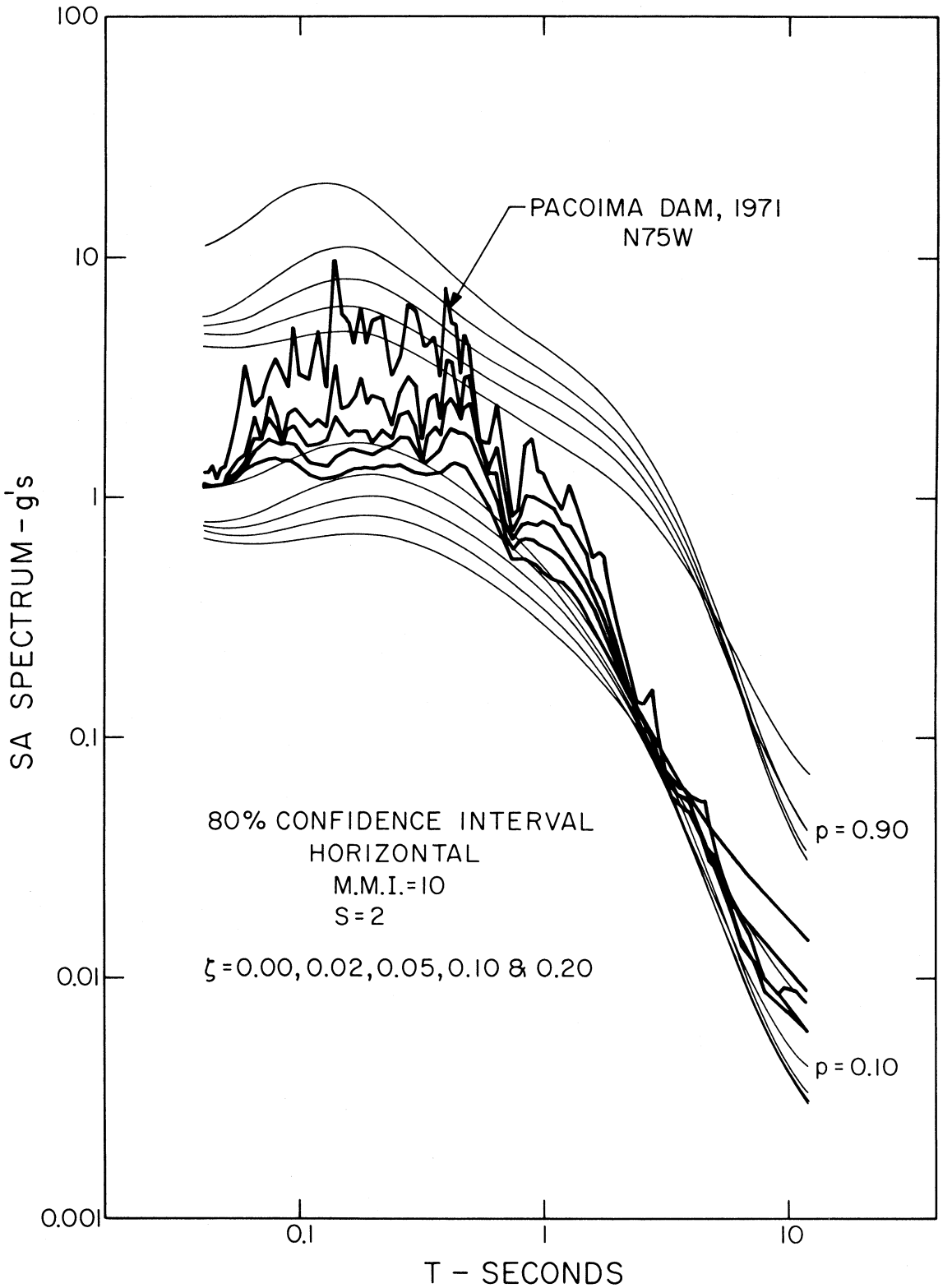
100
10
1
0.1
0.01
0.001
SA SPECTRUM - g's
PACOIMA DAM, 1971
N75W
80% CONFIDENCE INTERVAL
HORIZONTAL
M.M.I.=10
S=2
ζ=0.00, 0.02, 0.05, 0.10 & 0.20
p = 0.90
p = 0.10
0.1
1
10
T - SECONDS

FIGURE 46

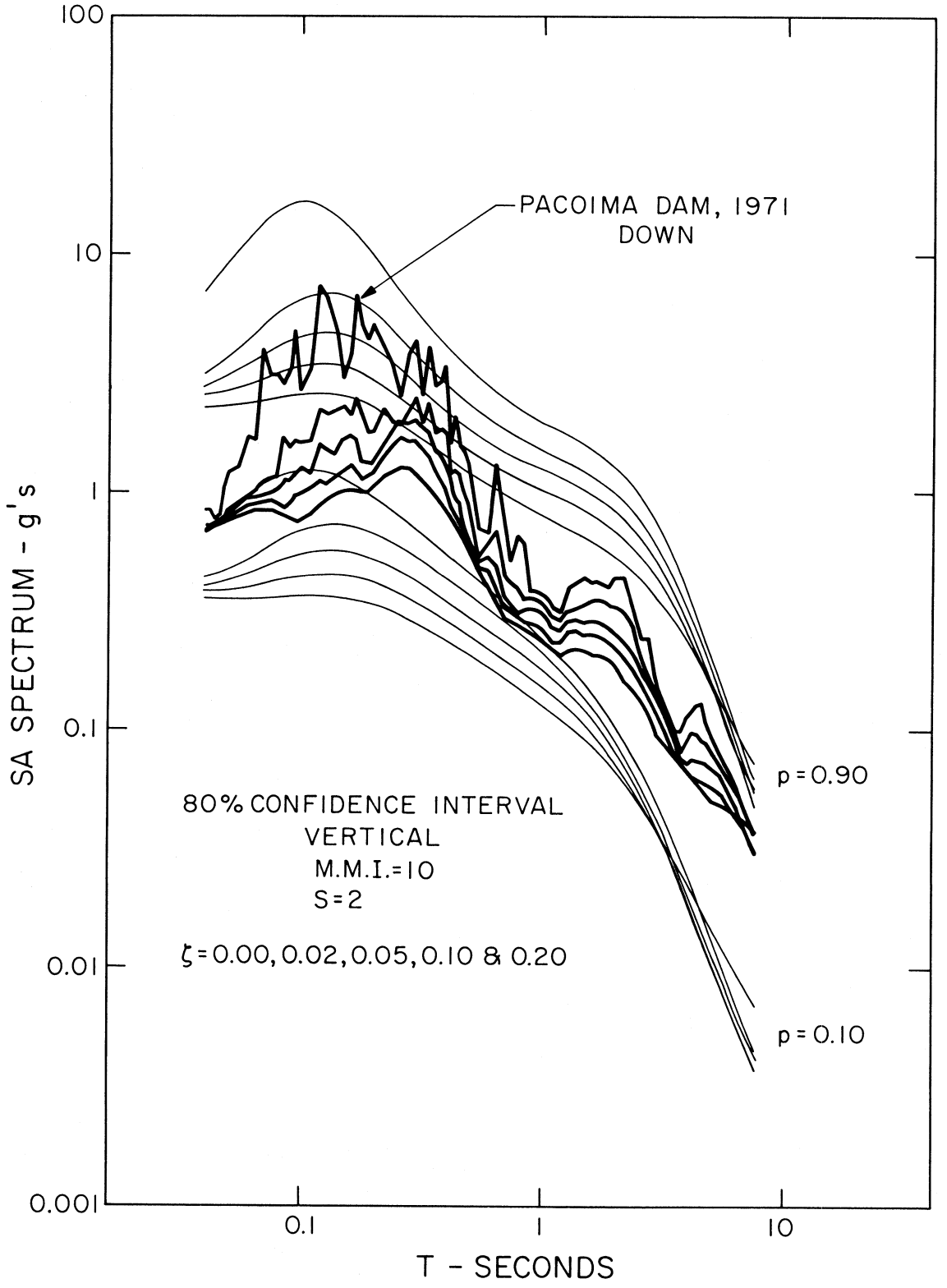
100
10
1
0.1
0.01
0.001
SA SPECTRUM - g's
PACOIMA DAM, 1971
DOWN
p = 0.90
p = 0.10
80% CONFIDENCE INTERVAL
VERTICAL
M.M.I.=10
S=2
ζ=0.00, 0.02, 0.05, 0.10 & 0.20
0.1
1
10
T - SECONDS

FIGURE 47

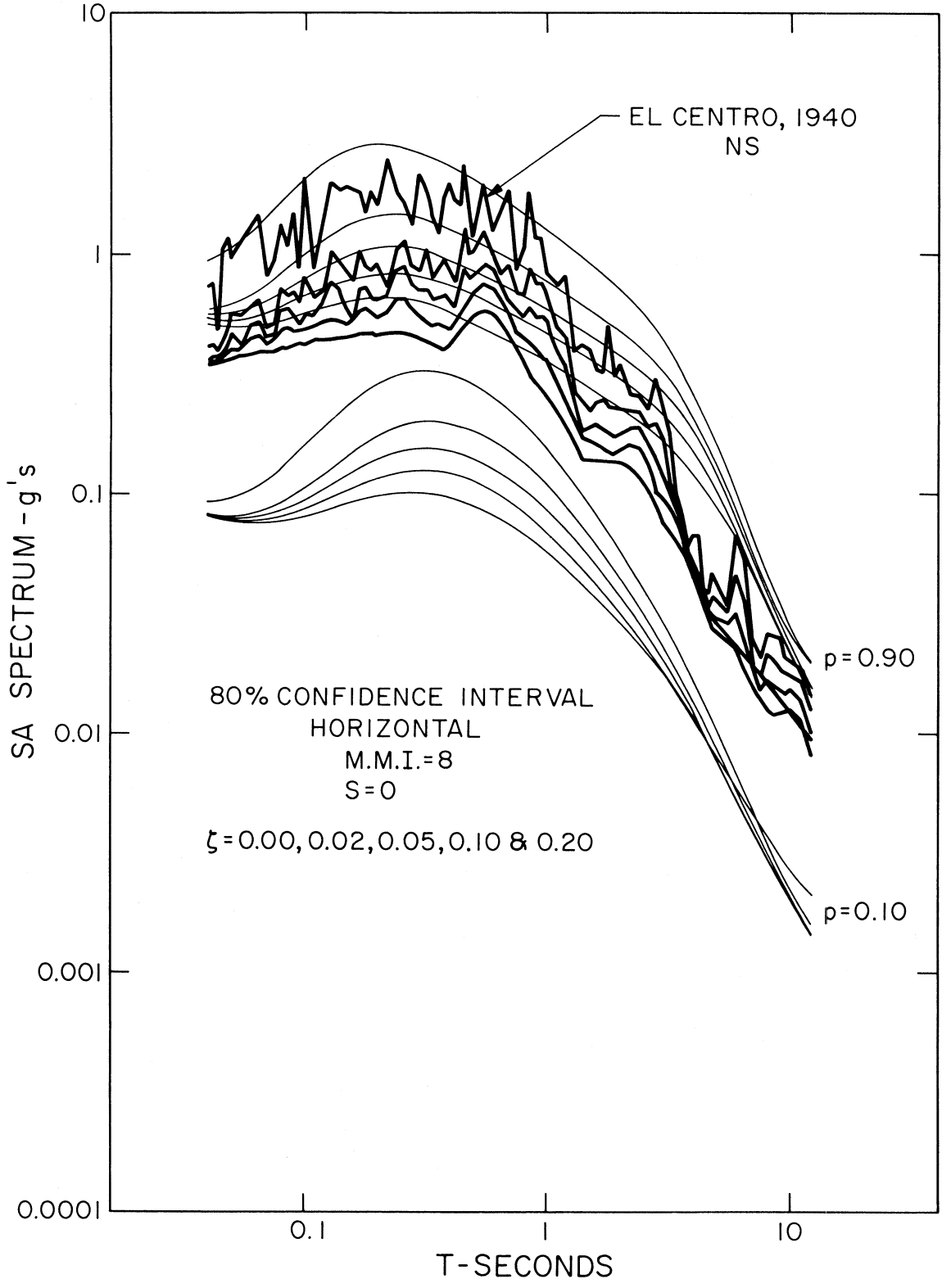
10
1
0.1
0.01
0.001
0.0001
SA SPECTRUM - g's
EL CENTRO, 1940
NS
p=0.90
p=0.10
80% CONFIDENCE INTERVAL
HORIZONTAL
M.M.I.=8
S=0
ζ=0.00, 0.02, 0.05, 0.10 & 0.20
0.1
1
10
T-SECONDS

FIGURE 48

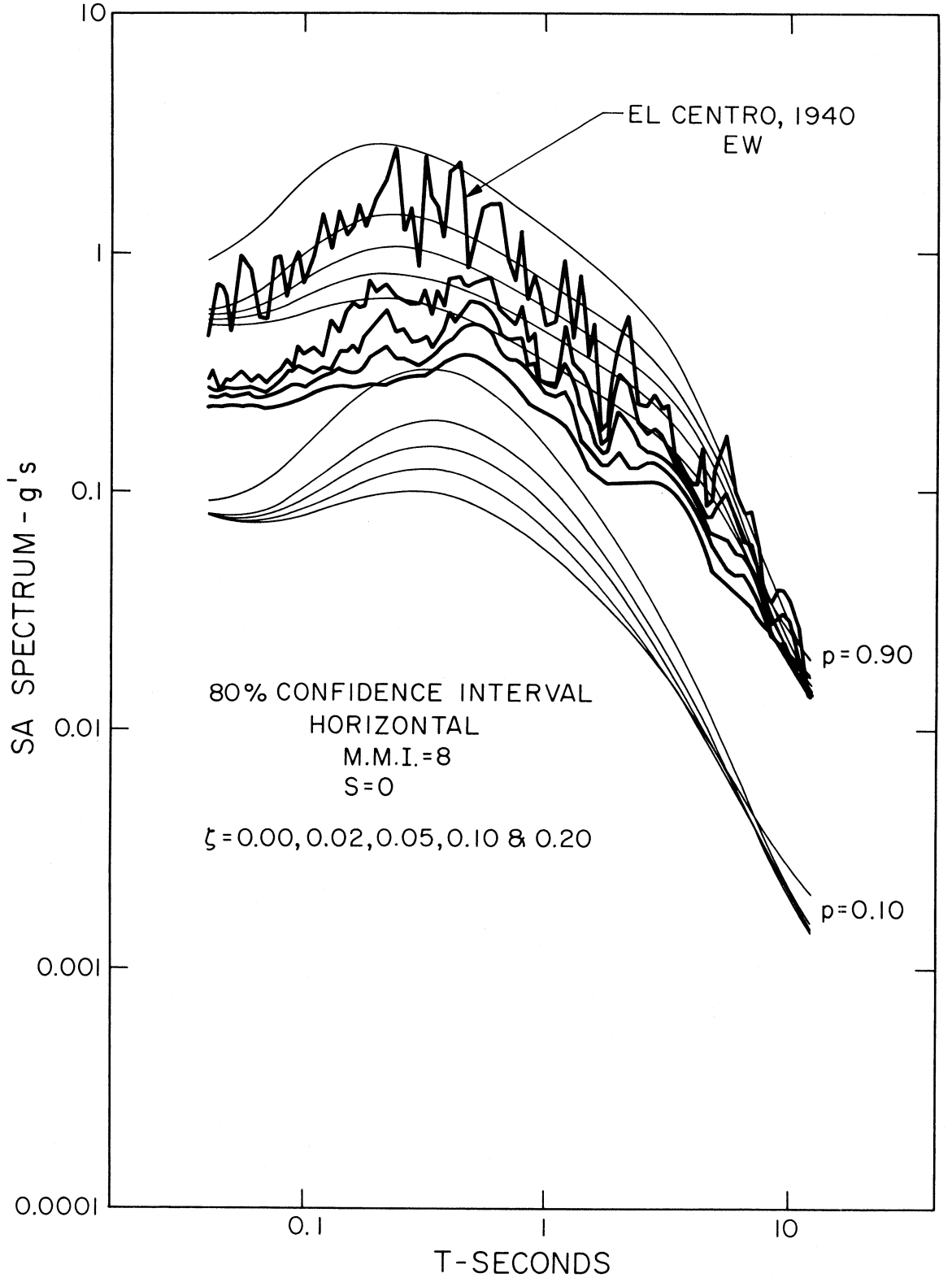
EL CENTRO, 1940
EW
p = 0.90
p = 0.10
80% CONFIDENCE INTERVAL
HORIZONTAL
M.M.I. = 8
S = 0
ζ = 0.00, 0.02, 0.05, 0.10 & 0.20
SA SPECTRUM - g's
T-SECONDS
10
1
0.1
0.01
0.001
0.0001
0.1
1
10

FIGURE 49

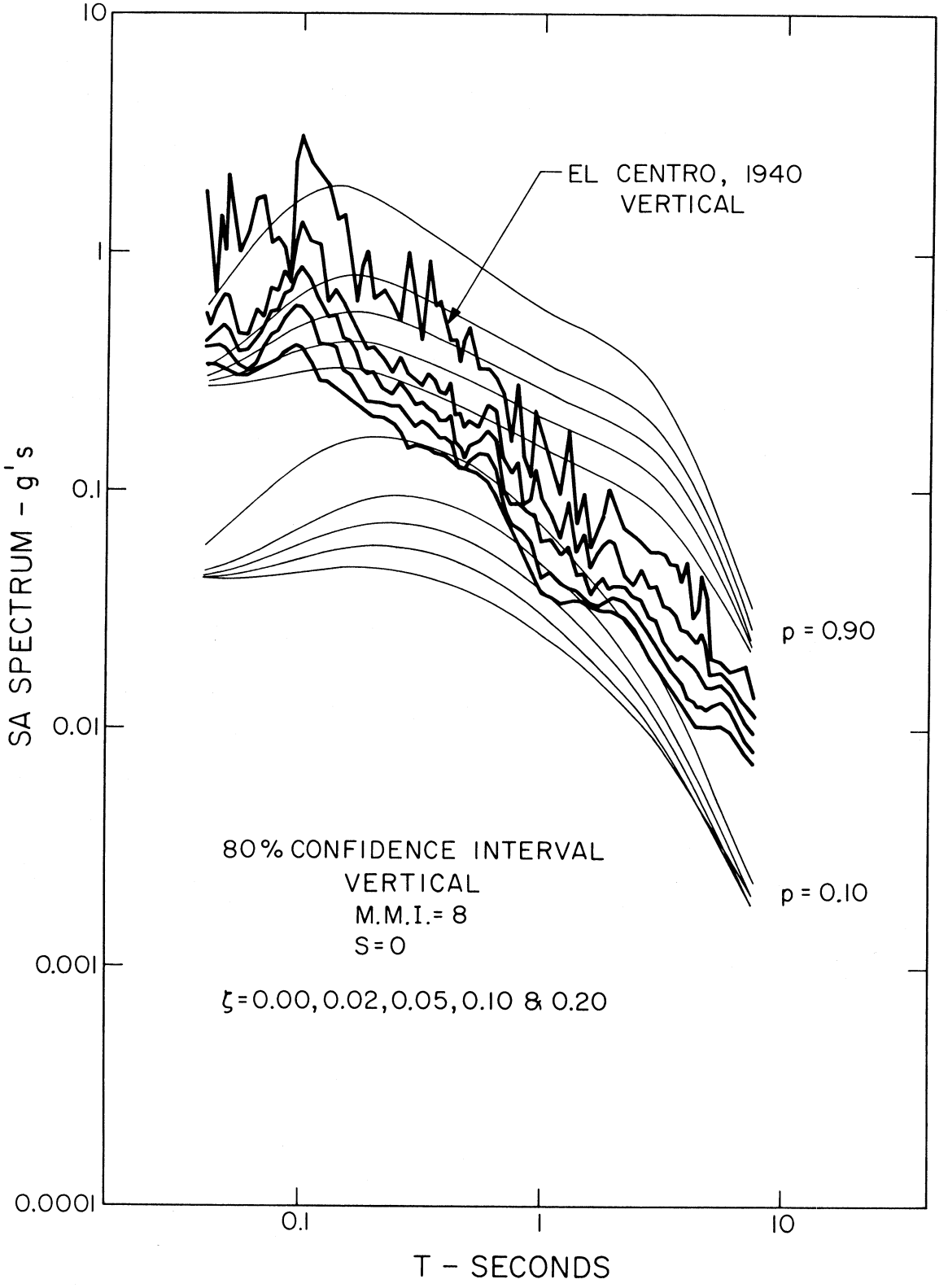
10
1
0.1
0.01
0.001
0.0001
SA SPECTRUM - g's
EL CENTRO, 1940
VERTICAL
p = 0.90
p = 0.10
80% CONFIDENCE INTERVAL
VERTICAL
M.M.I.= 8
S=0
ζ=0.00, 0.02, 0.05, 0.10 & 0.20
0.1
1
10
T - SECONDS

FIGURE 50

SOME TESTS OF THE PROPOSED EMPIRICAL SCALING FUNCTIONS

Scarcity of the recorded strong-motion accelerograms for epicentral distances less than about 20 km and for M.M.I. levels larger than VIII represents major weaknesses of the currently available data, since it is for these distances and intensity levels that strong shaking often becomes seriously damaging and needs to be scaled for earthquake resistant design purposes. Though equations (1) and (2) can be used formally to predict strong motion amplitudes in this range, there appears to be no independent reliable way of testing such estimates other than by strong motion recording during future earthquakes. In the meantime, two questions remain: (1) whether the predicted spectral amplitudes given by equations (1) and (2) are in agreement with other estimates of strong motion amplitudes based on the same data set, and (2) whether, with the scaling functions determined from the currently available data, equations (1) and (2) can be used as an interim basis for extrapolating the spectral amplitudes of strong shaking before adequate strong motion recordings become available.

It is well known that the amplitudes of absolute acceleration spectra of single-degree-of-freedom oscillators approaches the peak acceleration as the period approaches zero (e.g., Hudson et al., 1972). The required limiting conditions are not all achieved for our data set since all strong motion data used in this study have been low-pass filtered from 25 cps. However, at T = 0.04 sec, the SA amplitudes should be close to the corresponding peak accelerations. Therefore, the amplitudes of SA spectra computed from equations (1) and (2) for T = 0.04 sec should agree with the corresponding estimates of peak acceleration presented in Trifunac (1976a,c). Table IX therefore lists horizontal

TABLE IX

Comparison of SA Amplitudes for T = 0.04 sec With a Previous Estimate of Peak Acceleration

M	$\log_{10}$ of horizontal peak accelerations in g's from Trifunac (1976a) R = 0, p = 0.5, s = 0	$\log_{10}$ of horizontal spectral amplitudes for T = 0.04 sec (this study) R = 0, p = 0.5, s = 0	
		ζ = 0.00	ζ = 0.20
7.5	0.29	0.25	0.31
6.5	0.10	0.07	0.05
5.5	-0.46	-0.44	-0.45
4.5	-1.37	-1.16	-1.21

MMI	$\log_{10}$ of horizontal peak accelerations in g's from Trifunac (1976c) s = 0, p = 0.5	$\log_{10}$ of horizontal sepctral amplitudes for T = 0.04 sec (this study) p = 0.5, s = 0	
		ζ = 0.0	ζ = 0.20
(XII)	0.43	0.84	0.47
(X)	-0.16	0.16	-0.11
VIII	-0.74	-0.53	-0.70
VI	-1.33	-1.21	-1.29
IV	-1.91	-1.91	-1.88

peak accelerations computed for M = 4.5, 5.5, 6.5 and 7.5, as well as for M.M.I. levels IV, VI, VIII, X, and XII, for R = 0, p = 0.5 and s = 0, calculated from Trifunac (1976a,c). It also gives the range of absolute acceleration spectral amplitudes which is spanned by $\zeta = 0.0$ to $\zeta = 0.20$ at T = 0.04, using the correlations in this paper, for the same set of conditions. In light of the constraints which limit this type of comparison, Table IX shows that these estimates are in fair agreement.

Two facts related to the data processing methods used in this study differ when compared with the regression analyses in Trifunac (1976a) and Trifunac (1976c) and should be kept in mind when interpreting the comparison in Table IX. First the data of Trifunac (1976a) which was used in the derivation of the regression equation for computing peak accelerations contains some contributions from the digitization noise. In the processing of SA spectral amplitudes and in the derivation of a(T), b(T), ... for equation (1) (Figure 6) and (2) (Figure 34), average digitization noise was subtracted from spectral amplitudes. Second, the functions a(T), b(T), ... in Figures 6 and 34 have been smoothed by means of an Ormsby filter along $\log_{10}T$ axis. Although this has resulted in smoothing of spectral amplitudes, as computed from equations (1) and (2), this possibly introduced some distortion of the final spectral amplitudes as a result of the data processing assumption required to carry out digital filtering at the end of the data set (T = 0.04 sec). More precise comparison of SA amplitudes and the corresponding peak accelerations based on this and our previous studies are, of course, possible. One way to do this would be to use the actual distribution function of SA about the models (1) and (2) and about the corresponding models for

peak accelerations. We consider this approximate comparison in Table IX to be acceptable and postpone the discussion of actual probability distribution of spectral amplitudes for the later section of this report.

Next we examine the degree to which the models presented by equations (1) and (2) are mutually compatible in the epicentral distance range and for M.M.I. levels which lie beyond the range where the strong-motion data is now available. In particular, we compare the largest amplitudes of shaking which are predicted by the two models. Although there is no reason to expect the two models to agree in this respect, if they do we may be more confident that both are reasonable.

To this end we will assume that the Modified Mercalli Intensity XII represents the largest possible level of strong shaking. Then we compare the amplitudes predicted by equation (1) for R = 0 and for the largest recorded magnitude, say $M \approx 8.5$, with the amplitudes predicted by equation (2) and for M.M.I. equal to XII. Such comparison depends on a number of simplifying assumptions required for the derivation of equations (1) and (2). One of the most critical and most arbitrary assumptions in this respect is that it is permissible to assign numerical values ranging from 1 to 12 to the qualitative and descriptive categories of the M.M.I. scale. While some previous studies have suggested that this may be permissible for approximate correlations (Trifunac, 1976c) the limitations resulting from this assumption should be kept in mind.

Figures 51 and 52 present horizontal and vertical acceleration spectra for M = 8.5, R = 0 and s = 1, for ζ = 0.00, 0.02, 0.05, 0.10 and 0.20 and for M.M.I. level equal to XII. Spectral amplitudes computed

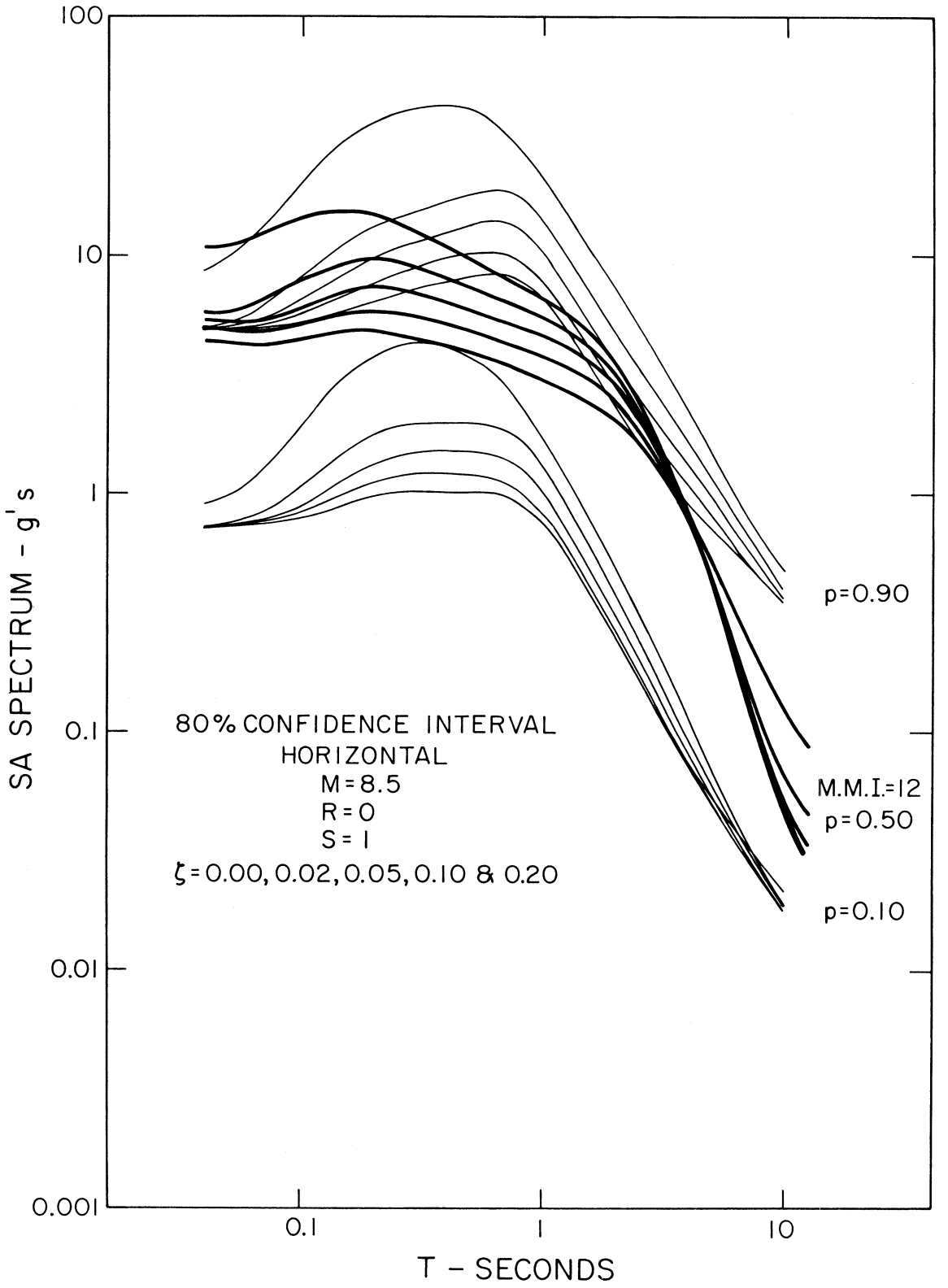
100
10
1
0.1
0.01
0.001
SA SPECTRUM - g's
0.1
1
10
T - SECONDS
80% CONFIDENCE INTERVAL
HORIZONTAL
M=8.5
R=0
S=1
ζ=0.00, 0.02, 0.05, 0.10 & 0.20
p=0.90
M.M.I.=12
p=0.50
p=0.10

FIGURE 51

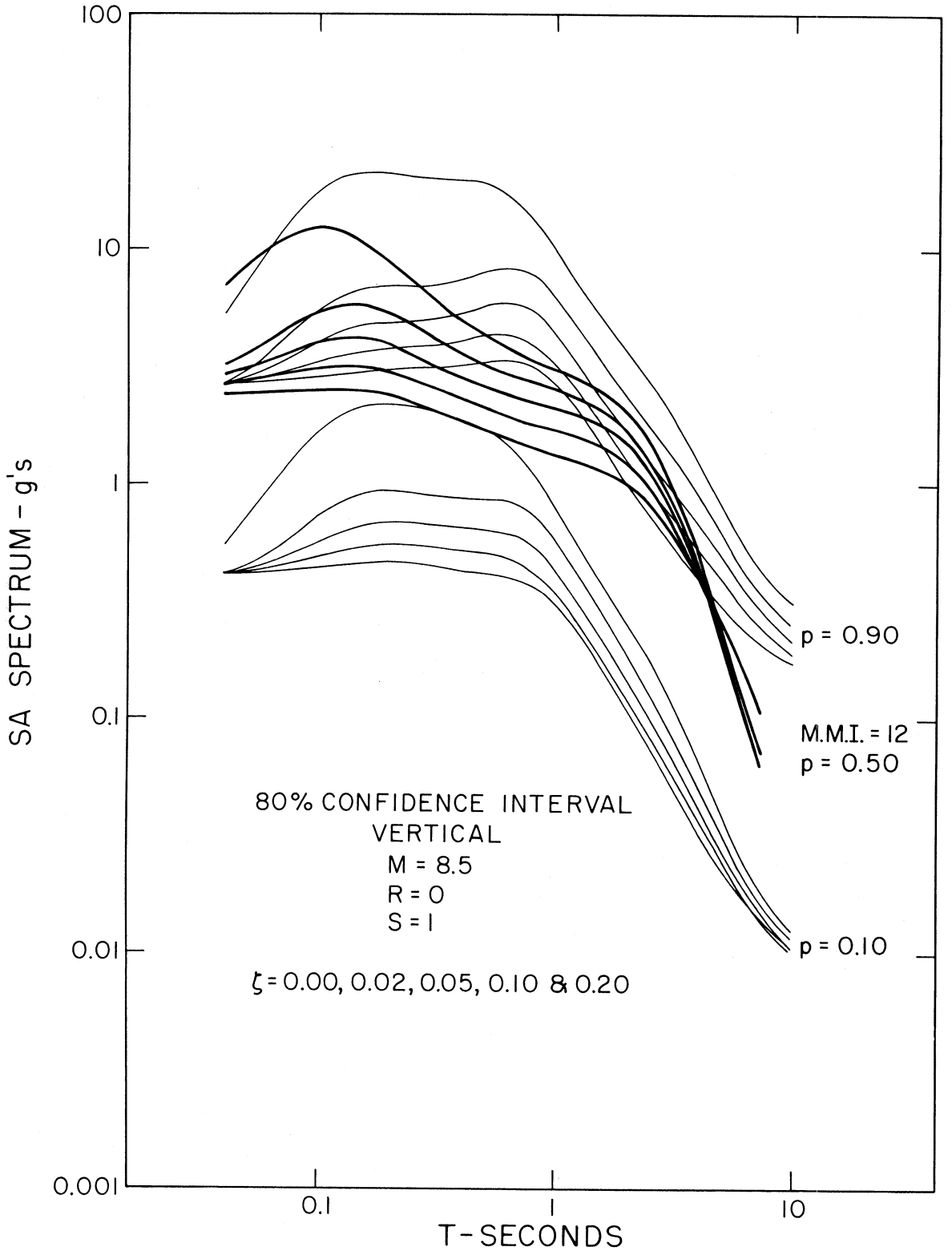
100
10
1
0.1
0.01
0.001
SA SPECTRUM - g's
0.1
1
10
T-SECONDS
p = 0.90
M.M.I. = 12
p = 0.50
p = 0.10
80% CONFIDENCE INTERVAL
VERTICAL
M = 8.5
R = 0
S = 1
ζ = 0.00, 0.02, 0.05, 0.10 & 0.20

FIGURE 52

from equation (1) are shown in light lines and for p = 0.1 and 0.9 while the spectra for M.M.I. of XII are shown with heavy lines for p = 0.50. The amplitude range between p = 0.1 and 0.9 then approximates the 80% confidence interval for M = 8.5, R = 0 and s = 1. These figures show that the average spectral amplitudes for M.M.I. equal to XII are in fair agreement with the model described by equation (1). Only for frequencies higher than about 10 cps the SA amplitudes seem to be overestimated by the linear functional form of equation (2). In our previous work (Trifunac, 1976c) dealing with peak accelerations we found that the parabolic regression does fit this type of comparison somewhat better than the linear regression (see Table IX of Trifunac, 1976c). However, the small contribution of the second order term in I_{MM} did not appear to be significant for the range between M.M.I. levels IV and VIII where most of the presently available data are distributed, and thus did not warrant the use of parabolic regression with respect to I_{MM} in this work.

When inspecting Figures 51 and 52 it should be kept in mind that the extrapolation range of equation (2) which is displayed there is equal to four intensity units on the assumed linear scale of M.M.I. levels. When it is further recognized that the available strong-motion data hardly covers the range from IV to VIII, also representing only four intensity levels, it becomes clear that the extrapolations presented in those figures for M.M.I. equal to XII are highly uncertain and cannot be accepted on the basis of equation (2) alone. On the other hand, the estimates of the largest SA amplitudes at R = 0 for a magnitude 8.5 earthquake might be somewhat more reliable since as is suggested by the physical nature of the near field shaking (Trifunac,

1973), and by the regression equation (1), the amplitudes of strong shaking seem to be only weakly dependent on earthquake magnitude (source dimension) for sufficiently large magnitudes and close to the source. Therefore, if one is willing to assume that the estimates of largest SA amplitudes in Figures 51 and 52 for M = 8.5 and R = 0 are plausible, then one should also suppose that the regression equation (2) does have approximately correct rate of growth with respect to the linear I_{MM} axis. Hence, this would also imply that the SA amplitude extrapolated from equation (2) and for I_{MM} greater than VIII may yield the estimates of spectral amplitudes which should not be too different from future, more reliable inferences.

DISTRIBUTION OF SPECTRAL AMPLITUDES

Relationship of P_a to P_ℓ

As noted earlier, the regression analyses in terms of equations (1) and (2) have been performed by using a correlation function which is linear in the so called confidence level, p, of not exceeding the spectral amplitude. It was pointed out that p is not a probability, but that the regression is done so that p will approximate the probability of not exceeding $SA(T)_p$ when $0.1 < p < 0.9$. To test the extent that this assumption is reasonable and to partially describe the actual distribution, Figures 53 and 54 present the fraction of data points which are smaller than the spectral amplitude predicted for 9 values of the confidence level (p). The procedure used to obtain this information is described in more detail in Trifunac (1976b).

Here we shall change notation and call the confidence level, p, in equations (1) and (2) by P_ℓ. If equations (1) or (2) are solved for P_ℓ, then it is clear that for some combinations of SA, M and R or MMI), s and v, P_ℓ can be less than zero or greater than 1. Next we will denote by P_a that fraction of data points less than the spectral amplitude associated with P_ℓ. The parameter P_a, then, is the empirically determined probability that $SA(T)_{P_\ell}$ will not be exceeded. Figures 53 and 54 show P_a as a function of period for 9 values of P_ℓ.

For some applications of the correlations (1) and (2), such as to seismic risk, for example, it is convenient to have a functional description of the relationship between P_a and P_ℓ. Anderson and Trifunac (1977) derived a functional relationship of this natrue for the distribution of Fourier spectral amplitudes. The object in this section is to find such a functional relationship for SA. Because we seek this

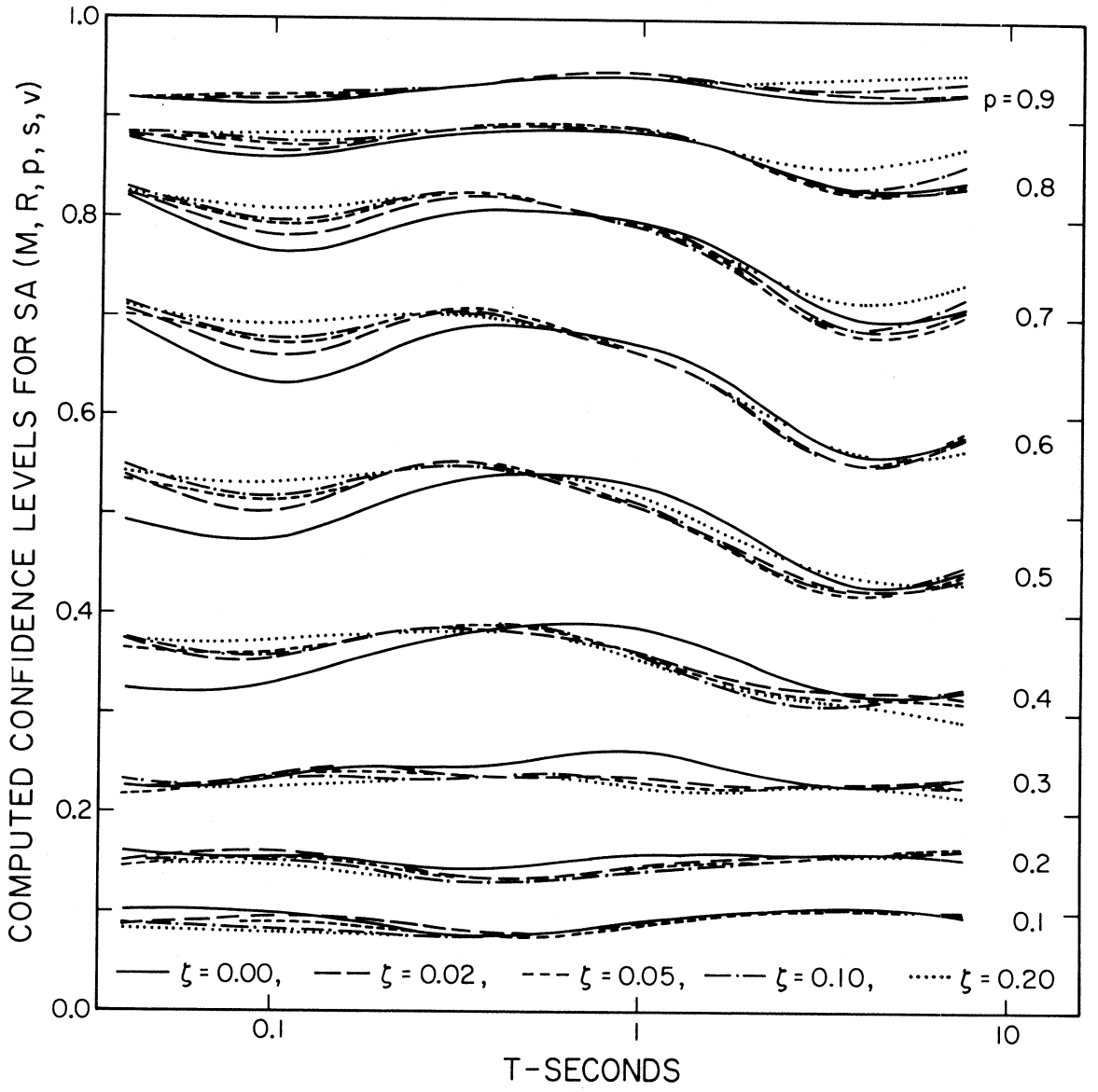
COMPUTED CONFIDENCE LEVELS FOR SA (M, R, p, s, v)
1.0
0.8
0.6
0.4
0.2
0.0
0.1
1
10
T-SECONDS
p = 0.9
0.8
0.7
0.6
0.5
0.4
0.3
0.2
0.1
ζ = 0.00, ζ = 0.02, ζ = 0.05, ζ = 0.10, ζ = 0.20

FIGURE 53

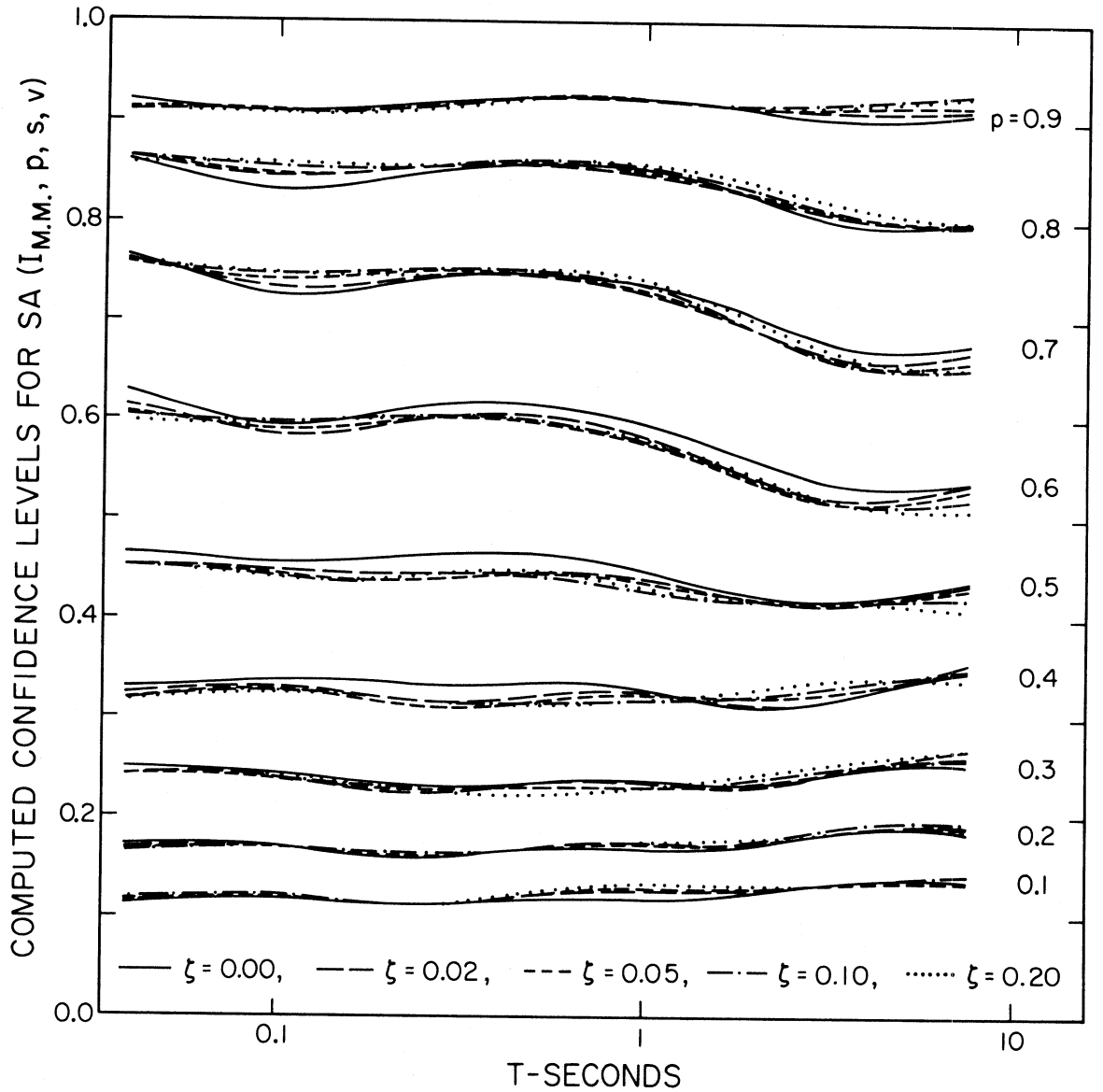
COMPUTED CONFIDENCE LEVELS FOR SA ($I_{M.M.}$, p, s, v)
1.0
0.8
0.6
0.4
0.2
0.0
0.1
1
10
T-SECONDS
p = 0.9
0.8
0.7
0.6
0.5
0.4
0.3
0.2
0.1
ζ = 0.00, ζ = 0.02, ζ = 0.05, ζ = 0.10, ζ = 0.20

FIGURE 54

relationship only as a convenience for future applications, the main criteria to be satisfied will be that it is consistent with the data points. An additional criteria will be that the function should physically be meaningful.

Anderson and Trifunac (1977) used a Gaussian distribution to relate P_a to P_ℓ for the Fourier amplitude spectrum. At the same time, they noted that a Gaussian distribution may not work for other spectra. Indeed, preliminary calculations for SA demonstrated that a Gaussian distribution is not satisfactory.

The statistics of random processes suggest a physical basis for a distribution of P_a vs. P_ℓ. The probability distribution of the maxima of a stationary random time series is a distribution which in the limit reduces to a Gaussian or to a Rayleigh distribution, depending on whether the parameter ε, which measures the width of the spectrum, is equal to 1 or to 0 (see, e.g., Udwadia and Trifunac, 1973). In particular, for a narrow frequency band process such as a response of a single-degree-of-freedom system with a small damping, the peak response amplitudes should be nearly Rayleigh distributed. If r is the peak amplitude, if $\bar{a}$ is the root mean square of the peak amplitudes ($\bar{a} = \frac{1}{N}\{a_1^2 + a_2^2 + \ldots + a_N^2\}^{\frac{1}{2}}$, where a_i are the amplitudes of N consecutive peaks), and if there are N peaks in the response of an oscillator to the strong shaking, then the probability that all the peaks have amplitude $a_i \leq r$ is

$$P\{a_i \leq r\} = \left[1 - e^{-\left(\frac{r}{\bar{a}}\right)^2}\right]^N \qquad (3)$$

For our application, r corresponds to the response spectral amplitude at one period, SA(T). Furthermore, as discussed in detail by

Anderson and Trifunac (1977), $P_a = P\{\text{all } a_i \leq r\}$. By replacing r with SA(T) in equation (3), and then substituting for SA(T) from equations (1) or (2), one obtains an equation of the form

$$P_a(T) = \left[1 - \exp(-e^{\alpha(T)P_\ell + \beta(T)})\right]^{N(T)} . \qquad (4)$$

All the terms depending on magnitude and distance (or intensity), and site conditions have been combined with the term in $\bar{a}$ to give $\alpha(T)$ and $\beta(T)$.

Careful attention to the step used in obtaining (4) yields a result in which $\alpha(T)$ and $\beta(T)$ have a functional dependence on M and R (or I_{MM}), s, v, and SA(T). Also, from the origin of (3), $\bar{a}$ and N will be functions of T, and will depend on the same parameters. Thus, formally, equation (4) gives the distribution of amplitudes for a single event or group of events which all have the same magnitude and distance (or intensity) and site conditions. On the other hand, the data shown in Figures 53 and 54 are derived from the entire set of response spectra. Although (4) may not formally apply to this entire set taken as a group, the calculations described subsequently demonstrate that (4) does have the capability to describe the observed relationship between P_a and P_ℓ (Figures 53 and 54).

We assumed that P_a and P_ℓ can be related by equation (4), found values of N(T), $\alpha(T)$, and $\beta(T)$ which could describe the data in Figures 53 and 54, and then tested the assumption using two statistical tests. If N is known, the parameters α and β can be found by first noting that

$$\ell n\,(-\ell n\,(1 - P_a^{1/N})) = \alpha P_\ell + \beta \quad .$$

Assuming P_ℓ is an independent variable and P_a is a dependent variable with possible noise, α and β are found by least squares. To avoid a difficult nonlinear fitting procedure, we evaluated α and β for several possible values of N ranging from 1 to 1000. Then we quantified the differences between P_a (derived) and P_a (data) for each of these combinations, and found the value of N which led to the best fit. Finally, this derived function of the best N vs. period was smoothed by eye, and the smoothed values used in final calculations.

We illustrate this process in Figures 55 through 57. Figures 55 shows the data of P_a vs. P_ℓ from Figure 53 for $\zeta = 0.02$ and $\log_{10}T = 0.034$. It also shows the function of form (4) for three selected values of N and with the corresponding optimum values of α and β. Also shown in Figure 55 are the values of X^2 and of the Kolmogorov-Smirnov Statistic (K-S) for the distributions shown. These statistical tests are applied in the manner described by Anderson and Trifunac (1977). Both statistical parameters have a distinct minimim at $N \cong 5$, verifying the visual impression that the curve for N = 5 fits the data best. Figure 55 also shows the values of X^2 and K-S which, if exceeded, would lead to rejection of the resulting distribution. The minimum in X^2 and in K-S is well below this threshhold level.

One can compile the information on the quality of fit such as is illustrated on Figure 55 for 11 periods and all five dampings of SA. The results are shown in Figures 56 and 57. Figure 56 summarizes the data for X^2 and Figure 57 for the Kolmogorov-Smirnov statistic. For the 11 periods, the best value of N (of those computed) is shown by a number which also serves to identify the damping: 1 for $\zeta = 0.0$; 2 for $\zeta = 0.02$; 3 for $\zeta = 0.05$; 4 for $\zeta = 0.10$; and 5 for $\zeta = 0.20$. The

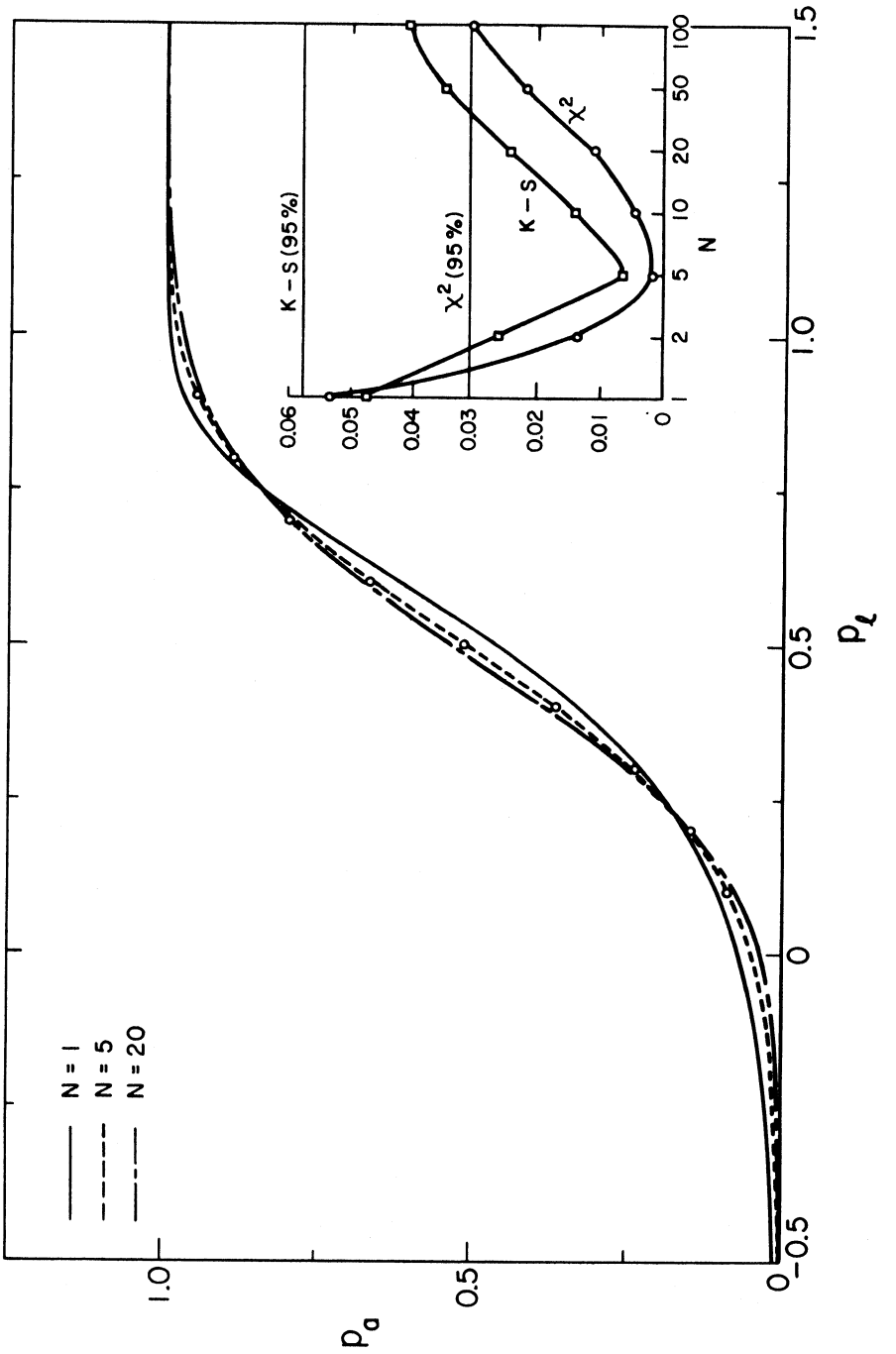

FIGURE 55

Best fitting functions of the form (4) for relating P_a to P_ℓ for three values of N. The data are shown by small circles. The insert at the right shows the results of two statistical tests for the goodness of fit. These statistical tests are shown for the three values of N illustrated, and also for some values which are not illustrated. If the Kolmogorov-Smirnov (K-S) statistics exceeds the line marked K-S (95%), then at the 95% confidence level, the trial distribution does not fit the data; the X^2 test is applied in the same way.

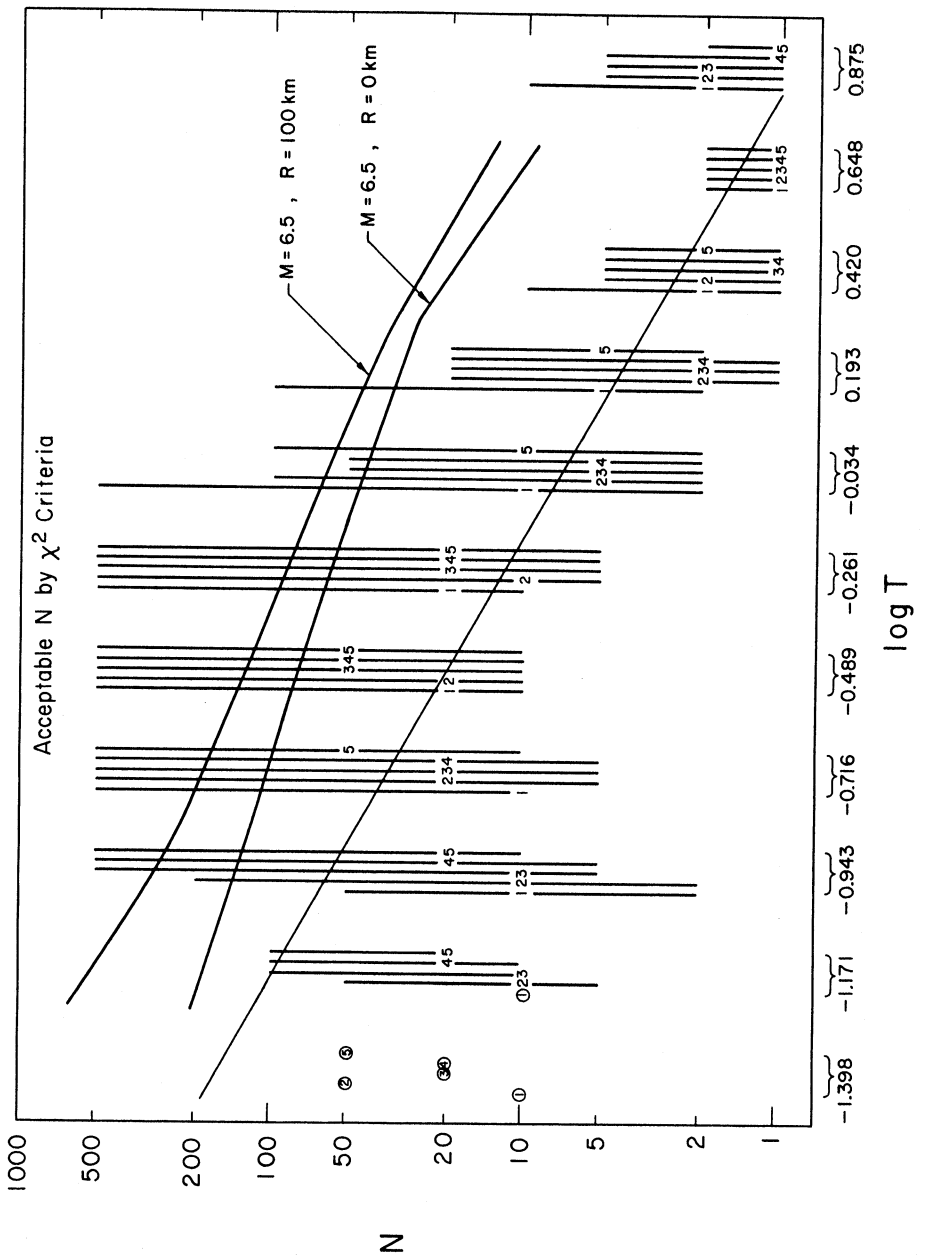

FIGURE 56

Summary of the results of the statistical X^2 test for distribution of form (4) relating P_a and P_ℓ for the regression of $\log_{10}[SA]$ as a function of P_ℓ, M, R, s, and v. For each of 11 periods, we have plotted an integer (1-5) at the value of N which leads to the smallest value of X^2. The vertical line shows the range of N which leads to a value of the X^2 statistic which is small enough that the corresponding distribution is not rejected at the 95% confidence level. Where the integer (1-5) is circled, the best value of X^2 is rejected. The integers 1-5 refer to the value of damping: 1 for $\zeta = 0.0$; 2 for $\zeta = 0.02$; 3 for $\zeta = 0.05$; 4 for $\zeta = 0.10$; and 5 for $\zeta = 0.20$.

The values of N which might be expected from the results of Trifunac and Westermo (1976a) for a magnitude 6.5 earthquake at 0 km and 100 km are shown. For reasons described in the text, we chose the value of N to be integers approximately equal to the straight line through the data, which has the equation $N = 6.5/T$.

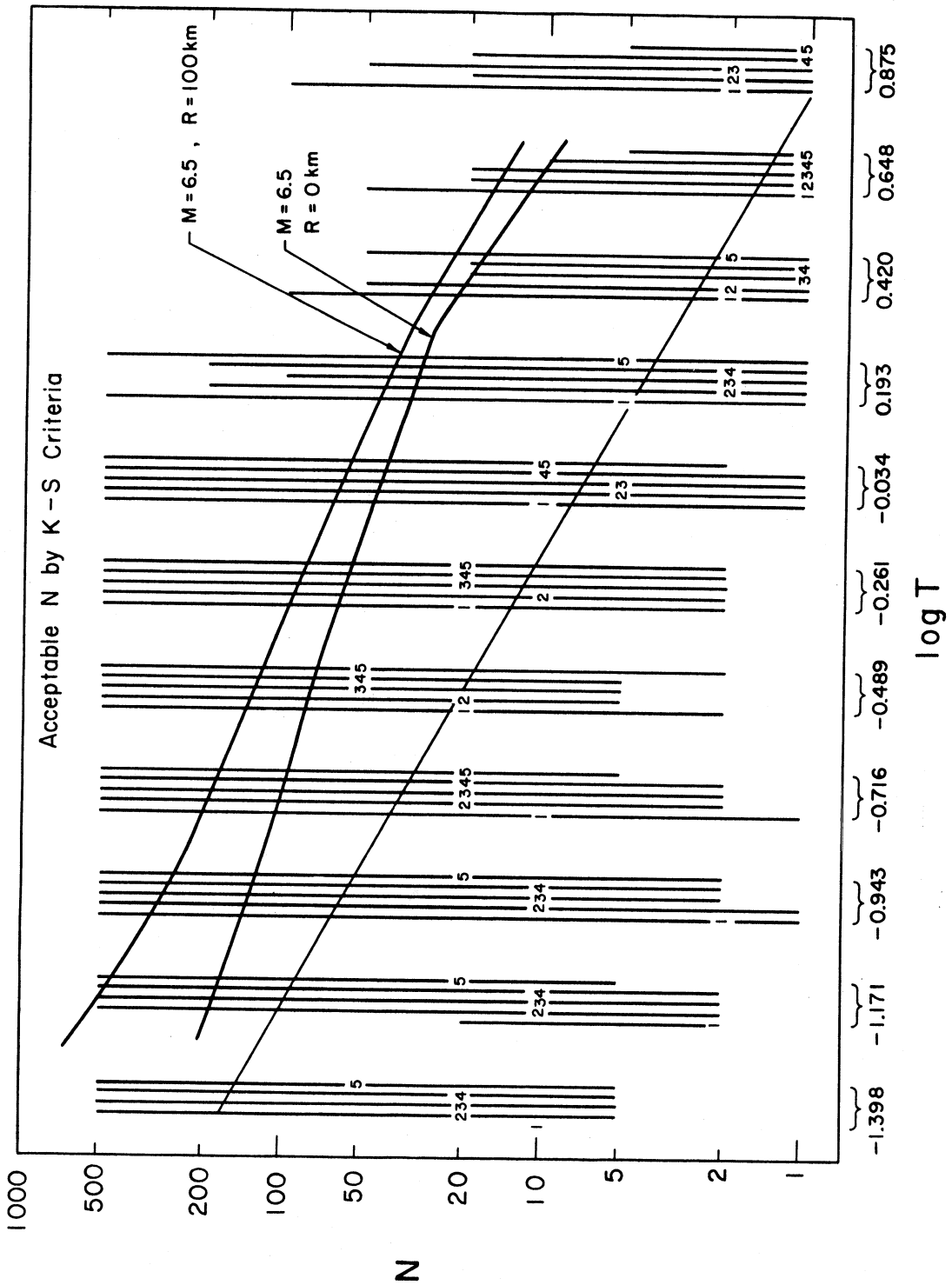

FIGURE 57

Results of the Kolmogorov-Smirnov statistical test to determine which values of N are acceptable to fit the data of P_a vs. P_ℓ for the regression of SA with magnitude and distance. Other symbols are as in Figure 56.

corresponding vertical line shows the permissible range of N according to X^2 (Figure 56) or K-S (Figure 57). Where the best value is not acceptable at the 95% confidence level, the digit 1-5 is circled.

The best value of N in Figures 56 and 57 is a strong function of the period T. This leads to values of α and β which are also strong functions of period, and these parameters jump discontinuously whenever the value of N changes from one integer to another. This contrasts with the characteristics of the spectra which must change continuously with changes in the frequency of shaking.

The problem arises from the way N is quantized. Because the SA spectra we are considering are for small values of damping, the number of cycles of shaking at some selected period is approximately the duration of the shaking divided by that period; there is no reason for this to be an integer. However, our probabilistic analysis is based on an integer number of peaks, and there, a fractional number does not make sense. Thus, the quantization of N is an artifact of the analysis.

Even though the values of $\alpha(T)$, $\beta(T)$ and $N(T)$ change discontinuously with changing periods, the parameters characterizing the probability distribution such as the most probable value or the various moments are nearly continuous. We will derive these next.

Consider the distribution:

$$P_a = F(P_\ell) = \left[1 - \exp(-e^{\alpha P_\ell + \beta})\right]^N$$

$$= \int_{-\infty}^{P_\ell} \left\{\frac{d}{dy}\left[1 - \exp(-e^{\alpha y + \beta})\right]^N\right\} dy \ .$$

We investigate the properties of the probability density function

$$\frac{d}{dy}\left[1 - \exp(-e^{\alpha y + \beta})\right]^N \ .$$

The n-th moment is

$$\overline{y^n} = \int_{-\infty}^{\infty} \left(\frac{x - \beta}{\alpha}\right)^n \frac{d}{dx} \left[1 - \exp(-e^x)\right]^N dx \quad . \tag{5}$$

If we use $I_N^{(n)} = \int_{-\infty}^{\infty} x^n \frac{d}{dx} \left[1 - \exp(-e^x)\right]^N dx$, then $I_N^{(0)} = 1$, and the the first two moments are

$$\bar{y} = (I_N^{(1)} - \beta)/\alpha$$

$$\overline{y^2} = (I_N^{(2)} - 2\beta\, I_N^{(1)} + \beta^2)/\alpha^2 \tag{6}$$

The standard deviation is $\sigma = \sqrt{\overline{y^2} - \bar{y}^2}$ (7)

Table X gives $I_N^{(1)}$ and $I_N^{(2)}$ for a large range of N. From this, the distribution P_a can be described in terms of $\bar{y}$ and σ. Given $\bar{y}$ and σ, from (6) and (7), one can show that:

$$\alpha = \frac{1}{\sigma} \sqrt{I_N^{(2)} - \left(I_N^{(1)}\right)^2}$$

$$\beta = I_N^{(1)} - \frac{\bar{y}}{\sigma} \sqrt{I_N^{(2)} - \left(I_N^{(1)}\right)^2} \quad .$$

Using these expressions, it may be possible in the future to choose $\bar{y}$, σ, and N to represent a particular earthquake. All these parameters could be a function of the size and distance of the earthquake, and possibly other factors. In this case, α and β could be found from the above expressions, and then (4) would apply formally. We are not adopting this approach at this time because we would like to see its validity demonstrated more directly than is possible with our data. However, it is instructive to substitute these parameters back into the probability function. Then:

$$F(P_\ell) = 1 - \exp\left[-\exp\left(I_N^{(1)} - \frac{\sqrt{I_N^{(2)} - \left(I_N^{(1)}\right)^2}}{\sigma} (P_\ell - \bar{y})\right)\right]^N \tag{8}$$

TABLE X

N	$I_N^{(1)}$	$I_N^{(2)}$	N	$I_N^{(1)}$	$I_N^{(2)}$
1	-0.5772	1.9781	28	1.3198	1.8366
2	0.1159	0.6975	29	1.3293	1.8603
3	0.4036	0.6114	30	1.3385	1.8831
4	0.5735	0.6729	31	1.3472	1.9052
5	0.6902	0.7612	32	1.3556	1.9266
6	0.7773	0.8508	33	1.3637	1.9472
7	0.8460	0.9353	34	1.3715	1.9673
8	0.9021	1.0134	35	1.3790	1.9867
9	0.9493	1.0852	36	1.3862	2.0056
10	0.9899	1.1513	37	1.3932	2.0240
11	1.0252	1.2123	38	1.4000	2.0418
12	1.0565	1.2687	39	1.4065	2.0592
13	1.0845	1.3212	40	1.4129	2.0761
14	1.1097	1.3703	41	1.4190	2.0925
15	1.1327	1.4162	42	1.4249	2.1086
16	1.1537	1.4593	43	1.4307	2.1243
17	1.1731	1.4999	44	1.4363	2.1395
18	1.1910	1.5384	45	1.4418	2.1545
19	1.2076	1.5748	46	1.4471	2.1691
20	1.2232	1.6094	47	1.4523	2.1833
21	1.2378	1.6423	48	1.4573	2.1973
22	1.2515	1.6738	49	1.4622	2.2109
23	1.2644	1.7038	50	1.4670	2.2242
24	1.2767	1.7325	51	1.4716	2.2373
25	1.2883	1.7601	52	1.4762	2.2501
26	1.2993	1.7866	53	1.4806	2.2627
27	1.3098	1.8121	54	1.4850	2.2750

TABLE X

(Continued)

N	$I_N^{(1)}$	$I_N^{(2)}$	N	$I_N^{(1)}$	$I_N^{(2)}$
55	1.4892	2.2870	83	1.5798	2.5544
56	1.4933	2.2989	84	1.5824	2.5621
57	1.4974	2.3105	85	1.5848	2.5697
58	1.5014	2.3219	86	1.5873	2.5772
59	1.5053	2.3331	87	1.5897	2.5846
60	1.5091	2.3441	88	1.5921	2.5919
61	1.5128	2.3549	89	1.5944	2.5991
62	1.5165	2.3655	90	1.5967	2.6062
63	1.5200	2.3760	91	1.5990	2.6133
64	1.5236	2.3862	92	1.6013	2.6202
65	1.5270	2.3963	93	1.6035	2.6271
66	1.5304	2.4063	94	1.6057	2.6339
67	1.5337	2.4161	95	1.6078	2.6407
68	1.5370	2.4257	96	1.6100	2.6473
69	1.5402	2.4352	97	1.6121	2.6539
70	1.5433	2.4445	98	1.6142	2.6604
71	1.5464	2.4537	99	1.6162	2.6669
72	1.5495	2.4628	100	1.6183	2.6733
73	1.5524	2.4717	101	1.6203	2.6796
74	1.5554	2.4805	102	1.6223	2.6858
75	1.5583	2.4891	103	1.6242	2.6920
76	1.5611	2.4977	104	1.6262	2.6981
77	1.5639	2.5061	105	1.6281	2.7042
78	1.5667	2.5144	106	1.6300	2.7101
79	1.5694	2.5226	107	1.6319	2.7161
80	1.5721	2.5307	108	1.6337	2.7219
81	1.5747	2.5387	109	1.6356	2.7278
82	1.5773	2.5466	110	1.6374	2.7335

TABLE X

(Continued)

N	$I_N^{(1)}$	$I_N^{(2)}$	N	$I_N^{(1)}$	$I_N^{(2)}$
111	1.6392	2.7392	139	1.6827	2.8798
112	1.6409	2.7449	140	1.6841	2.8843
113	1.6427	2.7505	141	1.6854	2.8887
114	1.6444	2.7560	142	1.6868	2.8931
115	1.6462	2.7615	143	1.6881	2.8974
116	1.6479	2.7669	144	1.6894	2.9017
117	1.6495	2.7723	145	1.6907	2.9060
118	1.6512	2.7777	146	1.6920	2.9103
119	1.6529	2.7829	147	1.6933	2.9145
120	1.6545	2.7882	148	1.6946	2.9187
121	1.6561	2.7934	149	1.6958	2.9228
122	1.6577	2.7985	150	1.6971	2.9269
123	1.6593	2.8036	151	1.6983	2.9310
124	1.6609	2.8087	152	1.6995	2.9351
125	1.6624	2.8137	153	1.7008	2.9392
126	1.6640	2.8187	154	1.7020	2.9432
127	1.6655	2.8236	155	1.7032	2.9472
128	1.6670	2.8285	156	1.7044	2.9511
129	1.6685	2.8334	157	1.7055	2.9551
130	1.6700	2.8382	158	1.7067	2.9590
131	1.6715	2.8430	159	1.7079	2.9628
132	1.6729	2.8477	160	1.7090	2.9667
133	1.6744	2.8524	161	1.7102	2.9705
134	1.6758	2.8571	162	1.7113	2.9743
135	1.6772	2.8617	163	1.7125	2.9781
136	1.6787	2.8663	164	1.7136	2.9818
137	1.6800	2.8708	165	1.7147	2.9856
138	1.6814	2.8753	166	1.7158	2.9893

Application to Correlation of SA with M, R, s, and v

Figures 56 and 57 present the quality of fit of the assumed distribution (4) to the relationship between P_a and P_ℓ. They show the range of values of N(T) for which an acceptable fit to the data points can be made, and also indicate the best values of N(T), among those computed.

The best value of N(T) decreases as the period of the waves increases. This trend is particularly apparent for intermediate periods. This could be predicted from a simple argument. Suppose the duration D is the same in all frequency bands. Then the number of peaks is $N(T) = \frac{2D}{T}$, where T, again, is the periods of the oscillators. The factor 2 arises because there are 2 peaks in each complete cycle of response. On Figures 56 and 57, we have drawn a line to connect the points $N = \frac{6.5}{T}$. This is consistent with the observed distributions for all but the highest frequencies. The inconsistency may arise because the signal to noise ratio of the original data is smaller at the high frequencies and because the duration depends on the period of the seismic waves.

The durations predicted by Trifunac and Westermo (1976a) can be used to estimate the number of peaks of strong shaking. The number of peaks predicted for a magnitude of 6.5 event at 0 and 100 km is shown in Figures 56 and 57. This procedure overestimates the "best" N, and does not provide a better estimate than the original line $N = \frac{6.5}{T}$. This is to be expected, however, because the definition of duration used by Trifunac and Westermo (1976a) does not exclude a decaying coda of strongly scattered waves, even though such a coda may not contribute to the peaks which control the statistics of the oscillator response.

The differences between the "best N" and the N estimated from the duration of strong shaking is smallest for the intermediate periods where the signal to noise ratio is largest. Where the signal to noise ratio is small, the definition of duration used by Trifunac and Westermo (1976a) may include the duration of some noise; this effect also will tend to cause the number of peaks estimated from the duration determined by Trifunac and Westermo (1976a) to be larger than the "best N" in Figures 56 and 57. At periods where we expect this effect to be strongest, the differences between the two methods are greater than where we expect this effect to be small.

As mentioned previously, the distribution function (4) applies to a single event; the data, however, is derived from a large number of events recorded over a large range of distances. Since the duration of strong shaking is a prominent function of distance, it may be of some concern how combining the data modifies the resulting distributions (4). To illustrate this, we have plotted several distributions with the same values of the mean and standard deviations but differing values of N by using equation (8). The result (Figure 58) is that for most amplitudes (most values of P_ℓ) the corresponding probability (P_a) either increased or decreased monotonically as N increased. Thus, a combination of many points from the distributions with many values of N would tend to fit a distribution with some averaged value of N. This average would be weighted toward smaller values of N because the distribution changes most rapidly when N is small. This also might help to explain why the value of the "best N" tends to be smaller than the N derived from the average duration of the same data set.

Using the value of N = Greatest integer in $\frac{6.5 \text{ sec}}{T}$, and N = 1

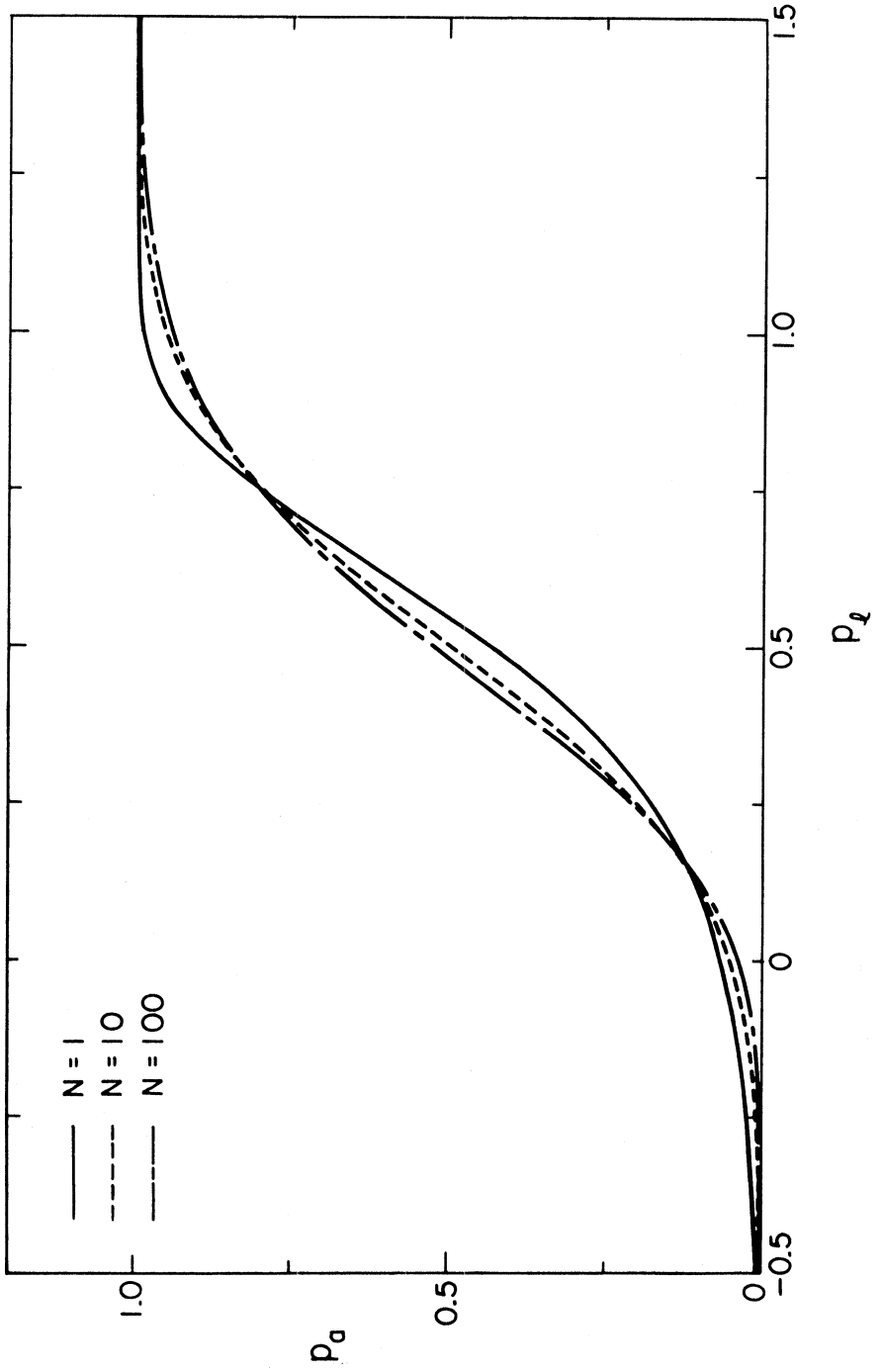

FIGURE 58

Comparison of the functional relationships of P_a to P_ℓ for fixed $\mu = 0.5$ and $\sigma = 0.3$ and for N = 1, 10, and 100. These results are obtained using equation (8).

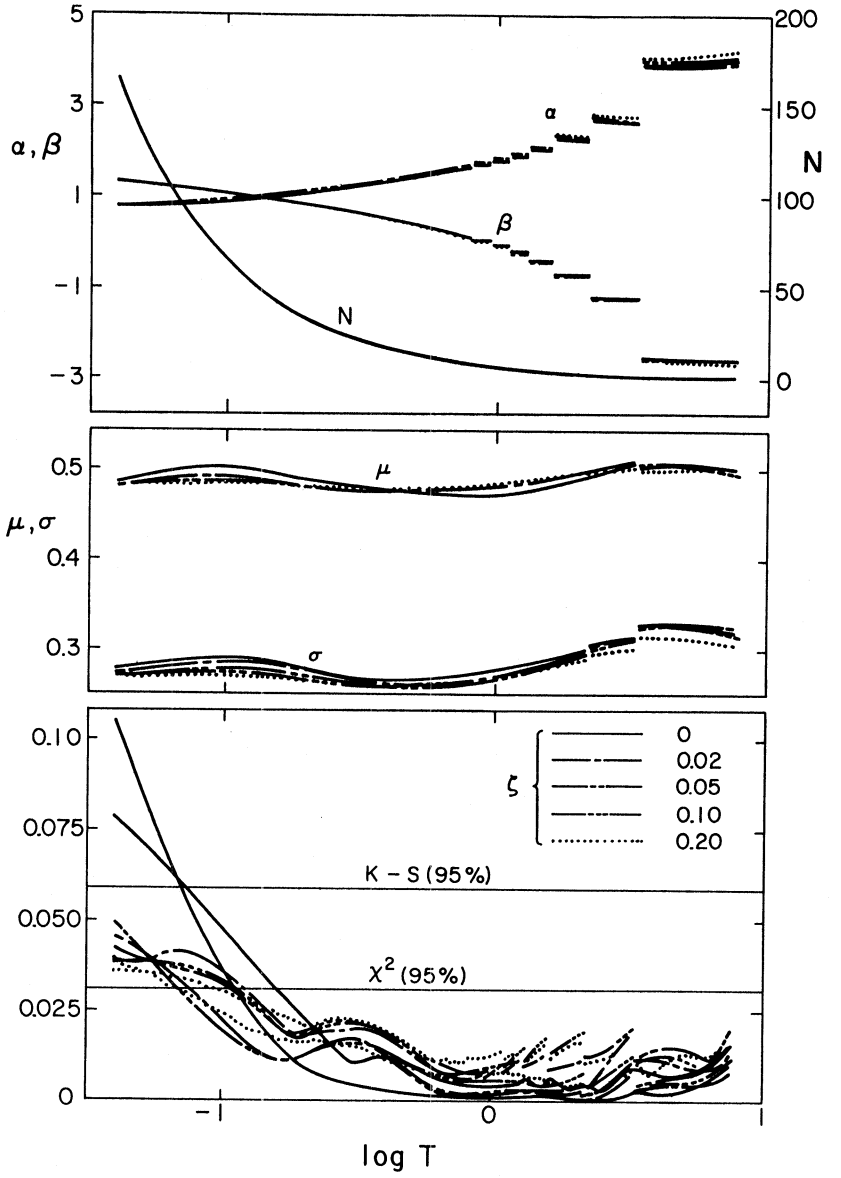

FIGURE 59

Parameters for one set of distributions (4) which approximately give P_a as a function of P_ℓ. The upper curves give α, β, and N (equation (4)). N is quantized, but the individual integers cannot be illustrated on this scale, so N is drawn as a continuous line.

The central section gives the parameters μ and σ derived from α, β, and N using equations (6) through (9). The lower section shows the statistical quality of fit by the Kolmogorov-Smirnov and the X^2 criteria. The X^2 test can be recognized by its smaller amplitudes for periods in the central portion of the graph. The levels marked K-S (95%) and X^2 (95%) are those which, if exceeded, lead to rejection of the assumed distribution at that frequency. The five lines are for the five values of damping, as indicated.

when $\frac{6.5 \text{ sec}}{T} < 1$, we have found the best values of α and β to fit the observed data relating P_a and P_ℓ as functions of period. The parameters α, β, and N, the corresponding mean and standard deviation (μ and σ), and the statistical tests for all five dampings are shown in Figure 59. Strictly, N(T), α(T), and β(T) should not be plotted as a continuous variable because they are quantized. The actual values of α(T), β(T), and N(T) are given in Table V for eleven periods. From Figure 59, it is apparent that the mean and standard deviation are nearly continuous, in spite of the way that N is quantized. The lower portion of Figure 59 shows the statistical tests for the associated distributions. These tests are applied as in Anderson and Trifunac (1977). For highest frequencies, these distributions fail and could be rejected; at all lower frequencies the assumed distribution is consistent with the data. Note that although (4), with the parameters in Table V, gives an adequate description of the relationship between P_a and P_ℓ for $0.1 \leq P_\ell \leq 0.9$, extrapolation using (4) to find the probabilities of amplitudes much larger or smaller than those impled by $0.1 \leq P_\ell \leq 0.9$ may not be justified on the basis of our data.

Application to Correlation of SA with I_{MM}, s, and v

Again, we assume that a Rayleigh distribution is appropriate to describe the distribution of peak amplitudes of single-degree-of-freedom viscously damped oscillators, and find the range of acceptable N and the best values of N by the X^2 and the K-S criteria. These are shown in Figures 60 and 61, respectively. Unlike the correlations with magnitude and distance, here only values of N equal to 1 or 2 are chosen as best values using the statistical tests.

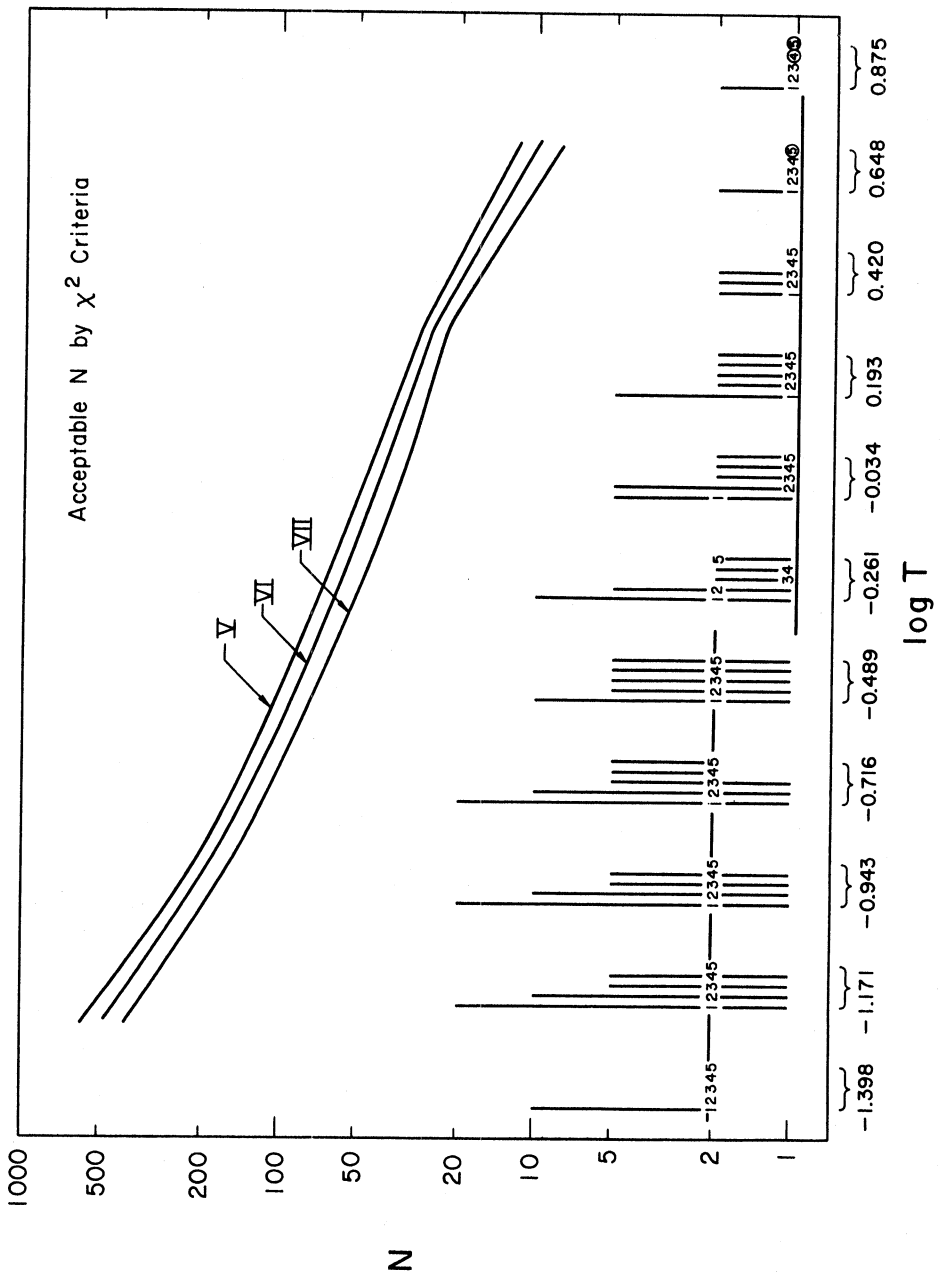

FIGURE 60

Results of the X^2 statistical test to determine which values of N are acceptable to fit the data of P_a vs. P_ℓ for the regression of SA with Modified Mercalli Intensity. The upper lines show those N which might be expected on the basis of results of Trifunac and Westermo (1976b) for intensity V, VI and VII shaking. For the later regression, we chose the N indicated by the light line. Other symbols are as in Figure 56.

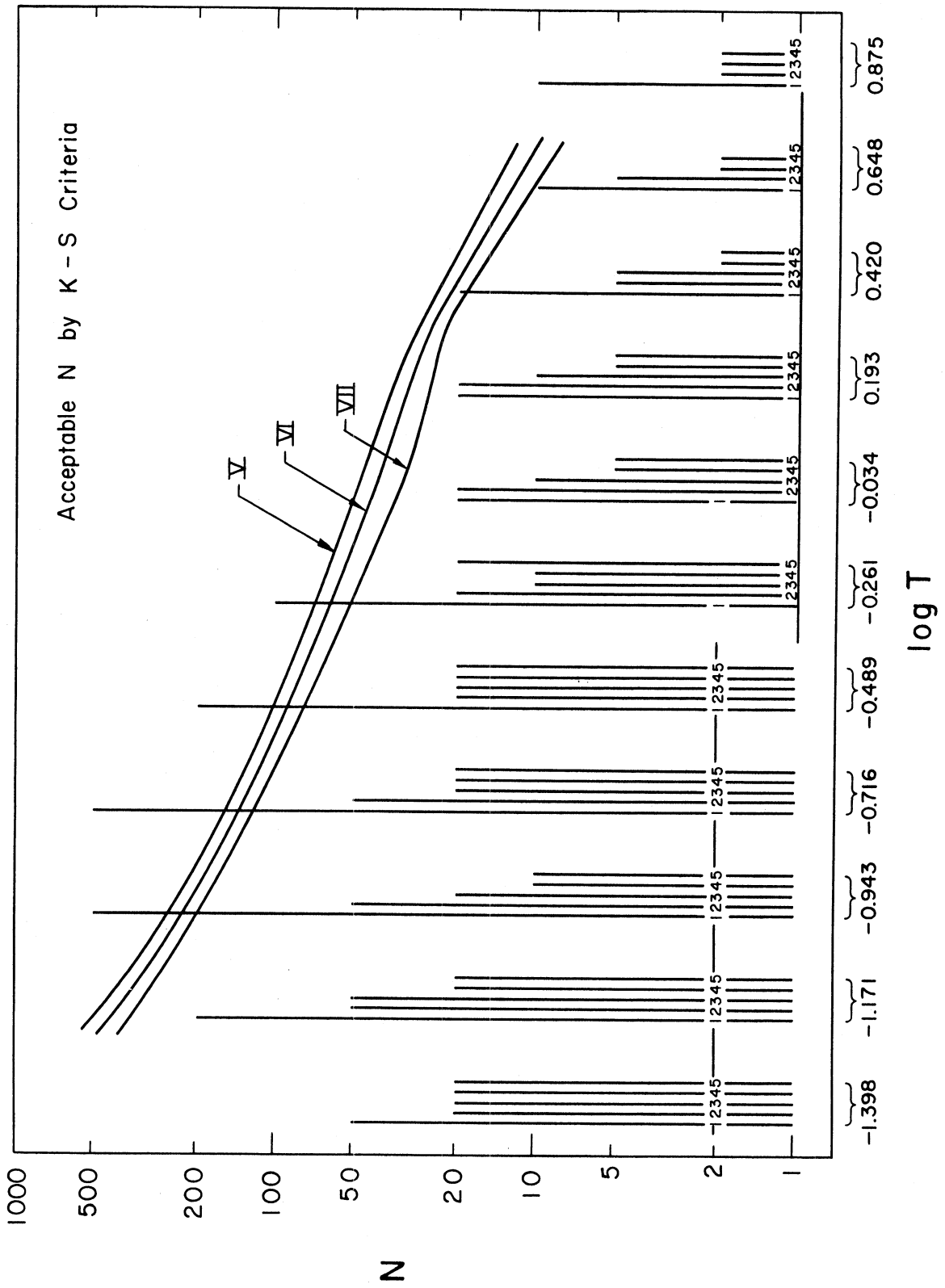

FIGURE 61

Equivalent of Figure 60, except that it shows the results of the Kolmogorov-Smirnov test.

In Figures 60 and 61, we again have plotted the values of $N = \frac{2D}{T}$ using average durations of these accelerograms for intensities V, VI, and VII given by Trifunac and Westermo (1976b). These values are generally over an order of magnitude larger than the "best N" found using our fitting procedure. We have mentioned three reasons why the results of Trifunac and Westermo (1976a) would tend to overestimate N for correlations with magnitude and distance: First, their definition of duration includes the decaying coda, which may not contribute significantly to the number of peaks in the oscillator response statistics. Second, their definition of duration can possibly include the presence of noise, which also would not contribute to the number of peaks in the oscillator response statistics. Third, our data points are combined from several distributions which each obey equation (4), and these several distributions may involve differing values of N; the best value of N when several distributions are combined in this way may tend to be smaller than the average of N over all the contributing distributions because for fixed mean and standard durations, equation (4) (or equation (8)) changes more rapidly for a change in N when N is small than when N is large. These factors are not adequate to explain why N is so small in the case of correlation with I_{MM} (equation (2)) because the correlations involving magnitude and distance (equation (1)) generally indicated larger values of N.

There is, however, another factor operating here which was not present in the correlations with magnitude and distance. This arises because I_{MM} is a function of both the amplitude of shaking and the duration of shaking among other factors. Because the correlations neglect duration, this can introduce another bias into the estimates

of N.

Let us assume that I_{MM} is a function of both duration (D) and amplitude of shaking:

$$I_{MM} = I_{MM}(D, A)$$

A contour of constant I_{MM} from this function is concave down, as sketched in Figure 62. For a fixed duration, we expect that as the amplitude of shaking increases, the I_{MM} will also increase. For a fixed amplitude, a longer duration will also tend to increase I_{MM} to a certain extent. However, for a fixed amplitude, a duration greater than some sufficiently long period of time may never cause the intensity to increase to the next larger value. For example, shaking strong enough to be felt by nearly everyone might continue indefinitely without being strong enough to move heavy furniture or damage chimneys. Because of this, a plot of a contour of uniform intensity on axes of duration (or distance) and amplitude, is concave downward as in Figure 62.

Now consider the consequences of data for a given intensity being distributed along one of these contours. We have shown this schematically for the $I_{MM} = V$ contour in Figure 62. When these data points are projected onto the amplitude axis, many tend to be grouped near small amplitudes, but the relatively fewer large amplitudes skew the distribution. A mean amplitude, as is found by regression, is then larger than the amplitude where most of the data occur; thus most of the amplitudes are smaller than the mean. As a result, when the distribution of amplitudes relative to the mean is found, it has an excess of amplitudes smaller than the mean. This may be exactly what we have found in our correlations of P_a and P_ℓ for I_{MM} because smaller

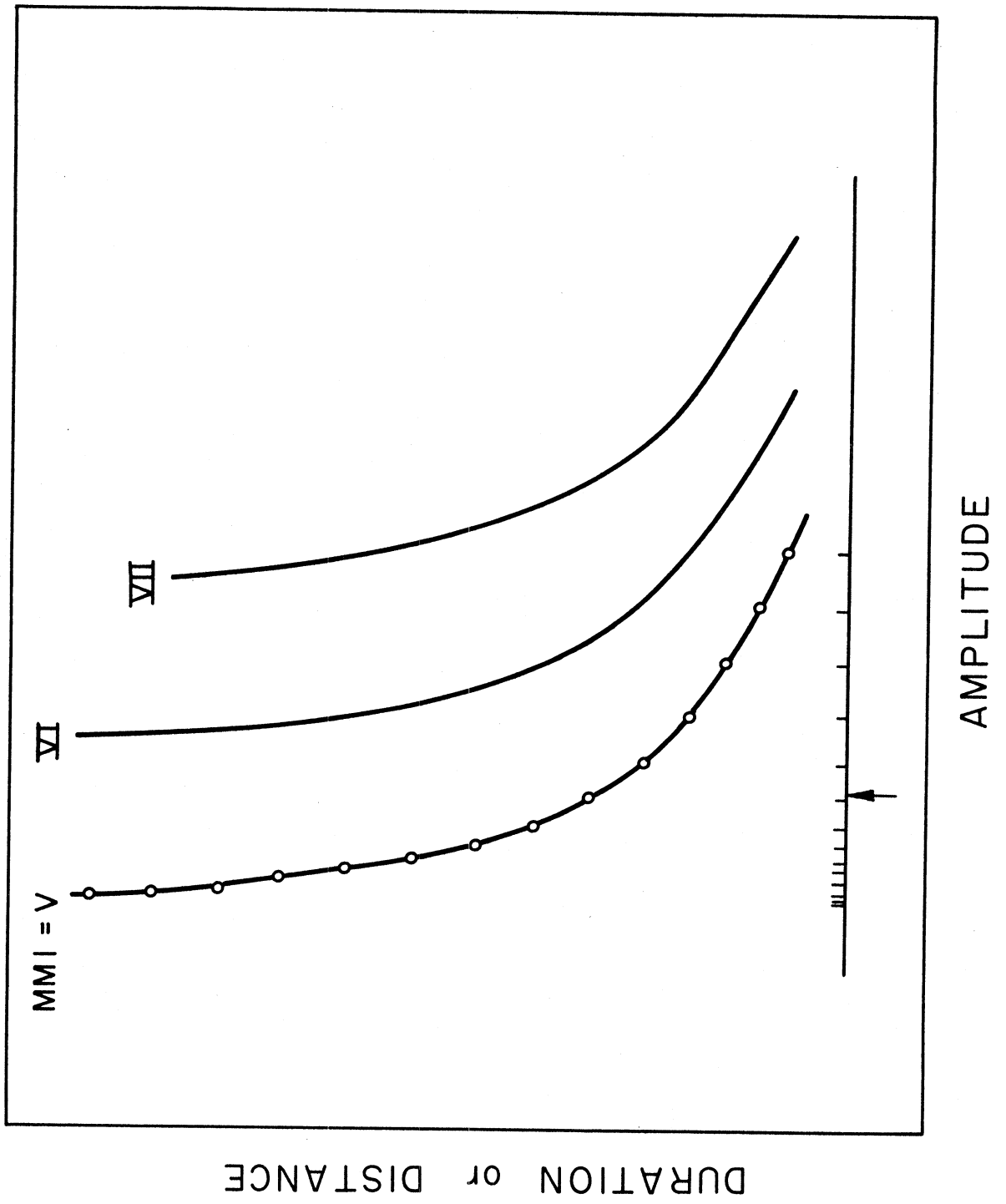

FIGURE 62

Schematic sketch showing the behavior of a contour of uniform intensity on a plot of duration (or distance) against amplitude of shaking. Below, the consequence of a correlation neglecting duration is illustrated: there is a tendency for a majority of the data points to be smaller than the mean (arrow).

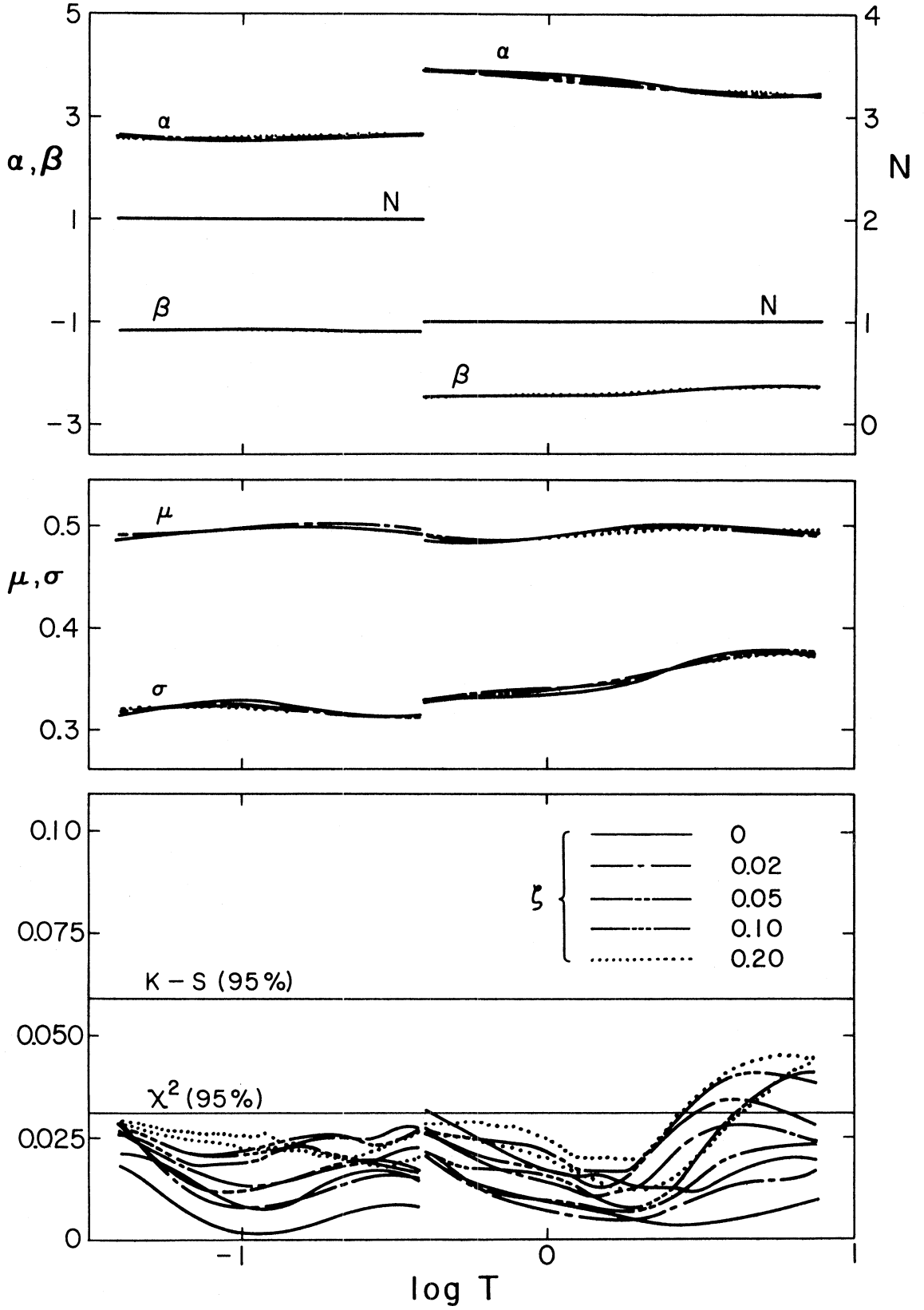

FIGURE 63

Equivalent of Figure 59 for the regression of SA with intensity.

N implies a distribution with a relatively greater number of small amplitudes. It is difficult to estimate the significance of this effect from this qualitative description; however, it appears from the Figures 60 and 61 that the effect might be strong.

Considering this effect, it may be possible to understand why the best values of N are so low in Figures 60 and 61. We choose:

$$N(T) = \begin{cases} 2; -1.398 \leq \log_{10} T \leq -0.400 \\ 1; -0.400 \leq \log_{10} T \leq 0.875 \end{cases}$$

From Figure 63, which shows the resulting statistical parameters, it is clear that the assumed distribution function is not contradicted by the data. The parameters $\alpha(T)$, $\beta(T)$, and $N(T)$ are also given in Table VI for eleven selected periods.

CONCLUSIONS

We have carried out two independent regressions for the amplitudes of absolute acceleration spectra (SA) using two regression equations. Equation (1) describes the dependence of SA on magnitude, epicentral distance, and site conditions; Equation (2) describes the dependence of SA on Modified Mercalli Intensity. Both regression equations are frequency dependent. The forms of the regressions were chosen to describe approximately the physical processes of the earth and in terms of those parameters which are readily available to the engineering community.

Before carrying out the regression analysis, we have partially eliminated digitization noise by subtraction of an average noise spectrum. Although this has not eliminated all noise, it has increased the reliability of the regression models.

The regressions show results which are consistent with previous related analyses and observations. Some of these results are that: the spectra increase less rapidly with increasing magnitudes at large magnitudes than at small magnitudes; spectral amplitudes at high frequencies tend to be larger on rock sites than on soil sites; and the scatter of SA about the scaling law in terms of MMI (equation (2)) is not worse than the scatter of SA about the scaling law in terms of magnitude and distance (equation (1)). The regression equations (1) and (2) give mutually consistent results when extrapolated to $M = 8\frac{1}{2}$ and $R = 0$ and to MMI = XII.

We have modeled the scatter of amplitudes about the mean trend by a distribution function derived from a Rayleigh distribution. One

parameter of this derived distribution function (equation (4)) is N(T), the number of peaks of the response of a single-degree-of-freedom system at the period T. The values of N(T) which best fit the observed scatter of amplitudes are smaller than the value of N(T) derived by independent considerations; however, there are several qualitative reasons why this might be the case. Nonetheless, the derived distribution is both physically motivated and is not inconsistent with the observed scatter in the data.

The results of this study, then, are the empirical scaling laws for modeling amplitudes of SA in either the case where the magnitude or the M.M.I. of a possible future earthquake can be estimated. Further calculation of P_a from equation (4) allows these results to be applied to seismic risk studies.

ACKNOWLEDGEMENTS

We thank J. E. Luco and A. Der Kiureghian for critical reading of the manuscript and for many useful comments and suggestions.

This research has been supported by a grant from the National Science Foundation and by a contract from the Nuclear Regulatory Commission.

REFERENCES

Alford, J. L., G. W. Housner, and R. R. Martel (1951). Spectrum Analysis of Strong-Motion Earthquakes, Earthquake Eng. Res. Lab., Calif. Inst. of Tech., Pasadena.

Anderson, J. G., and M. D. Trifunac (1977). On Uniform Risk Functionals which Describe Strong Earthquake Ground Motion: Definition, Numerical Estimation, and an Application to the Fourier Amplitude of Acceleration, Dept. of Civil Eng., Report No. 77-02, U.S.C., Los Angeles,

Benioff, H. (1934). The Physical Evaluation of Seismic Destructiveness, Bull. Seism. Soc. Amer., 24, 398-403.

Biot, M. A. (1941). A Mechanical Analyser for the Prediction of Earthquake Stresses, Bull. Seism. Soc. Amer., 31, 151-171.

Borcherdt, R., and J. F. Gibbs (1976). Effects of Local Geological Conditions in the San Francisco Bay Region on Ground Motions and Intensities of the 1906 Earthquake, Bull. Seism. Soc. Am., 66, 467-

Duke, C. M. (1958). Bibliography of Effects of Soil Conditions on Earthquake Damage, Earthquake Engr. Res. Inst., 47 pp.

Gutenberg, B. (1957). Effects of Ground on Earthquake Motion, Bull. Seism. Soc. Amer., 47, 221-250.

Hudson, D. E., A. G. Brady, M. D. Trifunac and A. Vijayaragharan (1971). Strong-Motion Earthquake Accelerograms, II, Corrected Accelerograms and Integrated Velocity and Displacement Curves, Earthquake Eng. Res. Lab., EERL 71-51, Calif. Inst. of Tech., Pasadena.

Hudson, D. E., M. D. Trifunac and A. G. Brady (1972). Strong-Motion Accelerograms III, Response Spectra, Earthquake Eng. Res. Lab., EERL 72-80, Calif. Inst. of Tech., Pasadena.

Hudson, D. E. (1976). Strong-Motion Earthquake Accelerograms, Index Volume, Earthquake Eng. Res. Lab., EERL 76-02, Calif. Inst. of Tech., Pasadena.

Housner, G. W. (1970). Design Spectrum, Chapter 5 in Earthquake Engineering, edited by R. L. Wiegel, Prentice-Hall.

Newmark, N. M., H. J. Degenkolb, A. K. Chopra, A. S. Veletsos, E. Rosenblueth and R. L. Sharpe (1977). Seismic Design and Analysis Provisions for the United States, 5-245, Sixth World Conf. Earthquake Eng., New Delhi, India.

Richter, C. F. (1958). Elementary Seismology, Freeman, San Francisco.

Seed, H. B., C. Ugas and J. Lysmer (1974). Site Dependent Spectra for Earthquake Resistant Design, Earthquake Eng. Res. Center, EERC 74-12, U. C. Berkeley.

Trifunac, M. D., and J. N. Brune (1970). Complexity of Energy Release During the Imperial Valley, California, Earthquake of 1940, Bull. Seism. Soc. Amer., 60, 137-160.

Trifunac, M. D. (1972a). Stress Estimates for San Fernando, California, Earthquake of 9 February 1971: Main Event and Thirteen Aftershocks, Bull. Seism. Soc. Amer., 62, 721-750.

Trifunac, M. D. (1972b). Tectonic Stress and Source Mechanism of the Imperial Valley, California, Earthquake of 1940, Bull. Seism. Soc. Amer., 62, 1283-1302.

Trifunac, M. D. (1973). Analysis of Strong Earthquake Ground Motion for Prediction of Response Spectra, International J. of Earthquake Eng. and Struct. Dyn., Vol. 2, No. 1, 59-69.

Trifunac, M. D., and V. W. Lee (1973). Routine Computer Processing of Strong-Motion Accelerograms, Earthquake Eng. Res. Lab., EERL 73-03, Calif. Inst. of Tech., Pasadena.

Trifunac, M. D., F. E. Udwadia, and A. G. Brady (1973). Analysis of Errors in Digitized Strong-Motion Accelerograms, Bull. Seism. Amer., 63, 157-187.

Trifunac, M. D. (1974). A Three-Dimensional Dislocation Model for the San Fernando, California, Earthquake of February 9, 1971, Bull. Seism. Soc. Amer., 64, 149-172.

Trifunac, M. D., and F. E. Udwadia (1974). Parkfield, California, Earthquake of June 27, 1966: A Three-Dimensional Moving Dislocation, Bull. Seism. Soc. Amer., 64, 511-533.

Trifunac, M. D., and V. W. Lee (1974). A Note on the Accuracy of Computed Ground Displacements from Strong-Motion Accelerograms, Bull. Seism. Soc. Amer., 64, 1209-1219.

Trifunac, M. D., and A. G. Brady (1975). On the Correlation of Seismic Intensity Scales with the Peaks of Recorded Strong Ground Motion, Bull. Seism. Soc. Amer., 66, 139-162.

Trifunac, M. D. (1976a). Preliminary Analysis of the Peaks of Strong Earthquake Ground Motion -- Dependence of Peaks on Earthquake Magnitude, Epicentral Distance and Recording Site Conditions, Bull. Seism. Soc. Amer., 66, 189-219.

Trifunac, M. D. (1976b). Preliminary Empirical Model for Scaling Fourier Amplitude Spectra of Strong Ground Acceleration in Terms of Earthquake Magnitude, Source to Station Distance and Recording Site Conditions, Bull. Seism. Soc. Amer., 66, 1343-1373.

Trifunac, M. D. (1976c). A Note on the Range of Peak Amplitudes of Recorded Accelerations, Velocities and Displacements with Respect to the Modified Mercalli Intensity, Earthquake Notes, Vol. 47, No. 1, 9-24.

Trifunac, M. D., and B. Westermo (1976a). Dependence of Duration of Strong Earthquake Ground Motion on Magnitude, Epicentral Distance, Geologic Conditions at the Recording Station and Frequency of Motion, Dept. of Civil Eng., Report No. 76-02, U.S.C., Los Angeles.

Trifunac, M. D., and B. Westermo (1976b). Correlations of Frequency Dependent Duration of Strong Earthquake Ground Motion with the Modified Mercalli Intensity and the Geologic Conditions at the Recording Stations, Dept. of Civil Eng., Report No. 76-03, U.S.C., Los Angeles.

Trifunac, M. D. (1977). Forecasting the Spectral Amplitudes of Strong Earthquake Ground Motion, Proc. Sixth World Conf. Earthquake Eng., New Dehli, India.

Veletsos, A. S., N. M. Newmark, and C. V. Chelapati (1965). Deformation Spectra for Elastic and Elastoplastic Systems Subjected to Ground Shock and Earthquake Motions, Third World Conf. Earthquake Eng., II, 663-680, New Zealand.

Udwadia, F. E., and M. D. Trifunac, (1973). The Fourier Transform, Response Spectra and Their Relationship Through the Statistics of Oscillator Response, EERL 73-01, Calif. Inst. of Tech., Pasadena.